Graft mechanical compliance in vascular patency

by

YeJin Jeong

A thesis

presented to the University of Waterloo

in fulfillment of the

thesis requirement for the degree of

Doctor of Philosophy

in

Chemical Engineering

Waterloo, Ontario, Canada, 2022

Examining Committee Membership

The following served on the Examining Committee for this thesis. The decision of the Examining Committee is by majority vote.

External Examiner	Dr. Lin-Yue Lanry Yung Department of Chemical and Biomolecular Engineering, National University of Singapore
Supervisor	Dr. Evelyn K.F. Yim Department of Chemical Engineering, University of Waterloo
Internal Member	Dr. Tizazu H. Mekonnen Department of Chemical Engineering, University of Waterloo
Internal Member	Dr. Tsui Yiu Ting Department of Chemical Engineering, University of Waterloo
Internal-external Member	Dr. Sean D. Peterson Department of Mechanical and Mechatronics Engineering, University of Waterloo

Author’s Declaration

This thesis consists of material all of which I authored or co-authored: see Statement of Contributions included in the thesis. This is a true copy of the thesis, including any required final revisions, as accepted by my examiners.

I understand that my thesis may be made electronically available to the public.

Statement of Contributions

YeJin Jeong was the sole author of Chapter 1, 5, and 6 which were written under the supervision of Dr. Evelyn Yim. The listed chapters do not contain any published information.

This thesis consists in part of two publications and one report. Exceptions to sole authorship of the material are as follows:

Review presented in Chapter 2:

Dr. Yuan Yao and Dr. Evelyn K.F. Yim were co-authors of the review article published on Biomaterials Science Journal - Royal Society of Chemistry. The review was conducted at the University of Waterloo by YeJin Jeong as the primary author, and Dr. Yao as co-author under the supervision of Dr. Yim.

Citation: Jeong Y, Yao Y, Yim EK (2020) Current understanding of intimal hyperplasia and effect of compliance in synthetic small diameter vascular grafts. Biomaterials Science.

Research presented in Chapter 3:

Dr. Yuan Yao, Dr. Tizazu H. Mekonnen, and Dr. Evelyn K.F. Yim were co-investigators of the research published on Frontiers in Materials. The research was conducted at University of Waterloo under the supervision of Dr. Yim. YeJin Jeong and Dr. Yim drafted the research aim. Dr. Mekonnen and Dr. Yao contributed in data analysis. YeJin Jeong wrote the draft manuscript, which other co-authors contributed intellectual input.

Citation: Jeong Y, Yao Y, Mekonnen TH, Yim EK (2021) Changing compliance of poly (vinyl alcohol) vascular grafts through modifying interlayer adhesion and crosslinking density. Frontiers in Materials 7:456

Research presented in Chapter 4:

Rebecca Danelon, Sarah Taylor, Suchi Vijayaraghavan, and Tim Wu developed the base form of automated dip-casting equipment under the supervision of Dr. Evelyn Yim and YeJin Jeong. The four authors contributed equally on the development of the equipment and written report. Dr. Evelyn Yim and YeJin Jeong provided guidance, resources, and contributed intellectual input to the design and experiments. The equipment was then modified by YeJin Jeong to increase the throughput. The modified automated dip-casting equipment was used for the experiments shown in this thesis.

Citation: Wu T, Taylor, S., Vijayaraghavan, S., Danelon, R (2019) Improving the Manufacturing Process for Biocompatible Vascular Grafts. 2019 Chemical Engineering Capstone Design Projects. University of Waterloo, University of Waterloo

Abstract

With the growing age of average population throughout the world, progress of biomaterials research is important to overcome current limitations. Vascular graft is one of the examples. Currently, synthetic vascular grafts made using expanded polytetrafluoroethylene (ePTFE) or Dacron are commercially available as treatments to cardiovascular diseases. These synthetic vascular grafts have good patency, which is a measure used to determine the success of the grafts, and are actively used in more than 400,000 life-saving procedures in the United States alone. However, the available synthetic grafts have limitations – their patency is poor when used in small-diameter application. Synthetic small diameter vascular graft (sSDVG) is defined by synthetic vascular grafts with internal diameter less than 6mm. sSDVG face limited success due to vascular wall thickening known as intimal hyperplasia (IH). IH develop at the distal anastomosis of the graft and are due to over proliferation and abnormal migration of vascular smooth muscle cells (VSMC). Mechanical compliance mismatch of the sSDVG is proposed as one of the key factors that contribute to the formation and development of IH. Compliance in vascular engineering is referring to the radial elasticity of the vascular graft or the blood vessel. Native blood vessels are highly elastic; compliance of human internal mammary artery with the diameter of 1-2 mm is reported to be 12% per 100mmHg. The compliance of sSDVG, however, is very low. The compliance of ePTFE graft, for example, is reported to be 1.2±0.3 % per 100mmHg. This discrepancy in the compliance of the native blood vessels and sSDVG is called compliance mismatch. Compliance mismatch is suggested to play an important role in IH because of mechanotransduction. Mechanotransduction refers to the cellular responses to mechanical stimuli. In the literature, many biological molecules inside VSMC, such as platelet-derived growth factor-BB (PDGF-BB), platelet-derived growth factor receptor, phosphorylated myosin light-chain kinase (pMLCK), have been found to be influenced by the mechanical stimulation. Compliance mismatch forces the cells around the anastomosis to be exposed to abnormal mechanical stimulation, which is translated to biological responses to increase proliferation and migration of VSMC.

Different biomaterials are being studied to develop compliant sSDVG. For example, polyurethane is being studied as a potential compliant vascular graft. Polyurethane vascular grafts were modified with gelatin and collagen to enhance endothelial cell adhesion and were modified using heparin to reduce thrombogenesis. Likewise, poly(vinyl alcohol) (PVA) vascular grafts were developed in 2008. PVA hydrogel is bio-inert, low-thrombogenic, and non-cytotoxic biomaterial with easily modified

mechanical properties. The compliance of PVA vascular graft developed by Chaouat et al. had comparable compliance to the native blood vessels. However, the compliance, as well as other mechanical properties, of the PVA grafts were heavily influenced by the conditions in which the crosslinking of the hydrogel occurred. While the variation was observed, it was not studied systematically to identify the effects of the fabrication conditions on mechanical properties. In this thesis, the roles crosslinking density and interlayer adhesion play in compliance and burst pressure of PVA vascular grafts were studied. Fabrication parameters were categorized based on their effects on either crosslinking density or interlayer adhesion. PVA tubes with different fabrication conditions were made to yield tubes with lower crosslinking density, higher crosslinking density, lower interlayer adhesion, and higher interlayer adhesion. It was found that the higher crosslinking density resulted in higher burst pressure and lower compliance. Furthermore, it was found that higher interlayer adhesion resulted in higher burst pressure and lower compliance as well. Elastic modulus and suture-retention strength of the control, higher interlayer adhesion, and higher crosslinking density were compared as well. The result displayed that only the circumferential elastic modulus was affected by the interlayer adhesion and crosslinking density. Therefore, the study concluded that it is important to balance crosslinking density and interlayer adhesion to fabricate PVA grafts with desired compliance.

Consistency is important for research to ensure reliable result. In part due to the sensitivity to fabrication condition, the consistency of PVA vascular graft suffered from person-to-person variation in fabrication process. PVA vascular grafts are fabricated using dip-casting method. In this method, a cylindrical mold is dipped into PVA crosslinking solution to produce thin layer of PVA hydrogel on the mold. The dipping is repeated until the PVA graft reach desired wall thickness. Also, while PVA hydrogel crosslinked using chemical crosslinking method is observed to be non-degradable, the stability of PVA grafts were not studied. The batch-to-batch consistency of PVA tubes made using automated process was studied, as well as the long-term stability of PVA grafts. The automated fabrication method developed displayed similar capacity as those made using manual fabrication method. The grafts made using automated process displayed consistent variation in wall thickness, burst pressure, and compliance. The grafts made using automated process and manual process exhibited comparable burst pressure and compliance when accounting for the wall thickness. Lastly, physical dimensions were compared to study long-term stability of the PVA grafts. Wall thickness, graft length, and dry weights displayed less than 5% change after 180 days of incubation.

PVA hydrogel is also a good platform to study the effects of compliance mismatch on VSMC. Mechanical stimulation is essential for understanding the responses of VSMC on formation of IH. Studies have found that PDGF-BB and pMLCK are upregulated when VSMC are exposed to cyclic stretching. Furthermore, VSMC have been observed increase in proliferation and changes to migratory phenotype when exposed to cyclic strain. However, understanding the isolated effects of compliance mismatch has been difficult due to lack of continuous sample with two distinct regions of stiffness. In this thesis, a hybrid method using both physical and chemical crosslinking was developed to form continuous compliance mismatched samples using PVA hydrogel. The samples were characterized and found to be continuous in both parallel and perpendicular to the mismatch line. The samples were then used to perform in vitro experiments using human umbilical arterial smooth muscle cells (HUASMC) with exposure to cyclic stretching at 10% strain for 4 hours. Exposure to mechanical stimulation resulted in higher proliferation, change into migratory phenotype, compactification of PDGF-BB, and higher expression of pMLCK for the all the groups Among the stretched groups, compliance mismatch resulted in highest proliferation, pMLCK expression, and highest number of cells with concentrated PDGF-BB signal. However, no nuclear localization of yes-associated protein (YAP) was observed. The experiments were repeated with samples with higher compliance mismatch. Nuclear localization of PDGF-BB and YAP was observed when HUASMC cultured on higher compliance mismatched samples were exposed to cyclic stretch of 10% strain for 4 hours. Therefore, it can be concluded that not only does compliance mismatch affect cellular responses to cyclic stretching, but also the extent of compliance mismatch plays a role in the responses.

Acknowledgements

I would like to acknowledge and thank Dr. Evelyn K.F. Yim for all of her effort in supervision and help throughout the Ph. D Program. I would like to thank my colleagues Dr. Yuan Yao, Dr. Aung Moe Zaw, and Dr. Tizazu Mekonnen for their help and guidance. I would also like to thank other lab members for helping with experiments and sample fabrication. I would also like to thank Rebecca Danelon, Sarah Taylor, Suchi Vijayaraghavan, and Tim Wu for the development of the automated PVA fabrication equipment. I would also like to thank Michael Tong and Dr. Keng Hwee Chiam for their help with development of simulation. Lastly, I would like to thank Clyde Overby III for his help in keeping me more-or-less sane throughout my endeavor.

Dedication

I dedicate this thesis to

My father, Jae Cheon Jeong (정재천).

And my Fiancé, Clyde Thomas Overby III,

I could not have done this without them.

Table of Contents

List of Abbreviations

Abbreviation	Definition
CVD	Cardiovascular Diseases
CDC	Centers for Disease Control and Prevention
USA	United States of America
sSDVG	synthetic Small Diameter Vascular Graft
PAD	Peripheral Artery Disease
CRF	Chronic Renal Failure
AVG	Arteriovenous Graft
IH	Intimal Hyperplasia
VSMC	Vascular Smooth Muscle Cells
PVA	Poly(Vinyl Alcohol)
HUASMC	Human Umbilical Arterial Smooth Muscle Cells
pMLCK	phosphorylate Myosin Light-Chain Kinase
PDGF-BB	Platelet-Derived Growth Factor-BB
YAP	Yes-Associated Protein
ePTFE	expanded Polytetrafluoroethylene
AF	Arteriovenous Fistula
STMP	Trisodium Trimetaphosphate
WS	Wall Stress
WSS	Wall Shear Stress
NO	Nitric Oxide
PGI_2	Prostacyclin
EC	Endothelial Cells
SMC	Smooth Muscle Cells
PDGF	Platelet-Derived Growth Factor
MMP	Matrix Metalloproteinases
TNF-α	Tumor Necrosis Factor-α
eNOS	endothelial Nitric Oxide Synthase
PDGF-A	Platelet-Derived Growth Factor-A
IGPR-1	Immunoglobulin and Proline-rich Receptor-1
PWV	Pulse Wave Velocity
AIx	Augmented Index
ARTSENS	Arterial Stiffness Evaluation for Non-invasive Screening
MPG	Magnetic Plethysmography
MRI	Magnetic Resonance Imaging
CFD	Computational Fluid Dynamics
FEM	Finite Element Modelling
TEVG	Tissue-engineered Vascular Grafts
BMF	Blood-mimicking Fluid
ISO	International Standard Organization
pAMPK	phosphorylated-Adenosine Monophosphate-activated Protein Kinase
NaOH	Sodium Hydroxide
LMW	Low Molecular Weight PVA. Chapter 3.

MMW	Medium Molecular Weight PVA. Chapter 3.
LS	Low (7.5% w/v solution) of Trisodium Trimetaphosphate. Chapter 3.
LN	Low (15% w/v solution) of Sodium Hydroxide. Chapter 3.
PBS	Phosphate Buffered Saline
DIW	Deionized Water.
NaCl	Sodium Chloride
15W	15-min Wait between dips. Chapter 3.
30W	30-min Wait between dips. Chapter 3.
HH	High Humidity (60±5%). Chapter 3.
60-2D	Dried in 60°C post fabrication for 2 weeks. Chapter 3.
60-4D	Dried in 60°C post fabrication for 4 weeks. Chapter 3.
18-2D	Dried in 18°C post fabrication for 2 weeks. Chapter 3.
18-2D	Dried in 18°C post fabrication for 4 weeks. Chapter 3.
PLA	Polylactic Acid
FTIR	Fourier-transform Infrared
DCS	Differential Scanning Calorimetry
PCA	Principal Component Analysis
FYDP	Fourth-Year Design Project. Chapter 4.
CAD	Computer-assisted design
C	Compliant PVA sample. Chapter 5.
M	Compliance mismatch PVA sample. Chapter 5.
NC	Not compliant PVA sample/ Chapter 5.
2M	Higher compliance mismatch PVA sample. Chapter 5.
2NC	Higher Not compliant PVA sample. Chapter 5.
CDI	Carbonyldiimidazole
DMSO	Dimethyl Sulfoxide
UV	Ultraviolet
UMT	Uniaxial Material Tester
DMEM/F-12	Dulbecco's Modified Eagle Medium/Nutrient Mixture-F-12
HEPES	4-(2-hydroxyethyl)-1-piperazineethanesulfonic acid
FBS	Fetal Bovine Serum
Pen-Strep	Penicillin-streptomycin
PFA	Paraformaldehyde
IF	Immunofluorescence
PDMS	Poly(dimethyl siloxane)
EdU	2-mercaptoethanol
EB	Electrophoresis buffer

List of Figures

List of Tables

Chapter 1
Introduction

This chapter will address brief background information, motivation, followed by the overall hypothesis of the thesis. Then, individual aims for each hypothesis will be explained in detail. Lastly, the outline of the thesis will be explained.

1.1 Background

With the advances in medicine, individuals are enjoying longer lifespan on average. Ironically, longer lifespan exposes people to more diseases. Cardiovascular diseases, chronic renal failure, Alzheimer's diseases, and cancer are but few of the examples of diseases that have old age as one of their risk factors. [1-5]. Numerous biomedical researches are performed worldwide to overcome the old age, but the solution is still far from present. Therefore, it is important to focus on the solutions that could be achieved sooner. For example, gene therapy is being studied to treat breast cancer [6]. Drugs are being developed to treat Alzheimer's diseases [7]. Vascular grafts are available for bypass surgeries for occluded arteries [8]. Dialyzers are developed for cleaning blood of patients with chronic renal failure [9].

Cardiovascular diseases (CVD) still remain as one of the major causes of death worldwide [1]. According to Centers for Disease Control and Prevention (CDC) of United States of America (USA), approximately one person dies every 36 seconds in USA due to CVD [10]. Typically, CVD occurs due to occlusion of a blood vessel. Occlusion of blood vessel can occur due to build-up of plaque, also known as atherosclerosis, or due to thrombus formation. The biggest difficulty with CVD is that the diseases blood vessel does not allow for proper flow of blood. The disturbed blood flow can result in lack of oxygen and nutrients to the tissues and organs in the body, and can result in necrosis [11]. To ensure proper blood flow to all regions of the body, bypass surgeries are performed to implant vascular grafts to circumvent the occluded regions [12]. Many commercially available synthetic vascular grafts are successfully used in bypass surgeries each year [13]. However, synthetic small-diameter vascular grafts (sSDVG), which are grafts with inner diameter less than 6mm, still face limited success [14].

Peripheral artery disease (PAD) and chronic renal failure (CRF) are two examples of diseases that require sSDVG. PAD refers to the medical condition where the arteries in the extremities are either partially or completely occluded [11]. It can cause serious swelling and pain at the affected limb, and

bypass surgeries can be performed to redirect the blood flow to avoid the affected region of the artery. as the diameters of these arteries are small, they are especially vulnerable to the limitation of sSDVG. CRF also requires the use of synthetic vascular grafts. CRF refers to failure of the kidney to filter the waste and fluid from blood, resulting in the need of hemodialysis [2]. In order to perform hemodialysis, however, a connection between and artery and vein has to be made. This connection is called arteriovenous fistula if made using the native artery and vein [15]. If the fistula fails or cannot be made in the patient for some reason, then vascular graft is implanted to for arteriovenous graft (AVG). AVG typically use sSDVG because the diameter of the artery and vein used for AVG typically range from 3-5mm for artery and 6-10mm for vein [16].

The long-term success rate of synthetic small-diameter vascular grafts (sSDVG) is low. For example, the patency of expanded-polytetrafluoroethylene vascular grafts have 23% of patency after 2 weeks of implantation [17]. Another synthetic vascular graft sold under the trade name Dacron have 29% patency after 7 months when graft had less than 6mm in diameter [18]. The biggest reason for failure of sSDVG is development of intimal hyperplasia (IH). IH refers to the thickening of the blood vessel wall due to excessive proliferation and abnormal migration of vascular smooth muscle cells (VSMC) [14]. The development of IH has been observed at the distal anastomoses of the implanted grafts [19]. The thickening of the wall results in occlusion, resulting in the failure of the graft.

A hypothesized reason for the development and progression of IH is the mechanical mismatch between the native blood vessel and the implanted sSDVG [14]. Specifically, mechanical compliance mismatch is considered as one of the potential factors responsible for IH. Compliance in vascular engineering refers to the elasticity of the blood vessel or vascular graft [20]. Native blood vessels have high compliance, or high elasticity [21]. However, available sSDVG have low compliance, or low elasticity [21]. In healthy compliant blood vessel, the flow rate is decreased due to the fact that the blood vessel expands to accommodate for the blood flow. In non-compliant sSDVG, on the other hand, cannot expand to decrease the speed of the blood flow and cause abnormal wall shear stress and wall stress around the distal anastomosis [22].

Understanding the effects of compliance mismatch between the native blood vessel and the implanted graft is difficult due to many other factors. Studying the blood flow within the implanted graft *in vivo* is difficult due to resolution limitation of available equipment [14]. The limitation in *in vivo* measurement prevents validation of the values acquired through computational fluid dynamic

simulations. Therefore, the simulations are often compared to in vitro experiments [14]. The experiments often decouple shear stress and wall stress to understand the effects of individual component. Furthermore, suture-line stress is also unavoidable due to the fact that vascular grafts are sutured onto the native blood vessels [23]. Studying compliance mismatch requires a connection between a compliant side and a not compliant side. Studies have found that suture-line can cause abnormal localization of stress around the sutures [23, 24]. With the addition of suture-line, the isolated effects of compliance mismatch cannot be studied. Just like wall shear stress and wall stress being decoupled to simplify the experimental setup, suture-line stress and compliance mismatch has to be decoupled to understand the isolated effects of each component.

However, the effects of compliance mismatch alone are not well understood. One of the reasons for the lack of understanding of isolated effects of compliance mismatch is that a continuous hydrogel with distinct regions of different compliance has not been developed [14]. Poly(vinyl alcohol (PVA) vascular graft have been suggested as a potential compliant vascular graft in 2008 [25]. Later, dip-casting method was used to apply multiple layers of coating crosslinking solution onto cylindrical mold [26, 27]. After complete crosslinking, the hydrogel was removed from the mold to yield PVA vascular grafts. PVA is a bio-inert, low-thrombogenic, and low-cytotoxic hydrogel. While PVA without modification does not allow for cellular adhesion, it can be easily modified to increase cellular adhesion [28-30]. For example, PVA has been modified using gelatin, fucoidan, and other molecules that allows for cellular adhesion [28, 29, 31]. The grafts are actively used *ex vivo* as well as *in vivo* experiments.

In vitro mechanical stimulation has played a vital role in understanding IH in vascular graft engineering. Cellular responses to mechanical stimulation is a well-observed phenomena [32]. Mechanical loading on osteocytes are used to encourage alignment of lacunae [33]. VSMCs are also one of the cell types that are sensitive to mechanical stimulation. In the case of VSMC, platforms to expose the cells to shear stress in vitro are developed and used in various labs [34, 35]. There are commercially available devices that exposes samples to cyclic strain [36]. Likewise, mechanical stimulation is important for understanding the role compliance mismatch plays in IH. For the exposure to cyclic strain, however, the continuous compliance mismatch sample has to be made with good integration of the two sides with different compliance.

1.2 Motivation

While the PVA vascular grafts displayed good compliance in study published by Ino et. al [27], the compliance of the grafts varied depending on the fabrication condition. To identify the parameters that affect the compliance of PVA vascular grafts, different fabrication parameters were studied. The parameters were categorized as either affecting the crosslinking density of interlayer adhesion. The PVA grafts were fabricated with different fabrication conditions, and the effects of crosslinking density and interlayer adhesion had on compliance of the graft were studied. Additionally, mechanical parameters that are important for vascular graft were quantified to assess the effects of crosslinking density and interlayer adhesion.

Also, the consistency of PVA grafts were explored. Because PVA vascular graft fabrication process is prone to variation between batches, automated method was developed to test whether the consistency between batches could be improved. Also, PVA vascular grafts are fabricated in batches and are typically stored until use. Therefore, the stability of the PVA grafts were assessed to ensure the consistency of the PVA grafts before and after long-term storage.

Lastly, the hydrogel was used to make continuous compliance mismatched samples to study the effects of compliance mismatch on VSMC. One of the difficulties in studying effects of compliance mismatch decoupled from suture-line stress is the lack of available materials. In order to study the isolated effects, a continuous compliance mismatched sample with distinct regions of different stiffness has to be developed. Using the fact that PVA hydrogels can be crosslinked using both physical and chemical crosslinking methods, continuous compliance mismatched PVA hydrogel samples were developed. The developed compliance mismatched samples were then used to study the cellular responses of VSMC with exposure to cyclic stretching.

1.3 Hypothesis

The overall hypothesis is that compliance mismatch will result in higher proliferation and migration of VSMC with exposure to cyclic stretching.

In Chapter 3, we hypothesize that (i) the increase in interlayer adhesion will allow for higher compliance and higher burst pressure when the grafts have the same wall thickness, (ii) decrease in crosslinking density will result in higher compliance and lower burst pressure when the grafts have

the same wall thickness, and (iii) post-fabrication processing can cause physical crosslinking, and impact the compliance and burst pressure.

The hypotheses that will be addressed in Chapter 4 are: (i) the automation process will result in less variation in wall thickness, burst pressure, and compliance compared to the PVA grafts made using the manual fabrication method, and (ii) there will be no more than 5% loss of length, thickness, and dry weight of PVA grafts after 180 days of incubation.

In Chapter 5, we hypothesized that: (i) chemical and physical crosslinking can be used simultaneously to achieve a continuous film with compliance mismatch, (ii) human umbilical arterial smooth muscle cells (HUASMC) cultured on compliance mismatch film will result in higher proliferation rate compared to both compliant and non-compliant films, and (iii) HUASMC cultured on compliance mismatched film would result in higher phosphorylated myosin light-chain kinase expression, higher platelet-derived growth factor-BB expression, and nuclear localization of yes-associated protein.

1.4 Aims

The overall aim of this thesis is to use invitro experiments to investigate the above-listed hypotheses.

In Chapter 3, different fabrication parameters were altered to identify the factors that can influence the compliance of PVA vascular grafts. The chapter aims to identify the effects of crosslinking density and interlayer adhesion on the mechanical properties.

Chapter 4 aims to identify the methods to increase the consistency of the PVA grafts between batches, as well as to identify whether there is any significant loss in the physical properties of the PVA grafts after long storage.

Chapter 5 aims to study the isolated effects of compliance mismatch on VSMCs exposed to cyclic stretching. Continuous sample with distinct regions of different stiffness was developed using physical and chemical crosslinking methods. Using continuous compliance mismatch samples, cellular responses of VSMC were studied to identify the expression of biological factors associated with proliferation and migration.

1.5 Outline of the thesis

In Chapter 2, detailed literature review on cardiovascular diseases, current state of synthetic vascular graft engineering, and uses of synthetic vascular grafts. This chapter will also address the limitations of the currently available synthetic vascular grafts. Lastly, current state of poly(vinyl alcohol) vascular graft engineering and related research will be addressed.

Chapter 3 will address the mechanical characterization of PVA tubes. PVA tubes were fabricated under different fabrication condition to modify the crosslinking density and interlayer adhesion within the tubes. Compliance along with other mechanical properties of the PVA tubes were characterized to conclude on the effects of crosslinking density and interlayer adhesion on the compliance of the PVA tubes.

Chapter 4 will explore the consistency of PVA grafts between batches and after long-term storage. Automated dip-casting equipment developed by Fourth-Year Design Group under the supervision of Dr. Evelyn Yim and YeJin Jeong were modified to assess the capacity of automated production while maintaining consistency in quality. Also, the physical properties of the PVA grafts were assessed to ensure consistency after long-term storage.

Chapter 5 will address the cellular study on the effects of compliance mismatch using continuous compliance mismatched sample. Continuous compliance mismatched samples were fabricated and characterized to ensure cellular adhesion and application of uniform strain throughout during cyclic stretching. Then, the samples were seeded with VSMCs and exposed to cyclic stretching. Various biological molecules associated with proliferation and migration of VSMC were quantified to assess cellular responses.

Lastly, Chapter 6 will address the conclusions of each chapter, and explain the contribution of the thesis in research. This chapter will also suggest future directions and applications of the techniques developed and used in this thesis.

Chapter 2
Literature Review

In this chapter, brief overview of diseases requiring vascular graft intervention will be discussed. Then, conditions that result in blood vessel occlusion will be explained in more detail, followed by the applications of synthetic vascular grafts. The synthetic vascular graft engineering research that have been done using poly(vinyl alcohol) will be explained. Afterwards, the current state and limitations of synthetic vascular graft engineering will be addressed. Use of mechanical stimulation in understanding cellular behavior of vascular smooth muscle cells will be addressed. Finally, compliance in vascular graft engineering will be discussed

2.1 Diseases requiring vascular intervention

Cardiovascular system is an essential system that distributes oxygen and nutrients to the cells throughout the body. Any problem in cardiovascular system can result in serious complications, and therefore have been a focus of research for many decades. Through many efforts, synthetic vascular grafts have been developed and are actively being used in life-essential treatments [12]. In 2012, approximately 400,000 vascular implants were used for coronary artery bypass in USA [37]. Currently, synthetic vascular grafts are made using expanded polytetrafluoroethylene (ePTFE), polyethylene terephthalate (Dacron®), or polyurethane [38]. Synthetic vascular grafts are used because they can be made and be readily available [38]. In the case of autografts, the grafts have to be harvested from the patient. However, the synthetic vascular grafts can be mass-produced and be used without needing to go through another surgical procedure. Also, synthetic vascular grafts have been improving over time. Different modifications have been tried to improve the patency of the grafts. In 1998, Walpoth et al. found that they can reach 100% patency after 8-week of implantation in mouse when using heparin-coated ePTFE [39]. The efforts to make higher patency synthetic vascular graft continued, and synthetic vascular graft became a reliable option for large-diameter vascular grafts.

However, limitation to the synthetic vascular graft engineering remains. The synthetic vascular grafts have low success rate when the luminal diameter is less than 6mm [40]. These vascular grafts are called synthetic small-diameter vascular grafts (sSDVG). With sSDVG the patency of the grafts can be as low as 23% after 2 weeks of implantation [17]. One of the proposed problems with the available sSDVG is the compliance mismatch between the native blood vessels and the synthetic vascular grafts [41]. The limited success of sSDVG is due to formation of intimal hyperplasia (IH)

[42]. IH refers to thickening of the blood vessel walls due to excessive proliferation and migration of vascular smooth muscle cells (VSMC) [43]. One of the hypothesized reasons for the formation of IH in sSDVG is compliance mismatch between the native blood vessels and the vascular graft [44]. Compliance is a measurement of the luminal volume due to change in internal pressure [45]. sSDVG have low compliance, and the abnormal wall stress (WS), wall shear stress (WSS), and suture-line stress. Detailed affects of compliance mismatch on sSDVG will be addressed in Section 2.4.

Here, the clinical problems that necessitates the development of sSDVG with high success rate are explained. Cardiovascular system is the system connecting the heart and blood vessels to allow for blood circulations throughout the body. Blood is pumped by the heart with each heartbeat. The blood flows through the blood vessels of different sizes to all parts of the body for oxygen exchange as well as transport or nutrients. If something within this process goes awry, it could cause cardiovascular disease (CVD) [1]. In the case of occluded blood vessels, synthetic vascular grafts are implanted to circumvent the blockage. Synthetic vascular grafts are also used in patients with chronic renal failure (CRF) [2]. Patients suffering from CRF requires surgical intervention to connect artery and vein, usually in the forearm of the patients [46]. While the connection can be made by using the native blood vessels, sSDVG are implanted in the case where the use of native blood vessel is not feasible [47].

2.1.1 Cardiovascular diseases

Cardiovascular system spans throughout the entirety of the body serving a vital role. This role can be interrupted or hindered by various causes, potentially leading to development of CVD. CVD is any health condition that affects either the heart or the vascular system [1]. It is one of the leading causes of death worldwide, accounting for approximately 17.9 million deaths worldwide each year according to World Health Organization [48]. Some of the known risk factors of CVD includes smoking, high cholesterol diet, diabetes, sedentary lifestyle, genetic predisposition, and old age [49]. These factors are often shared on news and social media platforms, explaining the importance of keeping healthy lifestyle and diet [50-53]. The dangerous part of CVD is that having one CVD increases the risk of developing other or multiple CVDs. Having peripheral artery disease (PAD), for example, can increase the risk for developing coronary artery diseases. In the case of heart failure, it could be due to malfunction of the heart or the heart valve because of damaged tissue, or because of interrupted blood supply due to blood vessel occlusion [54]. A clot formation can give rise to ischemic stroke if

the clot blocks a blood vessel in the brain. Because the focus of the thesis is on vascular graft, the review in this section will be limited to the vascular systems.

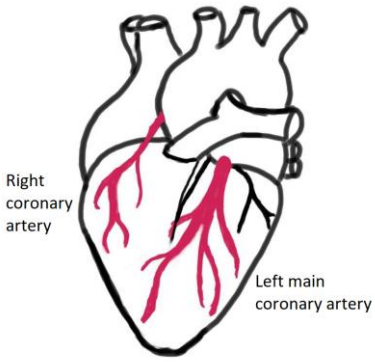

Figure 2.1. Schematic of the heart with left and right coronary arteries in red [55].

Coronary arteries are the major arteries that supplies blood to the heart muscles. There are two major coronary arteries: left main coronary artery, and right coronary artery (Fig. 2.1. in red) [55]. As coronary arteries supply blood to the heart muscles, any blockage of coronary arteries can result in increased strain on the heart, potentially leading to heart attacks, and even heart failures [54]. The severity of the coronary arterial diseases can affect the type of heart disease that may occur. If the blockage of coronary artery is minimal, then the patient may have a mild case of angina - which is also known as chest pain [50]. However, if significant amount of the coronary artery is blocked, then it can cause heart attack.

Heart attack, also known as myocardial infarction, is a well-known leading cause of death [51]. It occurs when the blood flow to the heart is significantly reduced [51]. The symptoms of heart attacks are typically pressure, tightness, pain in the chest, nausea, shortness of breath, fatigue, and dizziness [51]. The type of symptoms or the severity of the symptoms may vary depending on the person. Heart attacks can be sudden and deadly. Because of this, people are encouraged to seek emergency medical attention immediately after the display of one of the symptoms [51, 54]. One of the dangers of heart attack is that it can result in long-lasting damage. Heart attack results in disruption of blood flow throughout the body. In severe case, heart attack can result in brain damage due to the interruption of blood flow. Bypass surgeries are performed as treatments to heart attacks caused by coronary arterial blockage to circumvent the blockage, and to restore blood flow to the heart [55].

Peripheral arteries refer to arteries that are in the peripheries of the body. They allow for blood flow away from the heart to the arms and legs. The names and the diameters of some of the peripheral arteries are shown in Table 2.1. Typically, the diameter of the arteries in the left and right side are not different [56].

Peripheral artery disease (PAD) is a medical condition where the blood flow within these arteries is reduced due to blockage [64]. PAD typically occurs due to plaque build-up on the arterial all that results in reduction in luminal diameter. Some of the symptoms of PAD are pain, aches, or cramps at the location of blockage [11]. Also, people may feel weakness in the affected limbs, as well as hair-loss, smooth and shiny skin, slow healing, and coldness [11]. However, about 40% of people with PAD are asymptomatic [53]. PAD is known to be highly affected by age, affecting 6.5 million people that are older than 40 years of age in the United States of America (USA) [65]. Healthy lifestyle is suggested as preventative measure of PAD. PAD is typically treated using antiplatelet medication along with change in lifestyle [11]. However, bypass surgery may be needed if the disease is too severe to be treated using medication [53]. Due to the diameters of the peripheral arteries, PAD requires implantation of sSDVG.

Table 2.1. Names and diameters of peripheral arteries in healthy individuals.

Name	Diameter	Reference
Arteries in the legs		
Iliac artery	18.8 - 20.9 mm	[57]
Femoral artery	7 - 8 mm	[58]
Popliteal artery	4.9 - 6.9 mm	[59]
Tibial artery	3.1 - 3.4 mm	[56]
Fibular artery	3.08 - 3.10 mm	[56]
Arteries in the arms		
Subclavian artery	7 - 10 mm	[60]
Axillary artery	6.38 - 6.52 mm	[61]
Brachial artery	2.0 - 6.4 mm	[62]
Ulnar artery	2.358 ± 0.39 mm	[63]
Radial artery	2.329 ± 0.4 mm	[63]

2.1.2 Chronic renal failure

CRF, also known as chronic kidney failure, refers to the decrease in the function of the kidney to filter waste and fluid from the blood due to kidney damage [66, 67]. Insufficient removal of waste and fluid from the blood can cause swelling in the extremities, pulmonary edema, and hyperkalemia [2, 66]. The risk factors of CRF includes diabetes, high blood pressure, smoking, obesity, and old age [66]. There are reversible and irreversible kidney failure. In the case of reversible renal failure, the kidney function can be restored when the causes are resolved. Irreversible kidney failure, on the other hand, is as the name indicates – the damage to the kidney is too severe that the function of kidney cannot be restored. Irreversible renal failure is treated using one of three methods: kidney transplant, peritoneal dialysis, or hemodialysis [2]. Kidney transplant is a surgical process where the damaged kidney is replaced by the donated kidney [2]. While kidney transplant is the preferred treatment because of good long-term outcome, it is limited due to the availability of the donor kidneys [2, 9]. Therefore, either peritoneal dialysis or hemodialysis is performed on patients who suffer from CRF. Peritoneal dialysis is a process of performing dialysis using the lining of the patients' abdomen [68]. While the process is less invasive to people, peritoneal dialysis is not suitable for people with low

renal function, obesity, or abdominal scarring [69]. Also, peritoneal dialysis failure can occur due to technique failure [70]. Hemodialysis is a process where the waste and excess fluid is removed from the blood using a dialyzer located outside of the body [9]. For hemodialysis, a connection between the artery and vein are made for easy access to the dialyzer. The connection is surgically made by connecting the artery and vein to create arteriovenous fistula (AF) [15]. In the case where the AF cannot be made or are not usable, then vascular graft is implanted to make arteriovenous graft (AVG) [2]. Hemodialysis is performed once every 2-3 days, requiring the AF and AVG to be robust and have self-sealing properties to prevent leakage of blood [71].

2.2 Causes of blood vessel occlusion

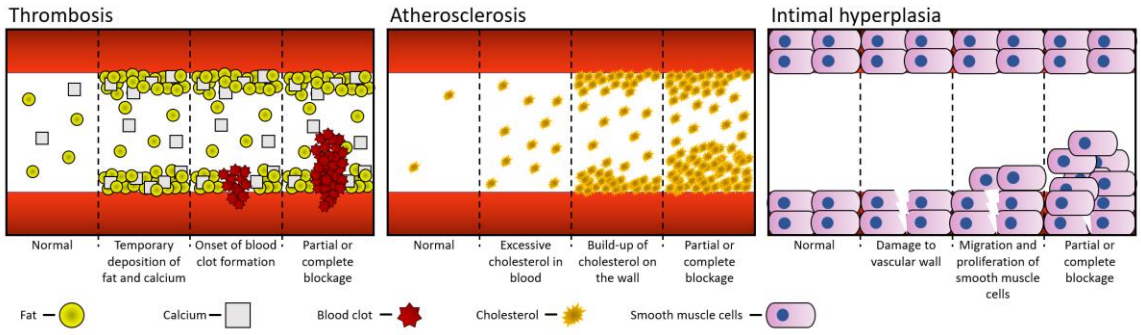

Figure 2.2. Schematic showing progression of thrombosis, atherosclerosis, and intimal hyperplasia [42, 72, 73].

The occlusion of blood vessels can occur due to thrombosis, atherosclerosis, or intimal hyperplasia (IH) [70-72]. Thrombosis is build-up of blood clots. In the case of atherosclerosis, it is caused by build-up of plaque. IH is thickening of blood vessel wall due to over proliferation and anomalous migration of vascular smooth muscle cells (VSMC). While one may trigger the onset of another, they all have distinct pathology. Summary of the progression of the three phenomena is shown in Figure 2.2.

2.2.1.1 Thrombosis

Thrombosis refers to formation of blood clots within blood vessel causing either partial or complete blockage of the artery or vein. Some of the symptoms of thrombosis can include pain, swelling, or numbness [11]. Development of thrombosis often are attributed to stiffening of the arteries [74, 75]. The stiffening can occur due to fat or calcium deposit build-up on the arterial wall [72]. Building up of the deposits further stiffens the vascular wall, encouraging thrombogenesis [76, 77].

Thrombogenesis can trigger inflammatory response near the site. The inflammatory response exacerbates thrombogenesis [72]. It can occur anywhere on the body, and can cause serious complications such as heart attack and coronary artery diseases [11]. Furthermore, the inflammatory response can also trigger onset of atherosclerosis [73].

2.2.1.2 Atherosclerosis

Similar to thrombosis, atherosclerosis initiates with deposition of particles floating in blood onto the blood vessel wall [73]. Atherosclerosis can also cause the symptoms such as pain, swelling, or numbness of the affected region. In the case of atherosclerosis, the particles that deposit onto vascular wall are cholesterol [73]. The collection of cholesterol that build-up on the vascular wall is called plaque. If plaque build-up continues, then the lumen of affected blood vessel can become either partially or completely occluded [11]. Immune responses have also been found to play a role in development and progression of atherosclerosis [73]. Similar to how thrombosis can cause atherosclerosis, inflammatory responses due to atherosclerosis can also cause thrombosis to occur [73]. The concurrent progression of thrombosis and atherosclerosis can expedite the blockage of the vascular lumen. It can occur anywhere in the body, and can also cause various cardiovascular complications.

2.2.1.3 Intimal hyperplasia

Intimal hyperplasia (IH) refers to thickening of the blood vessel wall due to anomalous migration and over-proliferation of VSMC. IH can occur when the cells composing the vessel wall gets damaged due to trauma, high shear stress, surgical injury, inflammation, etc. [15]. This type of occlusion of blood vessel occurs typically in vascular bypass, AF, and AVG [15, 78]. For the purpose of vascular graft engineering, IH is the biggest hurdle to overcome graft failures. Detailed review of IH will be addressed in the context of application of synthetic vascular graft in the later section of this chapter.

2.3 Applications of synthetic small-diameter vascular grafts

Two main applications of synthetic small diameter vascular grafts are bypass surgeries to circumvent blocked arteries and arteriovenous grafts for access for hemodialysis [79]. PAD is treated with medication and lifestyle changes initially [11, 50, 51]. However, if these measures are not sufficient and the disease progress, then bypass surgeries are needed. These surgeries are typically considered as last option since it is an invasive process. Hemodialysis is a procedure to remove waste and fluid

from the blood [9]. It is done for the patients with CRF [9]. In order to perform hemodialysis, a connection between artery and vein in the forearm is made surgically. AVG refers to the vascular grafts used to form the connection for the purpose of hemodialysis [9].

Vascular bypass surgeries involve the implantation of a vascular graft in order to circumvent blocked section of the blood vessel. Bypass surgeries are invasive, so it is used when other methods of treatment fail to prevent blood vessel occlusion, or if the blockage is significant enough to cause heart damage [55]. If bypass surgeries are considered necessary, the first choice for bypass graft are autografts. Autografts are the blood vessels of the patient harvested from another location of the body. For example, autografts that are used for coronary artery bypass are saphenous vein in the legs [80]. After autografts are harvested, they are immediately connected to create a bypass the occluded region of the blood vessel. They are least likely to be rejected by the body and have good patency [81]. However, autografts face some drawbacks such as limited availability and risks associated with additional surgeries [82]. If there are no autologous graft that can be used, then synthetic vascular grafts are used for the bypass surgery.

Similarly, autologous blood vessels are considered a good candidate to make the access for hemodialysis access. The access for hemodialysis using native artery and vein is called arteriovenous fistula (AF). For AF, native artery and vein in the arm of the patient is surgically connected [15]. The hemodialysis would be then connected to the fistula. Blood would be drawn from the remodeled superficial vein of the AF, filtered in the hemodialysis, then returned to the patient through the vein. Because connection of artery and vein is connecting two differently structured blood vessels together to expose them to abnormal blood flow for repeated access to hemodialysis, AF faces many difficulties in long-term maintenance [83]. Since AF is used as an access for hemodialysis, it is regularly punctured using needles. This repeated puncturing can damage the fistula. The damage then contributes to the failure of AF. Also, AF must mature correctly in order to be used as access for hemodialysis [84]. This maturation sometimes does not occur in some patients [84]. In the case of failed AF, AVG is used. AVG is the connection between artery and vein made using synthetic vascular graft.

2.3.1 Poly(vinyl alcohol) vascular grafts

Poly(vinyl alcohol) (PVA) hydrogel is bio-inert, have limited cytotoxicity, have low thrombogenicity, and have tunable mechanical properties [21]. It is used in many biomedical research areas due to

these beneficial properties. For example, when crosslinked using freeze-thaw cycles, PVA can have similar mechanical property as cartilage [85, 86]. Also, PVA has been used in the stem cell research. Stem cells have been shown to differentiate when cultured on a substrate with different stiffness [87]. In a study published in 2015, stiffness of PVA was varied using gradual freeze-thawing method to investigate stem cell differentiation [87]. In another study, PVA hydrogel crosslinked using trisodium trimetaphosphate (STMP) as the crosslinking agent was studied as a potential substitute of vitreous humor [88]. PVA hydrogel crosslinked with STMP has been found to be very compliant, and have been suggested as a material to make compliant vascular graft [89]. In this section, I will review usage of PVA in vascular graft engineering for the development of compliant sSDVG.

There are multiple methods of crosslinking PVA hydrogel. The two popular types are physical crosslinking method and chemical crosslinking method. The most common method of physical crosslinking of PVA uses freeze-thaw cycles to cause entanglement of the PVA molecules [90]. The relationship between the number of freeze-thaw cycles and the mechanical properties of resulting PVA hydrogel is very well characterized [90, 91]. There have been a few different chemical crosslinking methods of PVA hydrogels. PVA has been crosslinked using the glutaraldehyde, which resulted in PVA hydrogel with cytotoxicity [92]. Later, different chemical crosslinking methods of PVA were explored to result in PVA hydrogels without cytotoxicity. For example, Darabi *et al.* published a method of alkaline based crosslinking method of PVA hydrogel that is optically clear [93]. They also showed the method allowed for 3D printing of the PVA hydrogel [93]. Another group studied the crosslinking of PVA using different molecules [94]. In their study, crosslinking of PVA using citric acid, succinic acid, iron (II) sulfate heptahydrate, hydrogen peroxide, and sodium hydroxide [94]. PVA has also been crosslinked with epichlorohydrin as the crosslinker in 1992 [95]. PVA hydrogel have been crosslinked using STMP as the crosslinking agent in a basic solution [88, 96-98]. A review published in 2014 addressing crosslinking of hydrogel summarizes different crosslinking method of PVA [99].

The PVA hydrogels crosslinked using STMP is elastic, and was suggested to be a good material to make compliance vascular grafts [25, 29, 89, 96]. Recently, the detailed effects of different crosslinking parameters of PVA hydrogel crosslinked using STMP was studied in Chapter 3 [21]. This allows for the fine-tuning of the compliance and mechanical properties of PVA vascular grafts. Furthermore, some aspects of different sterilization methods on the mechanical properties have been studied [97]. Sterilization is an important and necessary step for implantation into the patients.

Therefore, understanding the effects of sterilization on the mechanical properties of the PVA grafts is important for the development of compliant PVA grafts.

One difficulty in using PVA hydrogel is that it does not allow for cellular attachment without modification. While the lack of cellular adhesion could be beneficial for other applications, it is important to allow cellular adhesion for vascular graft engineering. For sSDVG, endothelialization is key to long-term success of the graft [29, 100]. PVA has been modified using gelatin, collagen, and fucoidan to enhance cellular adhesion [28, 29, 101]. Among these, gelatin and fucoidan has been found to enhance endothelialization [28, 29]. The capacity to enhance cellular attachment is important also for using PVA hydrogel in *in vitro* experiments as well as for long-term patency of the grafts. PVA grafts are being studied in both *in vivo* and *ex vivo* animal models to test the performance of the PVA grafts. Improving the compliance and cellular interaction of PVA grafts would allow for positive results from these animal models, which is a prerequisite to proceeding to the FDA approval and clinical application.

2.4 Current state of synthetic small-diameter vascular graft engineering

Small-diameter vascular grafts, defined as vascular grafts with an inner diameter less than 6 mm, continue to show poor patency [102], most often caused by IH [46, 103]. sSDVG are small-diameter vascular grafts made using synthetic material. The lack of viable options for sSDVG impacts more than 52 million people who suffer from peripheral arterial diseases (PAD) in the United States of America (USA) alone due to maintenance of the [104, 105]. Furthermore, the lack of synthetic options for arteriovenous grafts (AVG), which are also sSDVGs, affects patients with end-stage renal disease [47].

The leading cause of poor sSDVG patency is IH. IH is the thickening of the tunica intima of blood vessel walls, which is believed to be caused by either proliferation or migration of smooth muscle cells (SMCs), that results in either partial or complete occlusion of the blood vessel [106, 107]. The factors associated with IH are mechanical or biological damage that leads to vascular endothelial injury [108-110]. Since IH development is detrimental to the patency of implanted vascular grafts, both biological and mechanical causes of IH have been studied extensively. A common treatment for vascular occlusion, for example, is angioplasty. In angioplasty, the occurrence of IH mainly derives from the destruction of the endothelium from scraping and stretching of the vessel wall, followed by the molecular and cellular reaction. Biomechanical factors, such as WS and WSS, also play a key role

in the generation of IH for particularly synthetic vascular grafts. These biomechanical factors have been shown to be affected by the compliance mismatch between the vascular grafts and the native arteries. One of the mechanical properties that is being revisited is vascular compliance. Compliance in cardiovascular engineering is defined as the inverse of stiffness – it is the circumferential elasticity of the vascular graft with application of pressure.

The theory that compliance mismatch could affect the patency of vascular grafts has been around since the 1970s [111-113]. Since then, many have tried to understand the effect of compliance mismatch using various methods—from flow analysis using simulations to in vivo graft implantation models. The significance of compliance mismatch remains controversial, as some studies found a significant drop in graft patency due to compliance mismatch [41, 113-115], while others showed that the effect was negligible [44]. This dispute could arise from comparing different types of grafts—biological vs. synthetic grafts. To avoid this potential confusion, this review will focus on the IH formation while using synthetic vascular grafts. This review aims to address the biological and mechanical factors that were found to affect IH and the significance of compliance mismatch in those mechanical factors. Lastly, this review will describe the current limitations in understanding the complete effect of compliance mismatch by assessing the methods that are used to analyse compliance mismatch.

2.4.1 Pathophysiology of intimal hyperplasia

Native blood vessel walls are made of three layers: tunica externa, tunica media, and tunica intima [116]. Tunica externa is the acellular outermost layer composed of collagenous fibers and elastic fibers, and tunica media is the thick middle layer composed of SMCs [117]. Tunica intima is the innermost layer composed of endothelial cells (EC) and connective tissues [106]. Intima is a single layer of EC, endothelium, and an endothelial-specialized basement membrane of tunica intima. It contains laminin, collagen type IV, glycosaminoglycans, and proteoglycans such as heparan sulfate [118, 119]. Adventitia is the outermost layer of the native blood vessel that consists of loosely packed fibroblasts.

The endothelium serves as a non-thrombogenic barrier between blood and tissues and participates actively in maintaining homeostasis. EC secrete various proteins and growth factors that prevents VSMC constriction and proliferation, such as nitric oxide (NO) and prostacyclin (PGI_2) [120], and synthesize heparin-like molecules that prevent platelet adherence, aggregation, and coagulation [121].

VSMCs, elastin tissue, and collagen form the medial layer of native blood vessel walls. In a normal blood vessel, VSMCs are contractile, differentiated, and quiescent. However, upon vessel injury or vascular surgical interventional process, VSMCs change phenotype to a proliferative state and eventually migrate to the intima and form IH.

Formation of IH involves all the components in the blood vessel and occurs through the following process. The initiation is due to the damage or dysfunction of EC, which exposes the underlying collagen and SMC to blood components. Immediately, platelets start to adhere, aggregate, and activate to form thrombus and are followed by leukocyte chemotaxis. The activated platelets release growth factors, such as platelet-derived growth factor (PDGF) [122-124]. In response to all the changes, SMC change phenotype from quiescent state to proliferative state, then start to proliferate and migrate from media to intima. Fibroblasts in adventitia also differentiate to myofibroblasts, proliferate, and then migrate to the lumen. Meanwhile, cells involved in the IH formation secrete and deposit extracellular matrix, further thickening the intima. Histological analysis of IH corroborates this process and shows abundant VSMCs, fibroblasts, myofibroblasts, and inflammatory cells [125-129]. Excessive damage to the adventitia can also lead to IH. During vascular surgeries, adventitia is frequently stripped by surgeons to enable a better grasp of vascular walls. However, studies have found that these injuries result in the remodeling of adventitia and increased proliferation of fibroblasts in adventitia within a few days [130, 131]. The proliferating fibroblasts would further migrate from adventitia to intima and form myofibroblasts, contributing to the formation of IH [125, 126, 132].

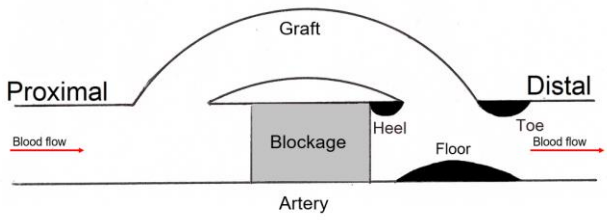

Figure 2.3. Locations of intimal hyperplasia formation in synthetic vascular grafts. IH in synthetic vascular grafts occur mainly at the floor of the native blood vessel and the toe, and heel and toe around the distal anastomoses [43].

2.4.1.1 Triggers of intimal hyperplasia in vascular grafts

The IH formation in synthetic vascular grafts show a common pattern of spatial distribution: IH develops mainly at distal anastomosis in bypass grafts [19, 133-135], and at graft-vein junctions of AVGs (Fig. 2.3) [136-138]. The IH is thought to develop around the distal anastomosis due to the fact that distal anastomosis is the region most heavily affected by combination of altered hemodynamic

and WS [133]. Surgical trauma, material bio-incompatibility, and biomechanical factors, have been found to contribute to IH formation in synthetic vascular grafts. Figure 2.4 summarizes the influence of these factors to the formation of IH [43, 73, 122-126, 130-132, 139-159]. This section will discuss material bio-compatibility and biomechanical factors and their effects on IH formation.

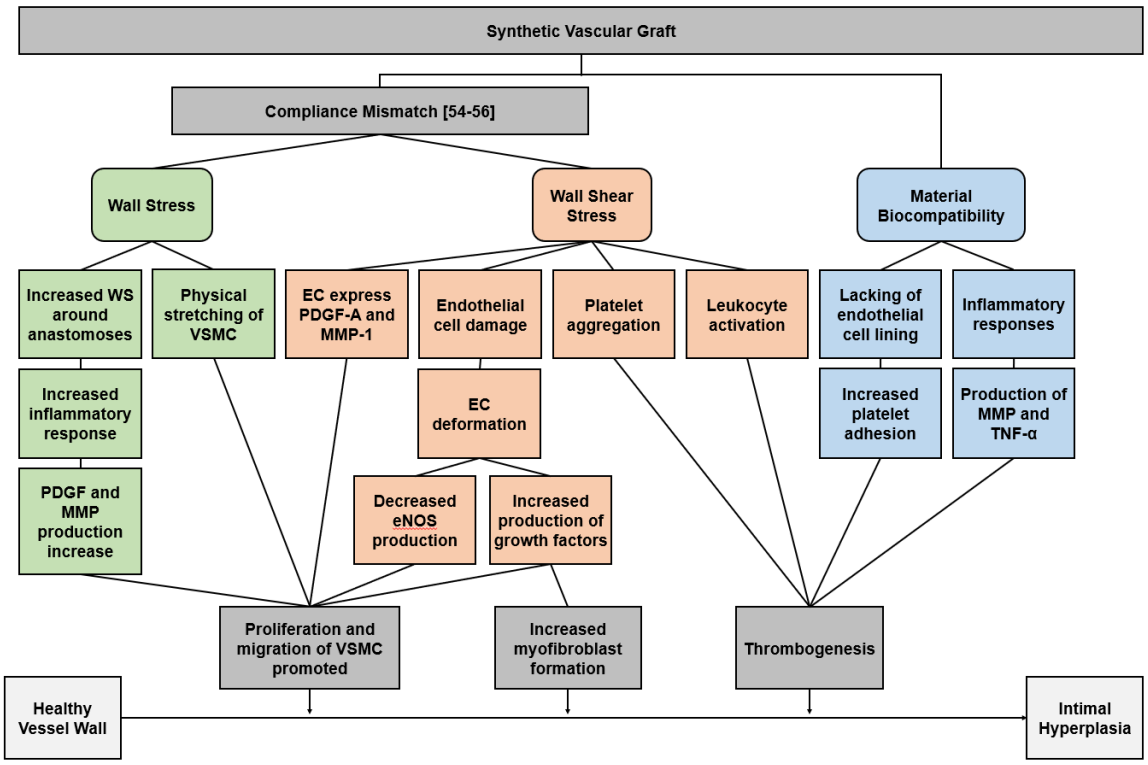

Figure 2.4. Factors that influence intimal hyperplasia formation. WS – wall stress, EC – endothelial cells, VSMC – vascular smooth muscle cells, PDGF – platelet-derived growth factors, MMP – metalloproteinase, TNF-α – tumor necrosis factor-α, and eNOS – endothelial nitric oxide synthase [43, 73, 122-126, 130-132, 139-159].

2.4.1.1.1 Material bio-incompatibility

Prosthetic, especially synthetic, vascular grafts are prone to triggering vascular inflammatory responses. Previous studies have shown an equal contribution of the inflammatory response and arterial injury to IH formation [139]. For instance, macrophages were commonly observed in expanded polytetrafluoroethylene (ePTFE) graft stenosis [140]. Furthermore, studies showed depleting macrophages could suppress IH, indicating the macrophages may regulate IH formation [141]. Meanwhile, the inflammatory response stimulates the production of matrix metalloproteinases (MMPs) by VSMCs, which facilitate the migration and proliferation of VSMCs [73, 142, 160]. T-

lymphocytes have also been observed in the intima of injured vessels. They secrete tumor necrosis factor-α (TNF-α), which has been proven to induce migration of SMCs [143]. In addition to inflammation, the lack of endothelial lining on the luminal surface of synthetic materials triggers platelet aggregation and thrombosis formation, resulting in narrowing of the lumen. Activated platelets and thrombin have also been demonstrated as mitogens of VSMCs and stimulate VSMC proliferation [144-146].

2.4.1.1.2 Biomechanical factors

The mismatch of mechanical properties between grafts and native blood vessels has been proposed to be one of the important factors leading to IH in vascular grafts. The compliant arterial wall acts as an elastic reservoir, absorbing energy during systole and releasing in diastole. Introduction of a rigid segment, such as a stiff synthetic graft, interferes with the function. Compliance mismatch between a native artery and prosthetic graft was hypothesized to affect graft performance and result in a loss of patency by Abbott *et al* [161, 162]. Later studies also confirmed the role of compliance mismatch in IH formation [45].

Accompanied with compliance mismatch, the geometric discontinuity across the anastomoses between grafts and native blood vessels causes a blood flow disturbance around the anastomoses. Due to the configuration and mechanical mismatch between native vessel and graft, there is turbulence or flow separation around the anastomosis area. The flow separation causes endothelial injury and endothelial dysfunction by inducing different flow patterns at the heel and the toe, releasing growth factors causing SMC and myofibroblast proliferation [19, 43, 147]. Also, the disturbed flow will trap platelets and cause platelets aggregation downstream, and will also promote fibrin thrombus formation [159].

WSS due to blood flow regulates the function and composition of blood vessels by affecting the phenotype and integrity of ECs [148, 149]. Under physiological WSS, the phenotype of ECs changes from random orientation to aligned with flow direction during neovascularization. With high steady laminar shear force, ECs produced more NO, lowering the proliferation of SMCs and thus inhibiting the pathways leading to IH [150]. However, with synthetic vascular grafts, ECs are exposed to abnormal shear stress and fail to express endothelial nitric oxide synthase (eNOS). Also, the distal anastomosis appears to induce a sharp shear stress change, with the directional change of shear force, which may lead to endothelial deformation [151]. Low WSS is also not good as it will cause slow

blood velocity inside the lumen and will decrease the proliferation of ECs and promote altered morphology. Monocyte adhesion was found to increase on the EC layer under low shear stress [152]. In addition to WSS, DePaola *et al*. found gradient WSS near arterial branches could induce a change of endothelium and potentially contribute to IH formation [163]. Later studies confirmed the

hypothesis that the gradient shear stress induces platelet-derived growth factor-A (PDGF-A) and monocyte attractant protein-1 expression in ECs [164], and potentially regulates the direction of SMC migration [165]. Ho *et al*. also found that immunoglobulin and proline-rich receptor-1 (IGPR-1) responded to shear stress and increased stiffness of the ECs [166]. EC stiffness contributes to the alteration in WSS and induces transdifferentiation of VSMCs, exacerbating IH [166, 167]. Meanwhile, endothelial NOTCH1 has been shown to affect cellular junctions and endothelial proliferation in response to shear stress [168].

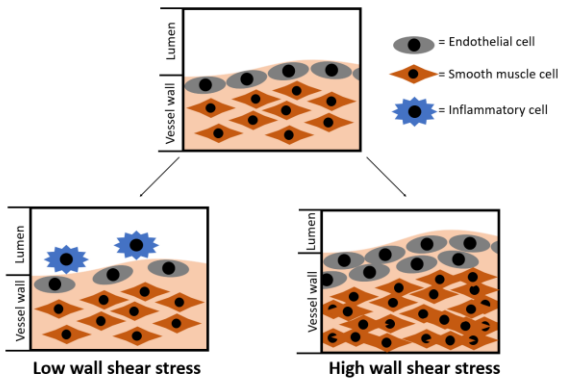

Figure 2.5. Vascular vessel wall remodelling due to alteration in wall shear stress [169, 170].

Other than in affecting ECs, the effect of WSS can be compounded with other factors that affect the blood vessel wall, such as SMCs, platelets, and leukocytes. In synthetic vascular grafts, vascular EC denudation at the anastomoses exposes underlying VSMCs to oscillatory WSS and regulates SMC proliferation, protein synthesis, and mitogenic activity [169]. Extensive studies have shown that high, yet still within physiological range, steady laminar WSS inhibited proliferation of SMCs [170-172]. However, when exposed to oscillatory shear stress, SMCs, had increased proliferation and cell survival [173]. Furthermore, low shear stress due to reduced blood flow speed traps platelets and leukocytes [153]. The attached platelets and leukocyte may become activated and trigger the formation of thrombus, further contributing to IH in a positive feedback loop (Fig. 2.5).

In addition to WSS, vascular WS (WS) also plays an important role in IH formation, mainly for vein grafts or the venous side of AVGs [174]. It has been found that compliance mismatch, and the resulting increase in WS, could also influence the formation and development of IH [43, 154, 159]. Compliance mismatch has been shown to cause increased WS around the anastomoses [154]. It was

found that high WS may serve as an initiator of the inflammatory response, such as increased PDGF and MMP expression, that is important for SMC proliferation [155, 156, 175]. Studies on PDGF responses to stress showed that upon increasing WS, PDGF secretion is promoted [176]. Also, increased suture-line stress has been found at compliance mismatch anastomoses [154]. As sutures are not elastic for the purpose of keeping the anastomoses closed, they result in contributing to the compliance mismatching at the anastomoses. The elevated suture-line stress may stretch SMCs and cause SMCs to proliferate, and contribute to IH formation [43, 158].

2.4.2 Compliance mismatch

Despite many advancements in the fields, the complete picture of the effect of compliance mismatch in IH formation still remains elusive. The difficulty in solving the question comes from the fact that IH formation in synthetic vascular grafts is due to complicated feedback loop. The difficulty is further exacerbated due to lack of consensus on a standardized measurement methods available for identifying the compliance of native blood vessels [177]. Furthermore, the difference in compliance of the vascular graft or native blood vessels are affected by the different measurement methods The lack of standardization is reflected on the equations used to calculate the compliance (Table 1). All of the equations can be applied to either *in vitro* or *in vivo* measurements. However, the sensitivity and accuracy of the measured value is dependent upon the measurement method used to make the measurements.

2.4.2.1 Measurement methods

One of the reasons why the influence of mechanical properties, specifically the compliance, is not well understood is that there is no set consensus on how to measure the compliance of native blood vessels. One of the fundamental disputes is of the parameters used to determine the compliance. Some use pulse wave velocity (PWV) by assessing fluid flow parameters along with augmented index (AIx) or resistance index [177, 178]. Others use changes in the diameter of the blood vessel or vascular grafts using echo tracking systems to determine the compliance. Lastly, an ultrasound based method called arterial stiffness evaluation for non-invasive screening (ARTSENS), developed in 2015, can be used to measure the arterial stiffness [179-181]. Different methods that can be used to measure the PWV and AIx (Table 2.2: Eq. 1–6), resistance index (RI; Table 2.2: Eq. 7), or compliance (Table 2.2: Eq. 8–15) are listed in Table 2.2. While all of the equations can be used in both *in vitro*, *ex vivo*, and *in vivo*, PWV and AIx equations are most suitable for measuring compliance *in vivo* due to accuracy.

Common measurement methods use PWV and AIx to overcome the limitations of the Doppler ultrasound—low accuracy and sensitivity [177]. In 2018, Joseph *et al*. developed magnetic plethysmography (MPG) to measure arterial compliance using PWV [182]. Another method developed in 2016 is ARTSENS® Pen. The benefit of ARTSENS® Pen is that it is an automatic and image free method of measuring arterial stiffness with good accuracy [183, 184]. This method is actively being tested for its accuracy, and recently showed repeatable and high sensitivity measurements through assessing 523 subjects in a clinical trial [185]. Radial artery tonometry is also used to measure the arterial stiffness in diabetic children using PWV and AIx [186]. AIx is a method using ascending aortic pressure waveform to measure the systemic arterial stiffness [186-188]. It is often used in conjunction with PWV as an indirect method of measuring arterial stiffness [189]. In clinical practice, AIx is used as a method to measure arterial stiffness because it is independent of geometry and is determined by age and aortic PWV [190]. The biggest benefit of AIx is the consensus in the equation used for calculation unlike others such as PWV and compliance.

The problem with these different types of devices lies with their potential for clinical applications. While many measurement options are commercially available, most clinicians still prefer to use Magnetic Resonance Imaging (MRI) or Doppler ultrasound due to ease of use for measuring arterial stiffness of the patients [177, 190-192]. Unfortunately, this yields inaccurate results depending on the resolution of the imaging instrument used, the location of the blood vessel, and size of the blood vessel [178, 193]. For example, some transcranial Doppler ultrasound cannot measure the arterial geometry, therefore requiring the flow velocity to be used for compliance measurement [193]. As means to minimize the errors due to the measurement method, RI is used to assess the vascular stiffness instead of measuring vascular compliance of the native blood vessels directly [178, 194]. Although these AIx and RI are closely associated with vascular compliance, they are not sufficient for the measurement of arterial compliance [195]. Validation of using Doppler ultrasound has also been performed by comparing with other available methods. Mechanotransduers have verified the reliability and reproducibility of Doppler ultrasound techniques [190, 196, 197]. However, these methods do not overcome the innate resolution problem Doppler ultrasound has; its accuracy and repeatability depend on the sonographer. The consensually most accurate method is using

Table 2.2. Equations used to calculate arterial stiffness.

	Equations	Unit	Ref.
1	$PWV=\frac{1}{\sqrt{\rho k}}$, $k=\frac{2\Delta D D_0+\Delta D^2}{\Delta P D_D^2}$ PWV = pulse wave velocity, ρ = blood mass density, k = distensibility, D = vessel diameter, P = pressure	$\frac{m}{s}$	[198]
2	$\text{Local PWV}=\frac{D}{\Delta t}$ PWV = pulse wave velocity, D = distance, t = time	$\frac{m}{s}$	[199]
3	$PWV=\sqrt{\frac{Eh}{2\rho R(1-v^2)}}$ PWV = pulse wave velocity = arterial stiffness, E = vessel wall Young's modulus, v = Poisson's ratio, R = lumen radius, h = wall thickness, ρ = density of the wall	$\frac{m}{s}$	[189, 200]
4	$C_i=\frac{V_i}{\rho}\frac{1}{PWV_i^2}$ C_i = volumetric compliance, V_i = volume, ρ = blood density, PWV_i = pulse wave velocity	$\frac{ml}{mmHg}$	[201]
5	$D=\frac{1+\eta}{\rho(PWV-u)^2}$, $C=VD$ D = distensibility, V = volume, u = axial flow velocity, ρ = density of incompressible fluid, PWV = pulse wave velocity, η = ratio of the wall deflection to internal wall radii, C = compliance	$\frac{mm^2}{mmHg}$	[202]
6	$AI=\frac{\Delta P}{PP}$ AI = augmentation index, ΔP = pressure difference between peak blood pressure during systolic period and break point, PP = pulse pressure difference	%	[188, 190, 203]
7	$RI=\frac{V_{max}-V_{min}}{V_{max}}*100$ RI = resistance index, V_{max} = peak systolic velocity, V_{min} = minimal diastolic velocity	%	[178]
8	$kp\frac{dP}{dt}+A_o\frac{du}{dx}=0, \frac{du}{dt}+\frac{1}{\rho}\frac{dP}{dx}+K_R u=0$ k_p = local vessel compliance, P = blood pressure, u = blood velocity, t = time, A_o = reverence vessel area, K_R = fluid resistance	$\frac{m^2}{Pa}$	[204]
9	$AC=\frac{\pi(D_s D_s-D_d D_d)}{4(P_s-P_d)}$ AC = aterial compliance, D_s = systolic diameter of the blood vessel, D_d = diastolic diameter of the blood vessel, P_s = systolic pressure, P_d = diastolic pressure	$\frac{mm^2}{kPa}$	[203]
10	$C=\frac{\text{stroke volume}}{K(P_{dist}-R_{end\ dist})}$, $K=\frac{A_s+A_d}{A_d}$ C = compliance, P_{dist} = pressure at the beginning of diastole, $P_{end\ dist}$ = pressure at the end of the diastole, A_s = systolic area, A_d = diastolic area	$\frac{ml}{mmHg}$	[205]
11	$\frac{Q}{C}=\frac{dP}{dt}+\frac{P}{RC}, Z_{in}=\frac{R}{1+jwRC}$ Q = flow, C = compliance, P = pressure, t = time, R = total resistance	$\frac{1}{Pa}$	[206, 207]
12	$C_{der}=\frac{dA}{dP}$ C_{der} = compliance, A = lumen area, P = blood pressure	$\frac{mm^2}{mmHg}$	[208]
13	$C=\left(D_s-\frac{D_d}{D_d}\right)*\frac{10^4}{P_s-P_d}$ C = diametrical compliance, D_s = systolic diameter, D_d = diastolic diameter, P_s = systolic pressure, P_d = diastolic pressure	% per $\frac{mmHg}{10^2}$	[209]
14	$C=\frac{d_{120}-d_{80}}{d_{80}}$ C = radial compliance, d_{120} = diameter of the graft at 120mmHg, d_{80} = diameter of the graft at 80mmHg	% per 40mmHg	[25]
15	$C=\frac{D_s-D_d}{(P_s-P_d)D_d}$ C = compliance, D_s = systolic arterial diameter, D_d = diastolic arterial diameter, P_s = systolic pressure, P_d = diastolic pressure	$\frac{\%\text{ radial change}}{mmHg*10^2}$	[210]

mechanotransducer [197]. This is an invasive method as a probe has to be inserted to measure the blood flow and pressure, and thus it is not used in clinical settings [196, 197]. Although many measurement methods are available, none of the currently available methods meet all of the requirements needed for accurate assessment of the mechanical properties affecting hemodynamics in both the clinics and in research.

2.4.2.2 Modelling methods

Recent advancement in computational fluid dynamics (CFD) and finite element modelling (FEM) made it possible to simulate the complex flow induced in vasculatures. CFD simulation allows researchers to model the effect of hemodynamics and the resulting WSS on the vessel walls without having to perform physical experiments. Similarly, FEM simulation allows estimation of WS applied on the vessel wall. For example, He *et al.* found that end-to-end anastomosis model showed the presence of significant disturbance in blood velocity, WSS and pressure at the compliance mismatch region [211]. Compliance mismatch can result in a change in the WSS exerted by the blood flow and, therefore, proper assessment of the flow regime gives insight to this phenomenon [211, 212]. This conclusion is consistent with the earlier findings of Steinman *et al*., who showed that the magnitude of shear stress is directly related to the pressure exerted by the flowing fluid [213]. As for WS, many tissue-engineered vascular grafts (TEVGs) use computational modelling to assess whether the TEVGs are suitable in physiological pressure [214]. However, as the models often overlook biological factors, the models are not capable of accurately predicting the generation of IH [187, 212, 215]. The computer models developed by Stewart and Lyman showed that protein transport patterns differ between compliance mismatched models and the compliance matched model, further giving weight to the importance of understanding compliance mismatch in vascular graft engineering [213, 215]. While the development of CFD allowed for a better understanding of the mechanical properties of graft effects on hemodynamics, many simplifications are still used for the CFD to sufficiently and accurately describe the development of IH. In 2018, Szafron *et al.* showed that the biological factors that were often overlooked can be incorporated into one computational modelling when assessing WS [216]. This is a great advancement for WS modelling, but it is yet to become the standard for WS computational modelling.

The improvement of computer simulations also shed light on the limitations of *in vitro* validation methods: the lack of high compliance materials and the lack of biomimetic available for *in vitro*

setups. For synthetic vascular grafts, there is a basic requirement of good mechanical integrity for safety. Dacron and ePTFE, synthetic vascular grafts that are currently available in the market, has high mechanical integrity and high safety margin. However, these grafts lack compliance. As hydrogel can often be modified to have different mechanical properties, hydrogels have been used to fabricate various sSDVGs. For example, Wise *et al*. made an elastin/polycaprolactone hybrid vascular graft that can match the compliance of the native blood vessel with the same diameter [217].

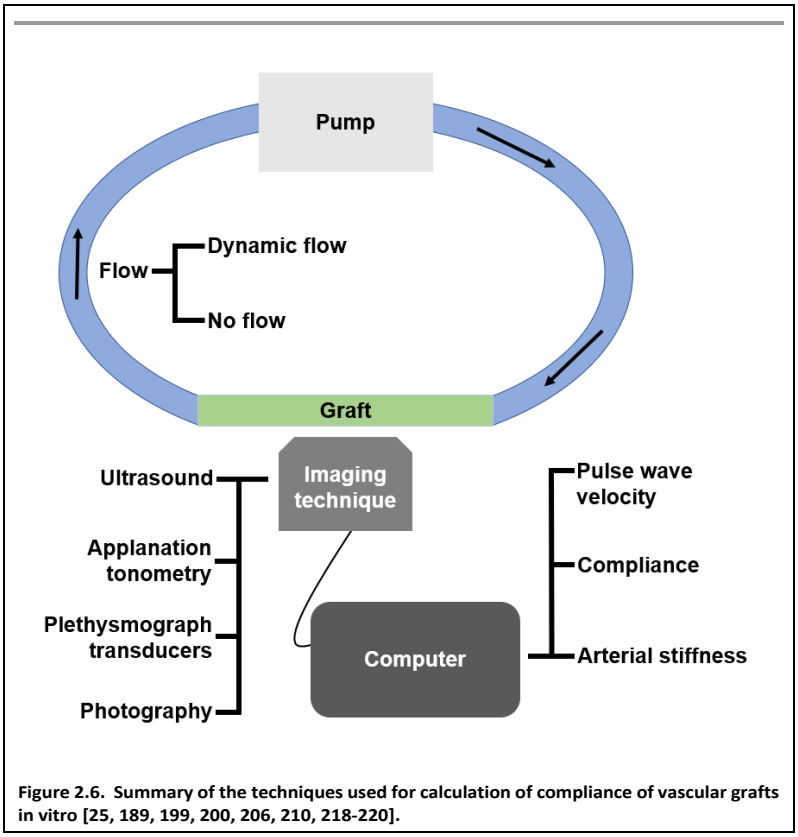

Figure 2.6. Summary of the techniques used for calculation of compliance of vascular grafts in vitro [25, 189, 199, 200, 206, 210, 218-220].

Similarly, polyvinyl alcohol grafts showed promise as a compliant synthetic vascular graft, and are being studied extensively [25, 29, 221, 222]. However, the problem with synthetic vascular grafts is that they lack the high compliance variability of native blood vessels. For example, the native artery has the compliance of 8 ± 5.9 percent per 10^{-2} mmHg, whereas poly(carbonate) urethane-based synthetic compliant vascular graft has the compliance of 8.1 ± 0.4 percent per 10^{-2} mmHg [209]. This is important as blood vessels must be able to compensate for different blood flow that naturally occurs due to physiological phenomena. Due to the fact that polyurethane vascular graft displaying compliance comparable to the native blood vessel, the grafts were studied as a potential candidate to be a sSDVG [209]. Poly(carbonate) urethane vascular grafts are being studied as a hemodialysis access in clinical trials [223, 224]. Despite the developments of new and improved biomaterials, the materials that displays the qualities required to mimic the mechanical properties of small-diameter blood vessels is yet to be found.

The other drawback of using *in vitro* model is that the experimental setup used to measure the compliance is not an accurate representation of the *in vivo* condition. As depicted in Figure 2.6, various techniques can be used for *in vitro* testing of synthetic graft compliance [25, 189, 199, 200, 206, 210, 218-220]. Due to the ease of setup, hydrostatic pressure-induced expansion has been used to measure the compliance of synthetic grafts [25]. While this model can be used to make basic compliance measurements, it is not suitable for assessing the dynamic compliance of the grafts. As blood flow within the body has been well-characterized, many *in vitro* tests and cell culture use simulated physiological pulsatile flow [161, 219, 225, 226]. For example, Gong *et al*. developed a culturing system that generated physiological pulsatile flow using a pump; they showed that dynamic culturing condition increased cellular attachment and improving compliance of the graft [219].

Even with the physiologically relevant culture conditions, it is impossible to get an accurate representation of the effect of mechanical properties on IH *in vitro*, as the biological factors involved, such as cells, platelets, and growth factors, in the formation and development of IH is either simplified or non- existent in the fluids used in *in vitro* cultures. The idea of blood-mimicking fluid (BMF) for the purpose of *in vitro* blood flow and vascular graft testing has been studied since late 1990's [227]. Despite the fact that BMFs are commercially available, these fluids mainly focus on the mimicking the biological acoustic noise for ultrasound imaging rather than the biological factors; they are mostly used for ultrasound imaging [228, 229]. As shown in Figure 2.4, the biological factors such as inflammatory responses and thrombogenesis play an important role in development of IH. Without blood factors and cellular interactions to simulate these interactions, *in vitro* tests cannot accurately represent the *in vivo* environment. Furthermore, performing *in vitro* WSS and WS experiments relating to compliance and compliance mismatch are still difficult as experimental methods are still not well established [230]. While particle tracing is the preferred method for measurement of WSS, this method is still yet to be used in conjunction with cell culture [231, 232]. Unlike, the effects of WS on cellular behaviors have been studied *in vitro* [154]. However, most of the recent publications focus on the FEM computer modelling rather than *in vitro* experiments [214, 233]. *In vitro* methods without multiple biological components cannot be useful beyond being a tool to understand only the basic interaction between one cell type and synthetic vascular grafts rather than assessing the interaction of various biological factors with different compliance.

To overcome the drawbacks of *in vitro* models, *ex vivo* models are used to perform more physiologically relevant experiments while minimize the use of animals. *Ex vivo* models are more

extensively used for biological or tissue-engineered vascular grafts as they provide a less invasive method to assess the graft's hemocompatibility than *in vivo* experiments. There are two different types of *ex vivo* models that can be used to assess the effect of compliance mismatch: the *ex vivo* shunt model and *ex vivo* organ culture. The *ex vivo* shunt is a well-established procedure to test the hemocompatibility of synthetic vascular grafts [98, 221]. *Ex vivo* shunts use externally reinforced vascular grafts surgically connected to a part of the animal. The limitation of this setup is that the shunt is supported by external structure, which masks any potential influence by the compliance. Recently, an *ex vivo* organ culture model for screening the synthetic vascular grafts have been developed [45]. This system is different from *ex vivo* shunt since it uses *ex vivo* bioreactor rather than the animal itself [234]. This system screens for the markers that are known to induce IH formation to screen for the synthetic vascular grafts their potential to form IH [45]. The strength of this model is that it allows for screening of the biological effects of vascular grafts with difference compliance. Further development of *ex vivo* models would enhance the ability to easily test synthetic vascular grafts with different compliance while having higher accuracy than *in vitro* models [234]. *Ex vivo* shunts or *ex vivo* bioreactors have the capacity to account for much higher variety of biological factors. Some have even developed *ex vivo* organ culture model for screening synthetic vascular grafts for compliance compatibility [45]. However, the techniques are still young and require further validation before application.

The best and most physiologically relevant method of studying the relationship between the biological and mechanical factors and IH is using *in vivo* model. An example of a well-established vascular graft implantation model for SDVG is end-to-end rabbit common carotid arterial implantation [235-237]. However, studies using *in vivo* model are extremely difficult due to many factors. First, non-invasive measurement methods are always preferred because of ethical concerns, easy procedures, clinical relevance, reduced trauma, and no unnecessary complications even though it is viewed as less accurate. But Doppler ultrasounds are not sensitive enough to isolate individual mechanical properties, and could not be used to accurately understand the extent to which the compliance and compliance mismatch influences IH [238]. MRI techniques can also be used to measure compliance, but this method requires expensive instrument, long imaging time, and specialized facility set up and, therefore, is oftentimes not accessible for research labs [20, 239].

Another limitation of *in vivo* models is inconsistency between protocols. When testing the biomaterials of vascular grafts *in vitro*, international standards and guideline such as International

Standard Organization (ISO) has been established to which researchers can refer [240]. However, there are still many different models to account for depending on the application, making it crucial to choose the most applicable models [236]. For example, even though the end-to-side anastomosis is more common method of implanting SDVG clinically, small animal models predominantly use end-to-end anastomosis [241]. On the other hand, end-to-side anastomosis in small animal model exists as well [222]. Surgical parameters such as anastomosis type is important as these parameters can directly impact the patency of the implanted grafts [236]. Finally, the type of animal used is very important. Different animals have different hemodynamic, different biological responses, different vascular sizes, and different compliances. All of these factors play a role in graft patency and IH formation. For example, having different diameters of vascular graft and the native blood vessel would decrease the blood flow around the anastomoses, which could cause thrombogenesis. Byrom *et al.* published a very comprehensive comparison between animal models and identified the potential animal models that are suitable for sSDVG application [236].

In vitro, *ex vivo* models, and *in vivo* models are used to understand the effects of compliance mismatch on the pathophysiology of IH. While *in vitro* models provide a convenient method to test the compliance and basic cellular interaction with the synthetic vascular grafts, there lacks a connection between the compliance mismatch and the onset of IH. *In vivo* testing models are still the best models for testing the performance of vascular grafts even with all the difficulties it entails. However, these models are particularly difficult for assessing the influence of compliance mismatch on IH as an accurate and non-invasive compliance measurement method *in vivo* does not exist. *In vivo* models must be carefully chosen to have appropriate animals, correct procedures, appropriate anastomoses, and correct diameters between vascular graft and native blood vessel.

Despite the advances in technology, understanding the complex roles of the biological and mechanical factors in vascular graft engineering are yet to be completely understood. IH is a well-observed phenomenon in medicine, and the biological mechanism of its development has been studied extensively. The field is now trying to make connections between the mechanical factors and their influence on biological responses.

The knowledge of compliance mismatch has been shown to be important in vascular engineering. Compliance mismatch between the synthetic vascular graft and the native blood vessel influences the hemodynamics. The altered hemodynamics influence WSS through irregular flow patterns. The

irregular mechanical signal then triggers irregular biological responses. These irregular biological behaviors then manifest as pathophysiological phenomena known as IH. While many strides have

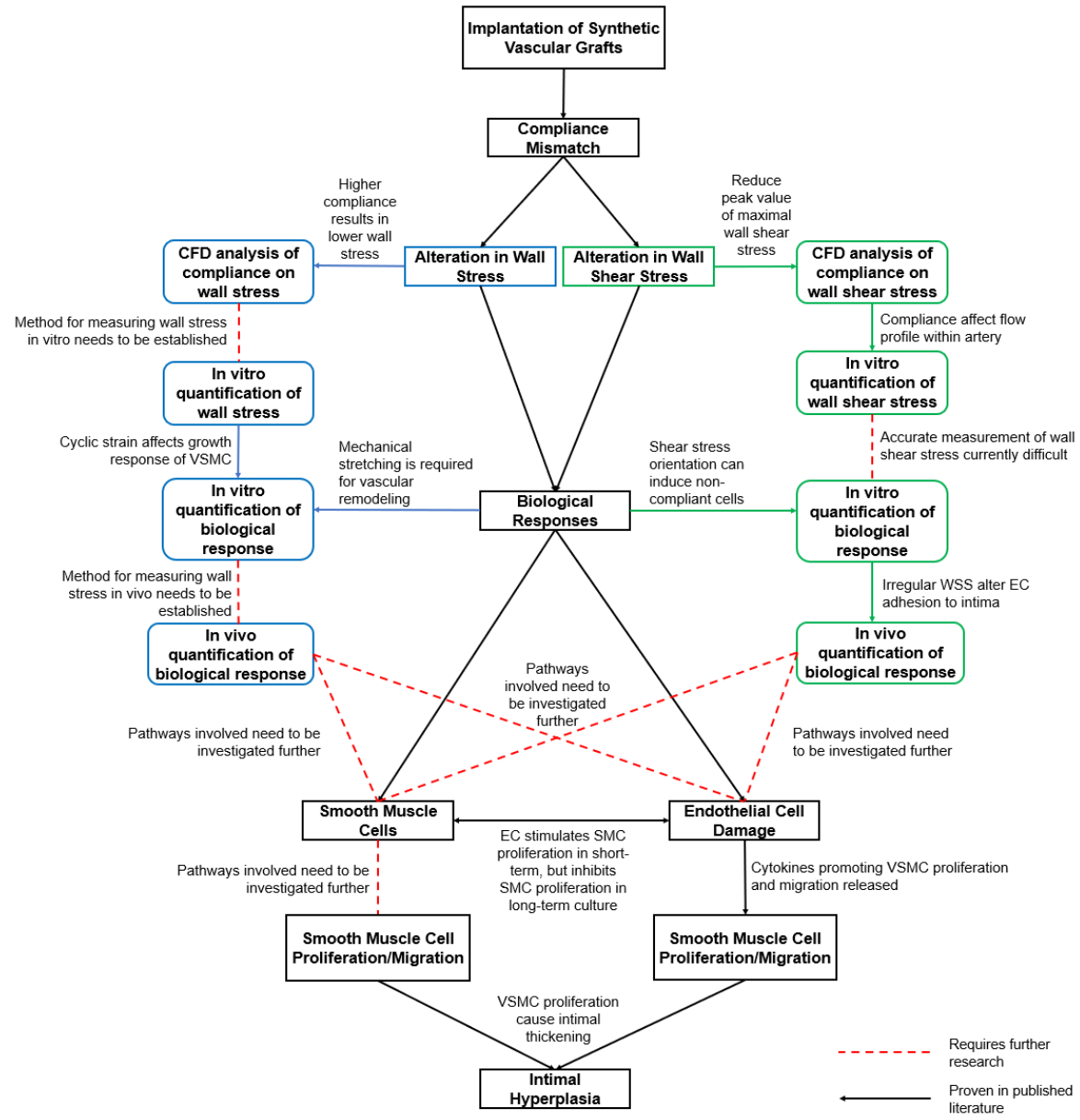

Figure 2.7. Summary of current progress in understanding intimal hyperplasia formation in synthetic vascular grafts [42, 211, 212, 231, 242-247].

been made to understand the links between compliance mismatch and IH, there is still missing information that must be identified before the links can be understood completely (Fig. 2.7 [42, 211, 212, 231, 242-247]).

With the number of cardiovascular disease incidences increasing as time passes, the need to fabricate better vascular grafts is evident—especially so for sSDVGs [248-250]. As IH is an important hurdle that must be overcome to achieve more successful AVGs and SDVGs, it is important to understand the biological factors associated with IH and the effect of mechanical properties, such as compliance mismatch, on hemodynamics that generate WSS. A platform that has the capacity to alter both the mechanical properties as well as the chemical properties is required so that the effects of the mechanical properties on the IH formation can be assessed without being influenced by the chemical and biochemical factors. Also, a way to ensure consistency in compliance measurements between *in vivo* experiments must be established so that the results from different vascular grafts can be compared to one another. This would not only enhance the reliability of the results, but also ensure the requirements of newly developed vascular grafts.

2.5 Responses of vascular smooth muscle cells to mechanical stimulation

The importance of mechanical stimulation in triggering biological functions have been studied in various cell types [32, 251]. For example, in the case of osteocytes, bones are exposed to compressive loading and torque [33]. Mechanical loading has been found to play a critical role in the shape of the lacunae formed by the osteocytes [33]. A study published in 2021 found that exposure to mechanical loading can activate the Yes-associated protein (YAP) pathway [252]. YAP is a known protein involved in extracellular and intracellular signaling pathways for regulating essential functions such as cell density, cell polarity, mechanical cues, cell proliferation, and survival [253]. Likewise, mechanical stimulation plays an important role in the function of VSMC.

Cells are exposed to mechanical stimuli *in vivo*. For example, VSMC are constantly exposed to WSS due to the blood flow and WS due to the stretching blood vessel wall [14, 243, 254]. WSS is the shear stress due to the flow of the blood. The extent of WSS experienced by the cells also vary depending on the location of the blood vessel in the body [147]. For example, the blood flow rate inside the aorta is significantly different from the shear stress within the arterioles [255] WS is the cyclic stretching the cells composing the vascular walls are exposed. Blood vessels are elastic tubes that expands to allow for the blood flow with each pulse. The repeated expansion results in exposing

the cells composing the blood vessel walls to cyclic stretching [256]. VSMCs in the body are formed, matured, exposed to, and undergo apoptosis in constant exposure to the combination of WS and WSS.

Presence of WSS is also important for understanding the behaviors of VSMC. The direction as well as the magnitude of the shear stress was found to influence the migration and orientation of VSMCs [257]. It was also suggested that shear stress can act as an inhibitor of VSMC proliferation [258]. In 2018, Sun et al. found that shear stress induced phenotypic modulation of VSMC [259]. In their study, VSMC were exposed to 15.28 dynes/cm^2 for 6, 12, and 24 hours and quantified the protein and DNA expressions. They found that the cells exposed to shear stress displayed elevated expression of phosphorylated-adenosine monophosphate-activated protein kinase (pAMPK) [259]. pAMPK is known to be involved in regulation of proliferation of mammalian cells [260]. In another study, Kim *et al.* found that the laminar shear stress suppressed the proliferation of VSMC through the AMPK pathway [34].

The application of mechanical strain in studying the behaviors of VSMC is widely accepted [261-263]. In 1998, Hu *et al.* found that exposure to strain can be used for the activation of PDGF receptor α in VSMCs [264]. The intracellular signaling pathway involving the PDGF receptor induced by the mechanical strain was suggested in 1998 as well [265]. PDGF-BB specifically have been found to be stimulated by cyclic stretching [266]. PDGF-BB is found to promote migration of VSMC even without mechanical stimulation [267]. The PDGF-BB is thought to be released by cells when exposed to cyclic strain, resulting in binding of the molecule to PDGF receptor [268]. The cyclic stretching is also found to influence the VSMC alignment. In 2002, Standley *et al.* found that nitric oxide signaling was responsible for the alignment of VSMC that are exposed to cyclic stretching [269]. In another study, cyclic stretch with 10% strain for 4 hours resulted in expression of vascular endothelial growth factor in VSMC [270]. The resulting upregulation of YAP1 has been found to inhibit apoptosis in VSMC exposed to cyclic stretching [271, 272].

2.6 Graft mechanical compliance in vascular patency

One of the hypothesized causes of the failures of sSDVG is compliance mismatch between the native blood vessels and the implanted grafts [273]. In vascular graft engineering, the volume change of the vessel due to internal pressure is defined to as compliance [274]. Compliance is affected by the stiffness of the arterial wall, with higher stiffness being associated with lower compliance [275, 276]. Currently available synthetic vascular grafts are much stiffer compared to the native blood vessel

[14]. This causes abnormal mechanical stimulation to the cells around the connection between the implanted vascular graft and the native blood vessel. The difference in compliance results in formation of abnormal WSS as well as WS around the implanted graft. Furthermore, the connection requires application of suture [277]. The gauge and type of suture technique used for suturing the vascular graft onto the blood vessel also poses additional mechanical stimulation that VSMC are not exposed to in a healthy environment.

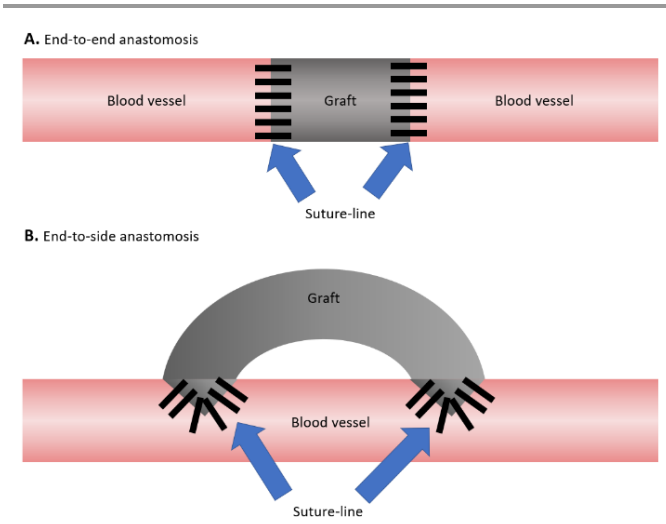

Figure 2.8. Two types of anastomoses. (A) end-to-end anastomosis, and (B) end-to-side anastomosis.

Implantation of vascular graft results in abnormal WS, WSS, as well as suture-line stress. The connection between the native blood vessel and the implanted grafts are called anastomosis. It can be made to be either end-to-end or end-to-side anastomosis (Figure 2.8) [278]. Simulation analysis of the shear stress caused by both types of anastomoses have been actively studied [213, 279-281]. The simulations tried to understand the effects of the compliance mismatch in WSS. The presence of compliance mismatch was suggested to exacerbate the disturbance by forcing the blood flow to increase through the graft, as the graft does not expand to allow for reduction of blood flow. While WSS in grafts implanted with end-to-end anastomosis is also affected by compliance mismatch [220], studies found that end-to-side anastomosis resulted in higher variable WSS [280]. The angle at which the end-to-side anastomosis are formed also played a role in formation of abnormal WSS, with the less acute change in flow path being found to cause least disturbance in WSS [282-284]. This leads to increased WSS around the distal anastomosis [285]. The increase in WSS also causes abnormally high WS around the distal anastomosis [285]. The abnormal WS causes direct effects to the cells around the anastomosis, but also affects suture-line stress. Suture-line stress is the stress around the anastomosis caused by the sutures. Computational analysis results shows that there are high concentration of stress around the sutures [23]. Others have studied the effects of suture-line stress, and reached the conclusion that compliance mismatch may affect formation of IH formation by altering the suture-line stress [23].

The isolated effect of compliance mismatch on smooth muscle cells is difficult to study. *In vitro* studies have been developed and performed to test the theoretical effects of compliance mismatch on WSS, WS, and suture-line stress studied in computational analysis. Platform to study the effects of WSS are developed by various labs and companies [219, 286, 287]. Similarly, devices to expose cells to cyclic stretching are developed to understand the effects of WS [268, 270]. The cellular behavior to suture-line stress was studied. Using gelatin modified PVA hydrogel, effects of cyclic strain on VSMC cultured on compliance mismatched PVA film were studied and is presented in this thesis. Lastly, preliminary data from simulation developed using the parameters are shown in Appendix A.

Chapter 3
Mechanical characterization of small diameter polyvinyl alcohol vascular grafts

This chapter will address the range of mechanical properties that is achievable through variation of fabrication process. This chapter will address different combinations of compliance in leu with other mechanical properties, and make conclusion on the fabrication method that results in the highest compliance while maintaining high graft integrity.

3.1 Introduction

Small diameter synthetic vascular grafts, which are grafts with diameter less than 6 mm, are not commercially available due to having low patency. The low patency has been attributed to many mechanical and biological factors [41]. Among the different factors, mechanical compliance has been shown as one of the potential parameters that can influence the performance of small diameter vascular grafts [14, 214]. Compliance is defined in vascular graft engineering as the elasticity of the conduit when exposed to internal pressure [214]. The commercially available synthetic grafts, such as expanded polytetrafluoroethylene (ePTFE) and Dacron, have significantly lower compliance than native blood vessels [209]. However, the exact role compliance plays in the failure of small diameter vascular graft still remains elusive [14]. This is partially due to the difficulty in fabricating grafts using one material with variable, controllable, and predictable compliance.

One of the materials that is being studied as a potential off-the-shelf small-diameter vascular graft is poly(vinyl alcohol) (PVA) [29, 89, 96, 288, 289]. PVA is a bioinert and low thrombogenic polymer that allows for easy chemical and topographical surface modification [29]. In addition to having beneficial biomaterial properties, PVA has tunable mechanical properties [89]. As a result, PVA is used in various applications. PVA vascular grafts are fabricated via dip-casting using cylindrical molds. PVA grafts have been shown to have dimensions and suture retention strength close to the native artery while withstanding burst pressure higher than that of the maximum systolic blood pressure [25]. Although PVA grafts have higher compliance than ePTFE grafts, PVA grafts are still not as compliant as the native blood vessels [290]. Therefore, there is a need to investigate the different fabrication conditions of PVA grafts to further increase the compliance of PVA grafts. One limiting parameter to increasing compliance is the mechanical integrity of the grafts. As the grafts

need to withstand the physiological pressure, increase in compliance cannot sacrifice the mechanical integrity of the grafts to ensure the safety of the patients. One of the parameters used to test the mechanical integrity of the vascular grafts is burst pressure. Burst pressure is the internal pressure at which the graft bursts, and is known to be closely correlated to the wall thickness of a tube [291]. The motivation of this study is to make grafts with varying compliance using PVA, and identifying the burst pressure at respective compliance.

To further identify the parameters that can contribute to the mechanical properties of the PVA grafts, the interlayer adhesion and crosslinking density were explored. Interlayer adhesion and crosslinking density have been shown to contributed to dip-casting polymer and hydrogel mechanical properties. An increase in interlayer adhesion is known to increase the mechanical integrity of hydrogels [292]. Interlayer adhesion is a critical factor since PVA grafts are fabricated through dip-casting multiple layers to reach the desired wall thickness. Additionally, the crosslinking density of the hydrogels can affect the mechanical properties of the polymer [292-294]. Increasing crosslinking density can result in stiffer hydrogels. PVA is a material with multiple mechanisms of chemical crosslinking with different chemical crosslinkers [295] and physical crosslinking with physical entanglement or via hydrogen-bonding [296, 297]. In an effort to increase compliance while maintaining high burst pressure, which will be 400mmHg, interlayer adhesion and crosslinking densities were altered by altering fabrication process. PVA grafts are fabricated using layer-by-layer additional of crosslinking solution. Therefore, interlayer adhesion, which is due to the adhesion between these layers, could alter the mechanical properties of the resulting PVA grafts. We hypothesize that the increase in interlayer adhesion will allow for higher compliance and higher burst pressure when the grafts have the same wall thickness. Also, we hypothesize that a decrease in crosslinking density will result in higher compliance and lower burst pressure when the grafts have the same wall thickness. Lastly, we hypothesize that post-fabrication processing can cause physical crosslinking, and impact the compliance and burst pressure.

3.2 Materials and methods

3.2.1 Polyvinyl alcohol vascular graft fabrication process

Standard PVA crosslinking method was used for graft fabrication as described previously [288]. Briefly, cylindrical molds are dip-cast in the crosslinking solution, then dried in controlled environment as shown in Figure 3.1A. The complete list of the parameters that were varied during the

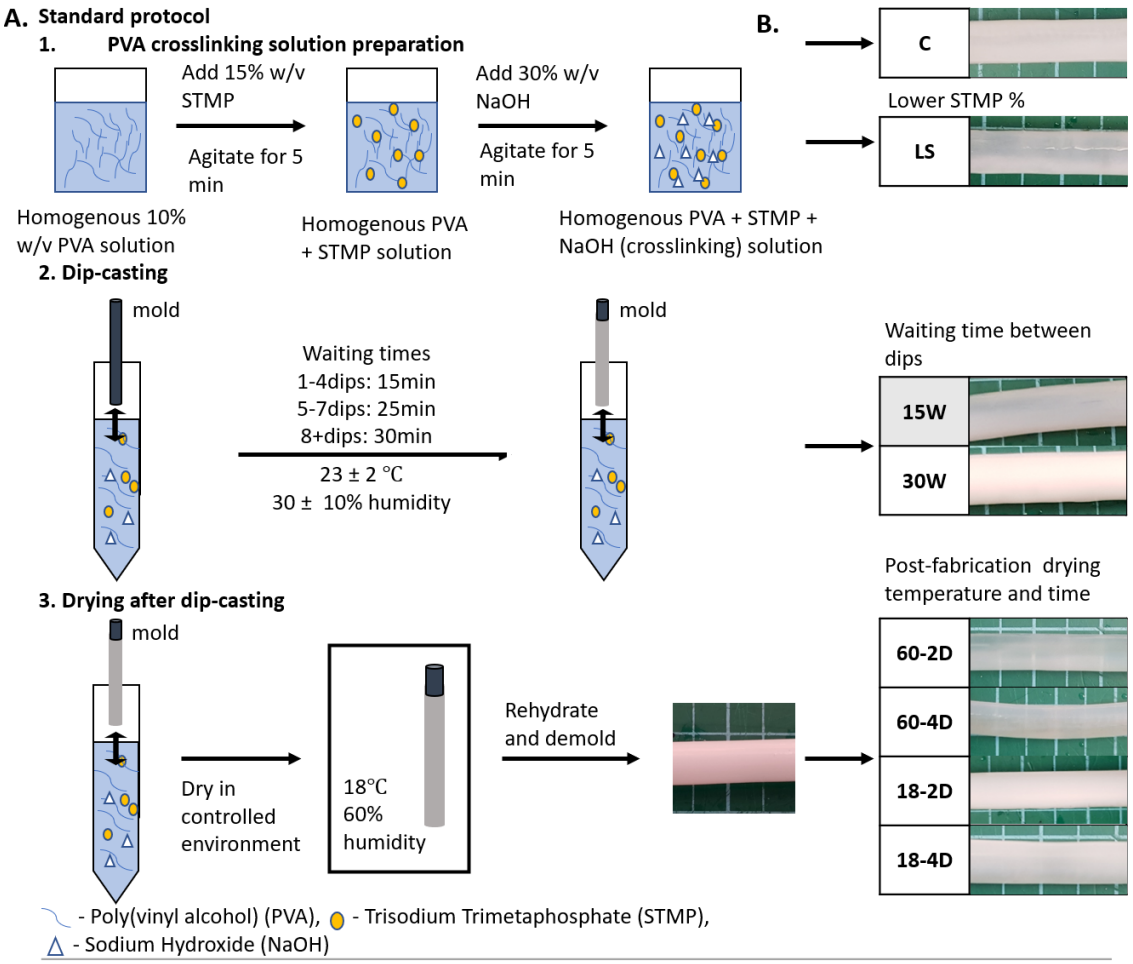

C.

Abbreviations	Description
C	Control. Made following standard protocol (shown above). Samples had 9 layers.
LS	Low STMP. Made using 7.5% STMP instead of the standard concentration. Samples had 9 layers.
15W	15-minute waiting between dips. Made using 15-minute dry times between dips instead of the standard drying times. Samples had 9 layers.
30W	30-minute waiting between dips. Made using 30-minute dry times between dips instead of the standard drying times. Samples had 9 layers.
60-2D	Dried in 60°C post fabrication for 2 weeks. Made using the standard protocol, then dried at 60°C post fabrication for 2 weeks. Samples had 9 layers.
60-4D	Dried in 60°C post fabrication for 4 weeks. Made using the standard protocol, then dried at 60°C post fabrication for 4 weeks. Samples had 9 layers.
18-2D	Dried in 18°C post fabrication for 2 weeks. Made using the standard protocol, then dried at 18°C post fabrication for 2 weeks. Samples had 9 layers.
18-4D	Dried in 18°C post fabrication for 4 weeks. Made using the standard protocol, then dried at 18°C post fabrication for 4 weeks. Samples had 9 layers.

Figure 3.1. Standard graft fabrication protocol and description of the varied parameter for each experimental group. (A) standard protocol, (B) representative images of the fabricated grafts for each experimental group, and (C) abbreviations and descriptions of the varied parameter for each experimental group. Samples for all groups were fabricated following the standard protocol except for the described parameter.

fabrication of the grafts is shown in Table 3.1. Variation in the fabrication process is highlighted in Table 3.1. All of the grafts made using different fabrication parameters had 9 layers. The images of the grafts that were successfully fabricated using different fabrication parameters are shown in Figure 3.1B. The abbreviations and the fabrication conditions that was altered from the standard fabrication conditions is explained in Figure 3.1C.

3.2.1.1 PVA crosslinking solution preparation

For standard crosslinking density grafts, a 10% aqueous solution of PVA (Sigma-Aldrich, 85-124 kDa, 87-89% hydrolyzed) was mixed with 15% w/v sodium trimetaphosphate (STMP, Sigma-Aldrich) and 30% w/v NaOH at the volumetric ratio of 12:1:0.4, respectively, to create crosslinking solution. PVA grafts were fabricated using base-catalyzed STMP crosslinking. The PVA crosslinking solution was immediately dip-cast on a cylinder mold to form tubular PVA grafts.

To fabricate PVA grafts with different crosslinking density, 10% w/v PVA solutions of different molecular weights were used. Instead of the standard molecular weight of PVA (Sigma-Aldrich, 85-124 kDa, 87-89% hydrolyzed,) low molecular weight PVA (Sigma-Aldrich, 13-23 kDa, 87-89% hydrolyzed) (LMW), or medium molecular weight PVA (Sigma-Aldrich, 31-50 kDa, 87-89% hydrolyzed) (MMW) were used while all other parameters were kept the same as the standard method. A low STMP (LS) concentration of 7.5% w/v was used to crosslink PVA with the standard PVA concentration and NaOH concentration. Lastly, low NaOH (LN) concentration of 15 %w/v was used to fabricate grafts with decreased crosslinking density.

3.2.1.2 Dip-casting PVA vascular graft

PVA vascular grafts were cast as previously described (Figure 3.1A) [96]. In short, the molds for the tubular grafts were plasma cleaned, then dipped in PVA crosslinking solution. The coated molds were dried at 20-21℃ and 30% humidity for 15 minutes, before dipping in the crosslinking solution again for the next layer. For the first four dips, the drying time between dips was 15 minutes, the drying time between dips in the fifth to seventh dip was 25 minutes, and drying time between dips for the eighth dip and higher was 30 minutes. The molds were inverted every-other dips to ensure even crosslinking throughout the mold. After the dipping completed, the PVA grafts were dried at 18℃ and 70-80% humidity for 3 days.

Upon completion of the final drying step, the PVA grafts were rehydrated in 10x phosphate buffered saline (PBS) for 2 hours, 1x phosphate buffered saline (PBS) for 2 hours, then in deionized (DI) water for 2 hours. For the samples used in phosphate quantification assay, samples were rehydrated in 9 % w/v sodium chloride (NaCl) for 2 hours, 0.9% w/v NaCl for another 2 hours, and

Table 3.1. Fabricated grafts and their fabrication conditions.

	PVA MW (kDa)	STMP (% w/v)	NaOH (% w/v)	Humidity during fabrication (%)	Dry time between dips	Post-fabrication	Graft fabrication
Control (C)	85-124	15	30	30 ± 5	1-4: 15min 5-7: 25min 8+: 30min	NA	Successful
Low MW (LMW)	13-23	15	30	30 ± 5	1-4: 15min 5-7: 25min 8+: 30min	NA	Not successful
Medium MW (MMW)	31-50	15	30	30 ± 5	1-4: 15min 5-7: 25min 8+: 30min	NA	Not successful
Low STMP (LS)	85-124	7.5	30	30 ± 5	1-4: 15min 5-7: 25min 8+: 30min	NA	Successful
Low NaOH (LN)	85-124	15	15	30 ± 5	1-4: 15min 5-7: 25min 8+: 30min	NA	Not successful
High humidity (HH)	85-124	15	30	60 ± 5	1-4: 15min 5-7: 25min 8+: 30min	NA	Not successful
15 min drying (15W)	85-124	15	30	30 ± 5	15 mins	NA	Successful
30 min drying (30W)	85-124	15	30	30 ± 5	30 mins	NA	Successful
Post-fabrication 2wk 60℃ dry (60-2D)	85-124	15	30	30 ± 5	1-4: 15min 5-7: 25min 8+: 30min	Dried in 60℃ for 2 weeks	Successful
Post-fabrication 4wk oven dry (60-4D)	85-124	15	30	30 ± 5	1-4: 15min 5-7: 25min 8+: 30min	Dried in 60℃ for 4 weeks	Successful
Post-fabrication 2wk 18℃ dry (18-2D)	85-124	15	30	30 ± 5	1-4: 15min 5-7: 25min 8+: 30min	Dried in 18℃ for 2 weeks	Successful
Post-fabrication 4wk 18℃ dry (18-4D)	85-124	15	30	30 ± 5	1-4: 15min 5-7: 25min 8+: 30min	Dried in 18℃ for 4 weeks	Successful

then in DI water for 2 more hours. The grafts were removed from the molds once they were fully rehydrated. The completed grafts were then kept in DI water until experiments. This procedure was kept the same as the standard method for the different groups unless otherwise specified. Grafts with different drying times were also fabricated as a method to test how the dry time could vary the interlayer adhesion. The drying times were either consistent 15 minutes (15W) or 30 minutes (30W) between dips for these samples. In sample group to test the role of drying rate on interlayer adhesion, PVA grafts were fabricated at higher humidity (HH) of 60±5% during fabrication.

3.2.1.3 Post-fabrication treatment of extra-dried PVA vascular grafts

After the rehydration step, some vascular grafts fabricated using the standard protocol were dried again to facilitate further crosslinking. Upon removal from the mold, the grafts were washed by submerging the grafts in DI water for 5 days. The grafts were dried again afterwards at different conditions. The post-fabrication drying conditions were: 2 weeks at 60 ℃ (60-2D), 4 weeks at 60 ℃ (60-4D), 2 weeks at 18℃ (18-2D), and 4 weeks at 18 ℃ (18-4D). Before testing, the grafts were rehydrated in DI water.

3.2.2 Storage of the fabricated grafts

The samples were kept at room temperature at all times. All samples were stored in DI water in a 50 mL conical tube upon completion of the fabrication. DI water was poured out and replenished with fresh DI water every 7 days during storage.

3.2.3 PVA film preparation

4g ± 0.2g of 10% w/v PVA solution was poured into petri dishes with diameter of 35 mm. The petri dish was covered and stored in a 18℃ chamber with a relative humidity of 70-80% for 3 days. The petri dish was then uncovered and stored at 18℃ and 70-80% humidity for another 4 days. The dried PVA film (Film) was removed from the petri dish. Films were stored in petri dish until use.

3.2.4 Inner-diameter and wall thickness

2 mm segment rings were cut from the tubular PVA grafts at the ends and at the center of the samples. Images of the 2 mm segments were taken, and the inner diameter and wall thickness of the segments were measured for each segment from the images using MatLab. For each individual

sample, the measurements of the inner diameter and the wall thickness from segments at different regions were averaged to yield the average inner diameter and the wall thickness of the sample.

3.2.5 Compliance

3 cm segments of PVA grafts were exposed to 120 mmHg and 80 mmHg of hydrostatic pressure. Images of the grafts were taken at the defined pressures. The outer diameters of the grafts were measured, then the compliances of the grafts were calculated using the following equation [25]:

$$\frac{diameter\ at\ 120m\ mHg - diameter\ at\ 80\ mmHg}{diameter\ at\ 120\ mmHg} * 100 = \%\ compliance\ per\ 40\ mmHg \quad \text{…Equation 1}$$

ePTFE vascular graft (Gore-Tex®, catalog number V04070L) with the inner diameter of 4mm was used to measure the compliance of the ePTFE graft with comparable size using the stated setup.

3.2.6 Burst pressure

Burst pressure measurement was performed following published method [97]. 4 cm segments of PVA grafts were exposed to internal pressure induced by nitrogen gas at room temperature. The pressure was increased gradually until the graft burst. The burst pressure was recorded at the pressure at which the graft burst. A normalized burst pressure was calculated as burst pressure normalized per unit thickness by dividing the burst pressure of the samples by their wall thickness.

3.2.7 Lap shear test

Lap shear test was performed following protocols described in published literature with modifications [298]. 1 cm segments were cut from tubular PVA grafts. The segments were cut open longitudinally, then they were held in a flat position and dried at 60 ℃ for 7 days. Segments prepared as such were partially rehydrated for 15 minutes and trimmed into 5 mm x 10 mm rectangular specimens. The surface of the specimens was patted dry using a paper towel. Then, the segment was glued onto two polylactic acid (PLA) holders so that the trimmed PVA segment was sandwiched between the two PLA holders. The PVA hydrogel segment was further rehydrated in DI water for 30 minutes. After rehydration, any residual water on the surface was removed. The non-overlapping parts of the holders were loaded onto a tensile testing equipment (AGSX Shimadzu, Japan), which was equipped with 1 kN load cell, and stretched at a rate of 25 mm/min until failure. Images of the samples after the test were taken using the laser confocal microscope (Olympus LEXT OLS5000-SAF, Japan) to measure

the thickness variation within the destroyed samples. The heights of the samples were measured using Olympus data analysis software.

3.2.8 Phosphate quantification assay

Phosphate quantification was performed according to the manufacturer protocol outlined in the phosphate quantification assay (Phosphate Assay Kit, Colorimetric, ab65622, Abcam). In brief, the rehydrated PVA grafts were dried at 60℃ for 7 days. The dried grafts were then degraded in 10% nitric acid, then diluted to varying concentrations. The degraded polymer solutions were added into micro-plate and allowed to react with the assay reagent. The absorbances of the solutions were then measured. Using the absorbance, the amount of phosphate in the PVA graft was calculated.

3.2.9 Fourier-transform infrared spectroscopy

Fourier-transform infrared (FTIR) spectroscopy was performed following a published protocol [290]. PVA grafts were cut to 1 cm segments, and the segments were then cut open longitudinally. The grafts were dried flat. Fourier-transform infrared (FTIR) spectroscopy was performed using Thermo Fisher Scientific FTIR (Nicolett 6700) fitted with germanium and a high sensitivity pyroelectric detector. Percent transmittance of the samples were collected between 400 and 4000 cm^{-1}. Sixty-four scans were acquired at a spectral resolution of 4 cm^{-1}. Data were normalized by modifying previously published protocol [299]. The data was normalized to the highest % transmittance and the PVA film spectrum was subtracted from the % transmittance spectra.

3.2.10 Differential scanning calorimetry

Differential scanning calorimetry (DSC; TA Instruments DSC Q2000) was performed following the published protocol [290]. In brief, the samples were dried at 60 ℃ for at least 1 week. 10g ± 0.1g of samples were measured and added into the Tzero Aluminum Hermetic pan. The heating cycle was set from 30 ℃ to 260 ℃ at the ramp rate of 10 ℃/min. Data were analyzed using the TA Universal Analysis software. Fractional crystallinity was calculated using heat of melting of 100% crystalline PVA of 138.60 J/g [300].

3.3 Swelling ratio

PVA grafts were submerged in DI water for at least a week to ensure thorough removal of charged ions from the grafts. Small sections of the tubular grafts were cut from the PVA grafts. Any residual

DI water lingering on the PVA sections were removed prior to measuring the weights of the sections. The sections were then dried at 60℃ for 5 days. The weights of the sections were measured every day for the subsequent days until the weight of the sections did not change further. Swelling ratio was calculated using the following equation [301]:

$$Swelling\ ratio = \frac{weight\ of\ hydrated\ polymer\ sample}{weight\ of\ dried\ polymer\ sample} \quad \text{…Equation 2}$$

3.3.1 Elastic modulus

For longitudinal elastic modulus and ultimate strength measurement, the grafts were cut into 8cm segments. The prepared samples were loaded onto the tensile machine (AGSX Shimadzu, Japan) with the gauge lengths of 2cm. The samples were then stretched at a rate of 25mm/min until the tensile failure of the sample. For circumferential elastic modulus and ultimate strength measurement, the grafts were cut into 2mm width rings. Curved holders were loaded onto the tensile testing machine grips. The PVA rings were loaded onto the holders so that the rings were held by the holders. The holders were then separated to achieve a gauge length of 5mm. The samples were then stretched at a rate of 10mm/min until the sample failed.

3.3.2 Suture retention strength

Suture retention strength of the PVA grafts were measured using published protocol with modifications [25, 290]. PVA grafts were cut into 4 cm segments. Using 7-0 suture, a single suture was made 5mm from the edge of the segment for each sample. The remaining suture end was taped securely onto an immovable surface so that the sample was hanging by the suture. Load was applied at 10 g/min onto the sample until the sample broke. The weight at which the sample broke was measured.

3.4 Statistical analysis

Statistical significance was determined using a two-way ANOVA followed by Tukey's multiple comparison analysis with 95% confidence interval using MatLab. The data are presented as mean ± standard deviation. For all the presented data, $p<0.05$ is denoted by * unless otherwise specified in the figure caption. The correlations between components were compared using principal component analysis (PCA). PCA plots were generated using JMP statistical software.

3.5 Results

3.5.1 Compliance and burst pressure of the grafts with varying wall thickness

The relationships between the burst pressure vs wall thickness and compliance vs wall thickness are shown in Figure 3.2. The cross-sectional images of the PVA grafts with different layers are shown in Figure 3.2A. The red arrow highlights the region in the graft that has different transparency. The wall thickness of the grafts increased linearly with the increased number of layers (Figure 3.2B). As shown in Figure 3.2C, a linear increase in burst pressure with increasing wall thickness was also observed. The compliance of the grafts displayed an inverse relationship with the wall thickness (Figure 3.2D).

3.5.2 Properties of the grafts fabricated using different fabrication conditions

All of the grafts that were made using different fabrication parameters had 9 layers. The complete list of conditions used for fabrications and their fabrication outcomes are shown in Table S1. The images of the grafts that fabricated successfully are shown in Figure 3.1B. The cross-sectional images of the successfully fabricated grafts are shown in Figure 3.3A. The wall thickness of the grafts was quantified (Figure 3.3B). LS, 15W, 60-2D, and 60-4D had significantly thinner walls than the control group, while 30W, 18-2D, and 18-4D showed no statistical difference from the control group. The wall thickness of 15W was significantly thinner than 30W. 60-2D and 60-4D did not show any statistical difference in wall thickness. Also, 18-2D and 18-4D did not show any statistical difference in wall thickness.

Despite having thinner walls than the control, grafts from LS, 60-2D, and 60-4D conditions had significantly lower compliance than the control group ($p<0.05$, Figure 3.4A). Regardless of the post-fabrication drying temperature, the samples that were subjected to extra dehydration process post-fabrication had significantly lower compliance than the control group (Figure 3.4A). 30W had lower compliance than the control group as well, despite having comparable wall thickness. Lastly, 15W did not have statistically significant differences in compliance compared to the control group despite having thinner wall thickness. Swelling ratio was used to estimate the crosslinking density. LS, 60-2D, and 60-4D had less swelling than the control group (Figure 3.4B). 15W had higher swelling ratio than the control group. No correlation between the swelling ratio and the wall thickness was observed

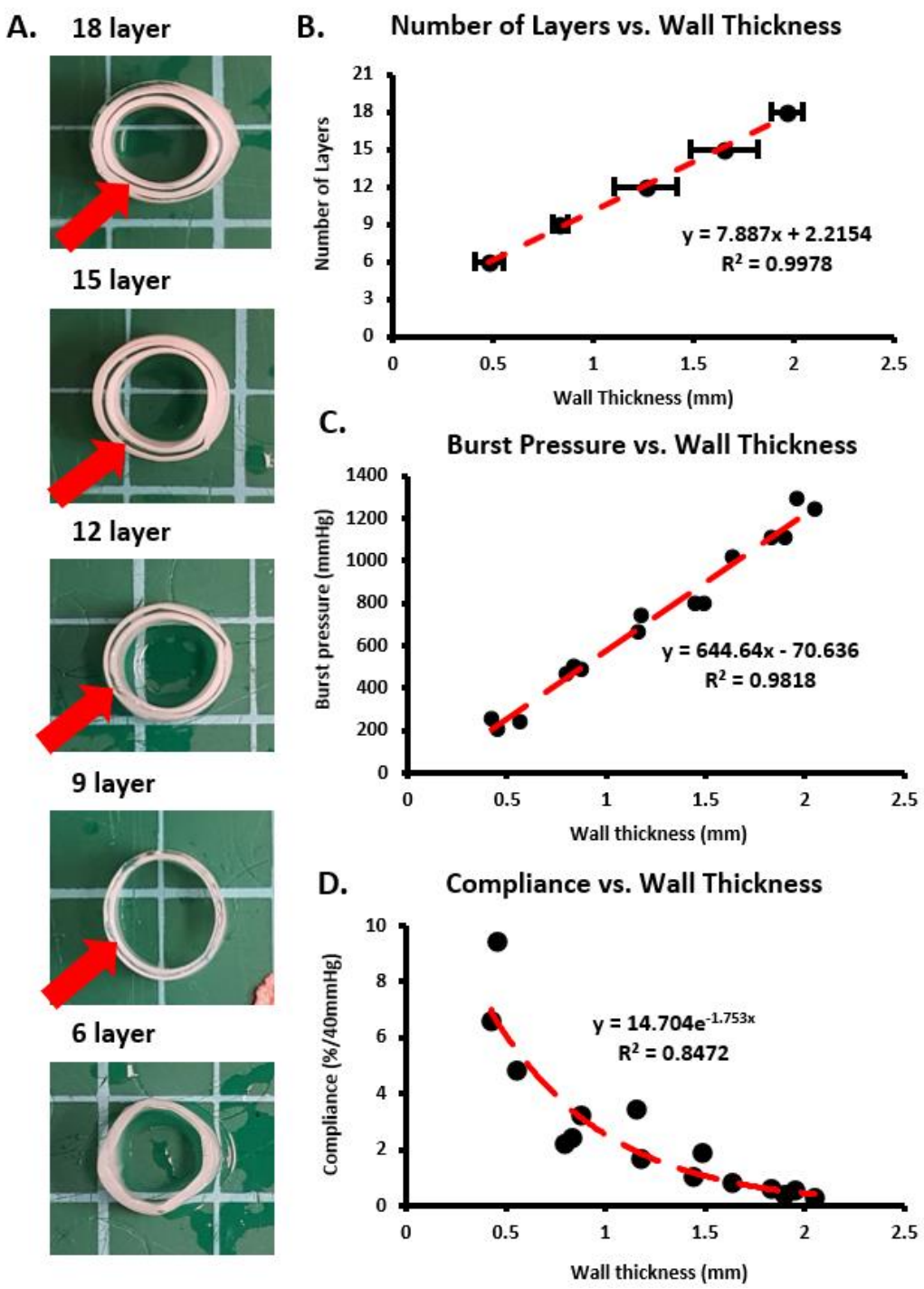

Figure 3.2 Physical and mechanical characterization of grafts with different number of layers. (A) cross-sectional images. Red arrows used to identify difference level of transparency between layers within a sample. (B) Wall thickness of the samples for different number of layers. (C) Burst pressure plotted against the wall thickness. (D) Compliance plotted against the wall thickness. * = $p < 0.05$ between indicated groups. n = 9 for all groups. Error bar represents standard deviation.

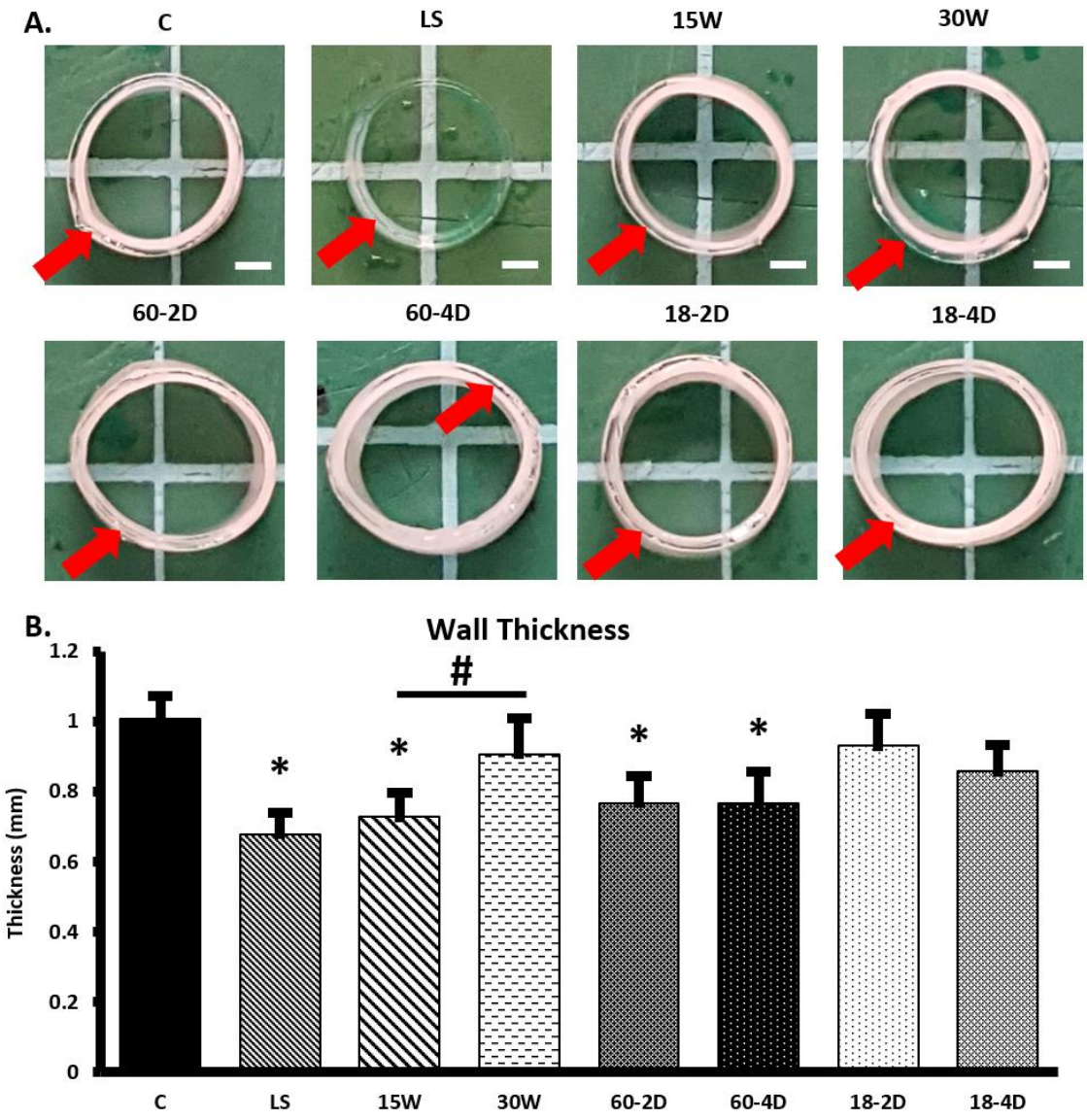

Figure 3.3. Ph**ysical characterization of the experimental groups.** (A) Cross-sectional images. Red arrows are used to identify difference level of transparency between layers within a sample. (B) Wall thickness of the samples for different number of layers. (B) wall thickness of the samples. * indicates p< 0.05 with respect to control group. # indicates p<0.05 between the groups being compared. n = 9 for all groups.

(Figure 3.4B). Burst pressure of 15W was significantly lower than control, which was as expected due to the lower wall thickness of the group (Figure 3.4C). However, 60-2D and 60-4D had higher burst pressure than the controls despite having thinner walls. LS, 30W, 18-2D, and 18-4D did not have significantly different burst pressure with respect to the control group. Further assessment of the

burst pressure was performed by normalizing the burst pressure per unit thickness (Figure 3.4D). When the data was normalized to wall thickness, LS, 60-2D, and 60-4D had significantly higher normalized burst pressure than the control group. Additionally, 60-2D and 60-4D had higher normalized burst pressure than 18-2D and 18-4D. Within each group with the same fabrication or post-fabrication variations, all of the groups showed positive linear relationship between the wall thickness and the burst pressure (Figure 3.4D).

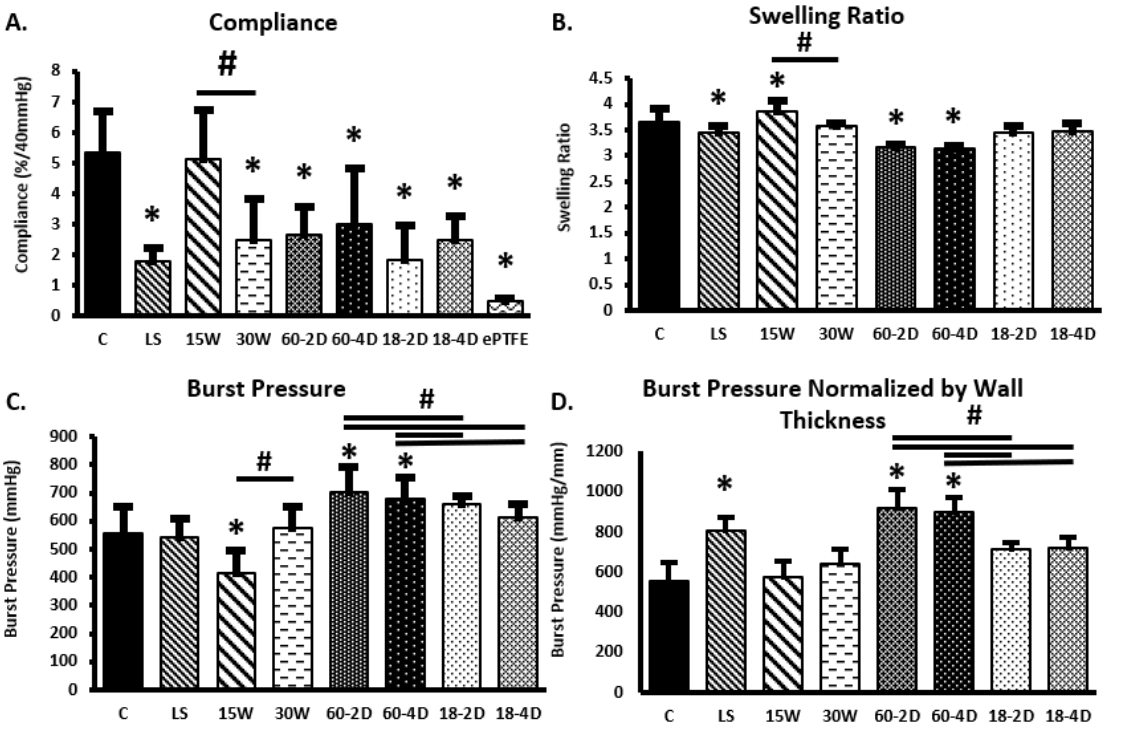

Figure 3.4. Bulk properties of the samples. (A) Compliance of each group. (B) Swelling ratio of each group. (C) Burst pressure of each group. (D) Burst pressure of each group normalized to their respective wall thickness. Average values of burst pressure and wall thickness of the internal replicates used to plot the graph. * indicates $p < 0.05$ with respect to control group. # indicates $p < 0.05$ between the groups being compared. n = 9 for all groups.

Figure 3.5 shows graphs of the different properties measured plotted against either the wall thickness (Figure 3.5A-3.5D) or compliance (Figure 3.5E-3.5H). Within each group with the same fabrication or post-fabrication variations, all groups displayed an inverse relationship between wall thickness and compliance (Figure 3.5A).

Phosphate content was quantified for the samples to verify the crosslinking density of the covalent crosslinking with STMP (Fig 3.6A). There was no significant difference in phosphate content among the control, LS, 15W, 30W, 60-2D, and 18-2D (Figure 3.6A). On the other hand, both LS and 15W

had significantly higher phosphate content than the 18-2D and Film. FTIR was performed to identify if there were any changes in crosslinking between the groups or if there were any changes in functional groups introduced due to change in the fabrication process. Figure 3.6B shows FTIR data using normalized percent transmittance of the control group (C), LS, 60-2D, and 18-2D rehydrated in NaCl. All of the groups displayed peaks at similar wavenumbers, indicating there were no noticeable differences between samples in terms of functional groups.

DSC was performed to further assess the degree of crosslinking. DSC is a reliable method [302]. After consulting the technician at the Analytical Facility in Chemical Engineering Department at University of Waterloo, the measurement was made using n=1 with repeated heating and cooling cycles. Figure 3.7A through Figure 3.7F shows the DSC plots of each of the group. The resulting values car compiled in Figure 3.7G. The DSC thermogram for control, LS, 15W, 30W, 18-2D, and 60-2D. LS, 15W, and 30W had higher heat of fusion than the control group (Fig. 3.7G). All of the experimental groups had higher fractional crystallinity compared to the control group.

The interlayer adhesion was assessed in Figure 3.8. The shear strength of all of the groups were not significantly different from the control group. However, 15W had the average shear strength of 3.75 MPa, which was more than twice higher than that of the control group (1.69 MPa). Statistical analysis between 15W and control revealed $p=0.057$. The interlayer adhesion of 15W was also significantly higher than 30W ($p<0.05$). The 3D images of the polymers after the adhesive shear tests are shown in Figure 3.8B, then were used to acquire the height profile used to plot graphs in Figure 3.8C-J. These height profiles were then used to identify whether the polymers had high interlayer adhesion. 15W had the highest slope, and therefore high interlayer adhesion, while other groups showed flat lines.

PCA analysis showed that the wall thickness and compliance showed a high positive correlation (Figure 3.9A). Also, it showed that the compliance and burst pressure showed a high negative correlation (Figure 3.9B). All other components did not display significant correlation (Figure 3.9C-3.9E). The component contribution plot is shown in Figure 3.9F. Lastly, correlations between components are shown in Figure 3.9G.

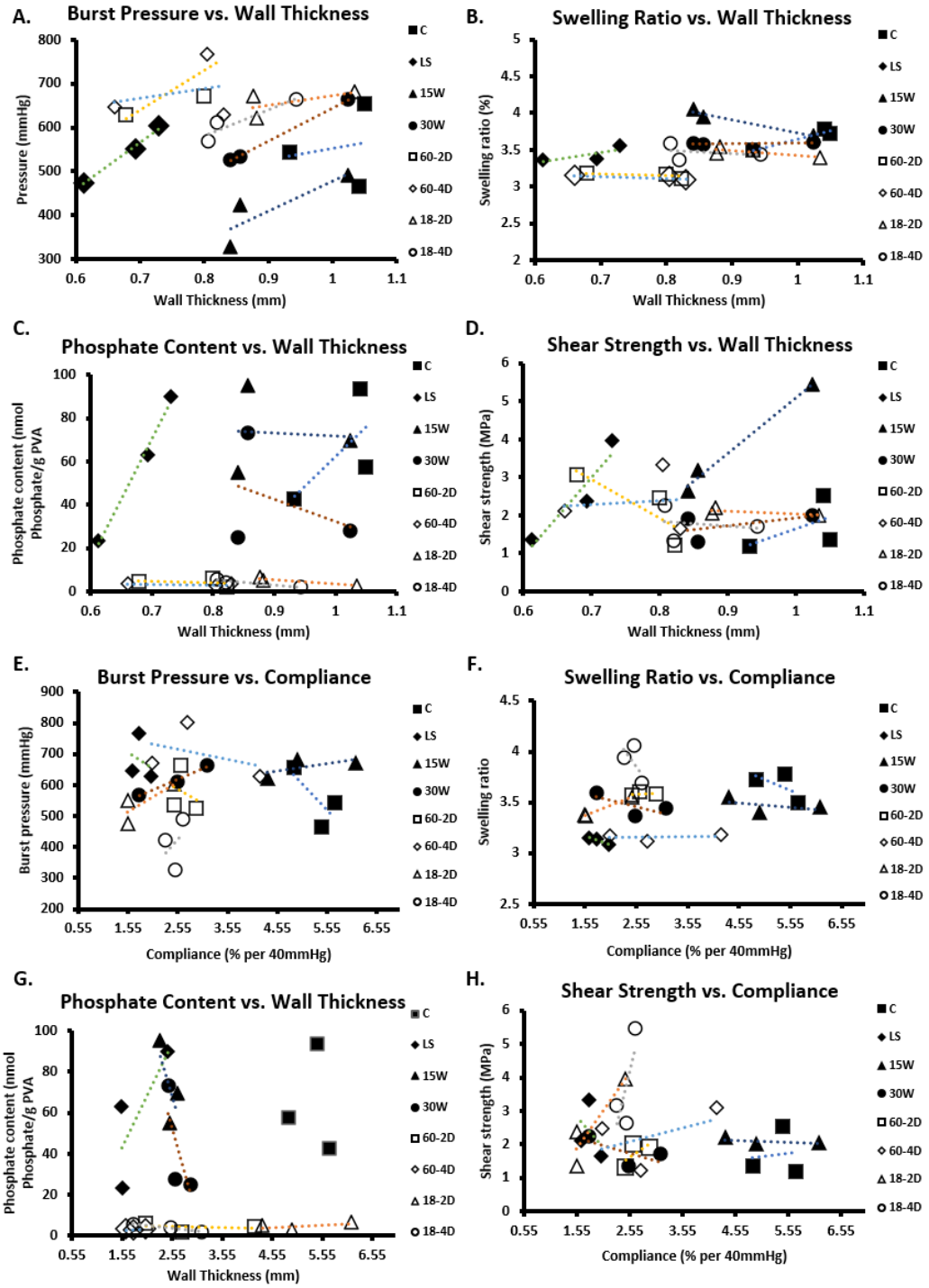

Figure 3.5. Plots of different properties plotted against wall thickness or compliance. (A) Burst pressure, (B) Swelling ratio, (C) Phosphate content, and (D) Shear strength plotted with respect to wall thickness. (E) Burst pressure, (F) Swelling ratio, (G) Phosphate content, and (H) Shear strength plotted with respect to compliance. No correlation was observed.

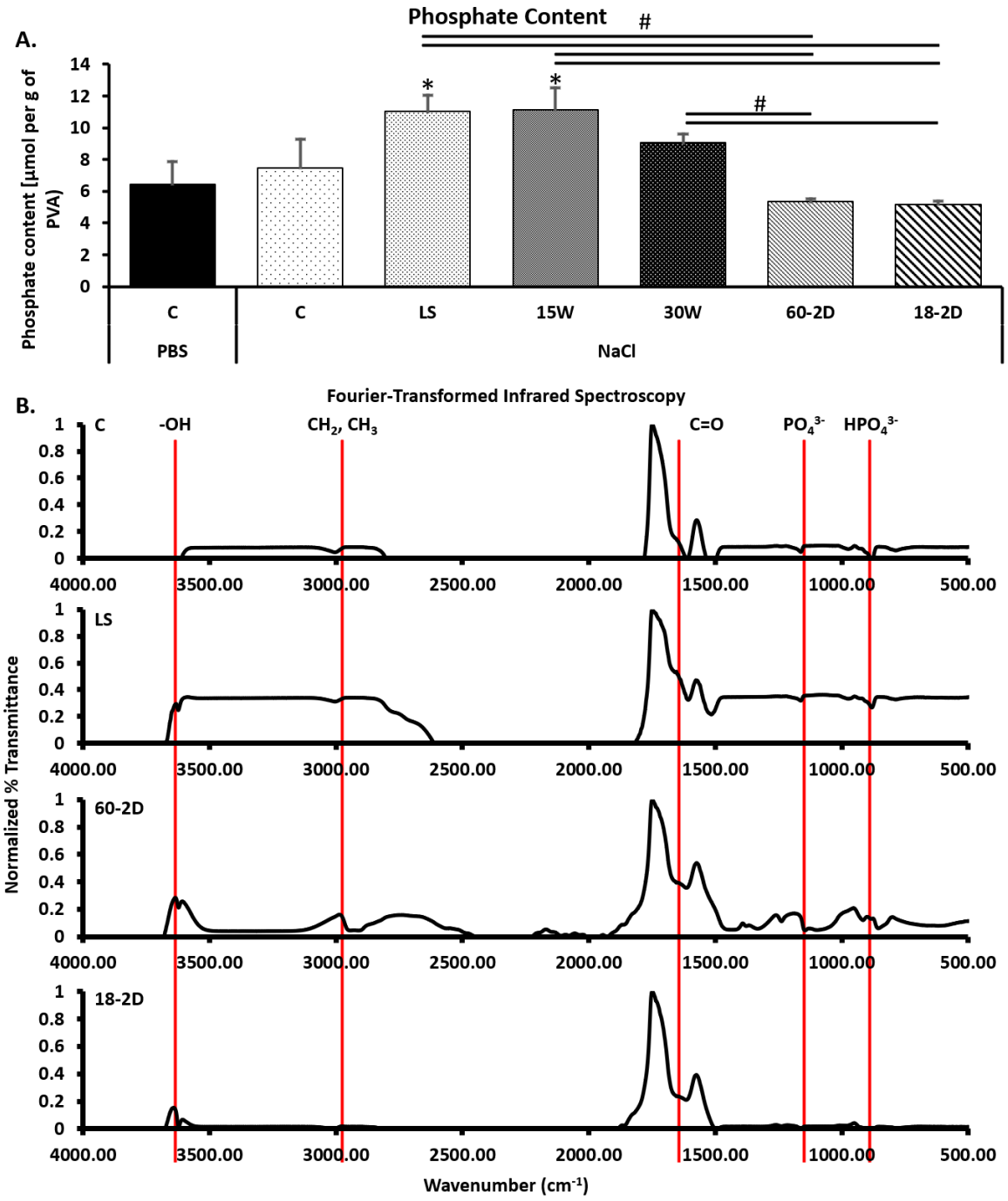

Figure 3.6. Functional groups and STMP crosslinking density in PVA films. (A) Quantification of phosphate content for the samples to characterize covalent crosslinking by STMP. * indicates p< 0.05 between the indicated groups. n = 6 for all groups. C PBS was control sample rehydrated in PBS. C, LS, 15W, 30W, 60-2D, and 18-2D were rehydrated in NaCl solution. * indicates p < 0.05 with respect to the control groups. # indicates p < 0.05 between the groups being compared. (B) Fourier-transform infrared spectroscopy data. Data was normalized to PVA films. n=3 for all samples.

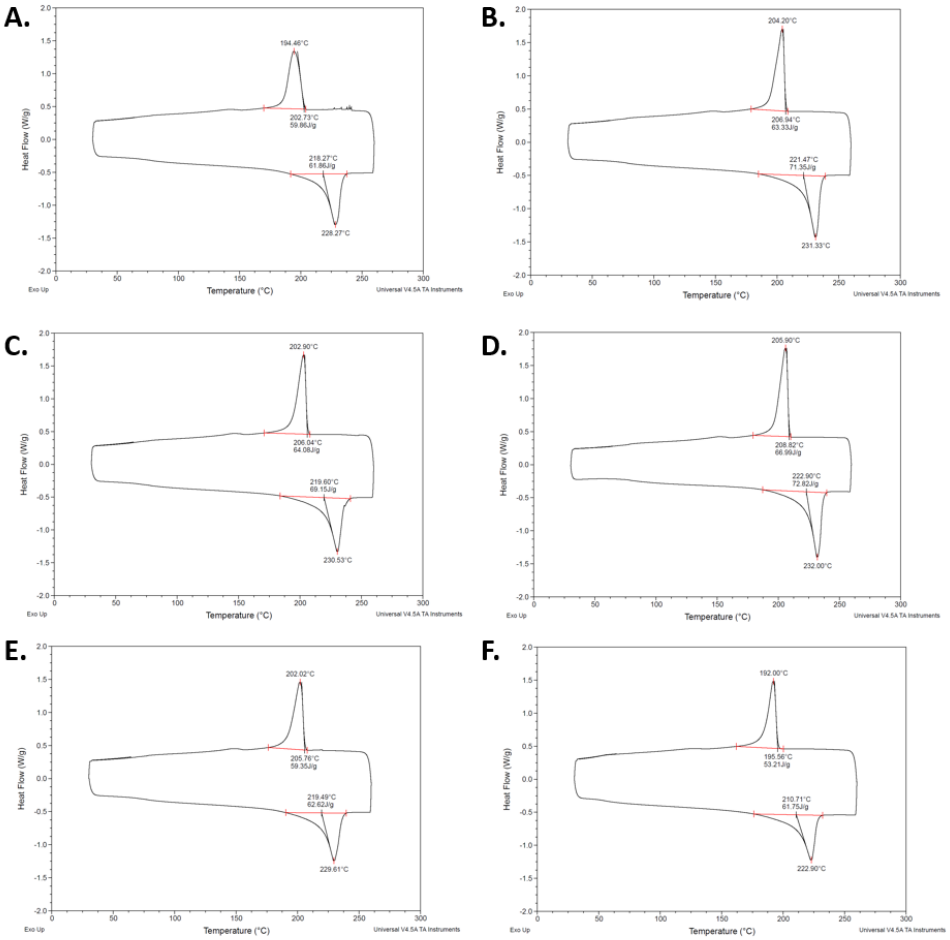

G.	Melting Temperature (℃)	Heat of Fusion (J/g)	Fractional Crystallinity (%)
Control	194.45	61.86	50.8
LS	204.20	71.35	52.8
15W	202.90	69.15	51.9
30W	205.90	72.82	52.1
18-2D	202.02	62.62	51.3
60-2D	192.00	61.75	53.7

Figure 3.7. Differential scanning calorimetry (DSC) used to measure crystallization and melting temperature. (A)-(F) DSC plot of (A) control, (B) LS, (C) 15W, (D) 30W, (E) 18-2D, and (F) 60-2D. Data is shown for the second heating and cooling cycle. (G) Heat of fusion and fractional crystallinity of the samples.

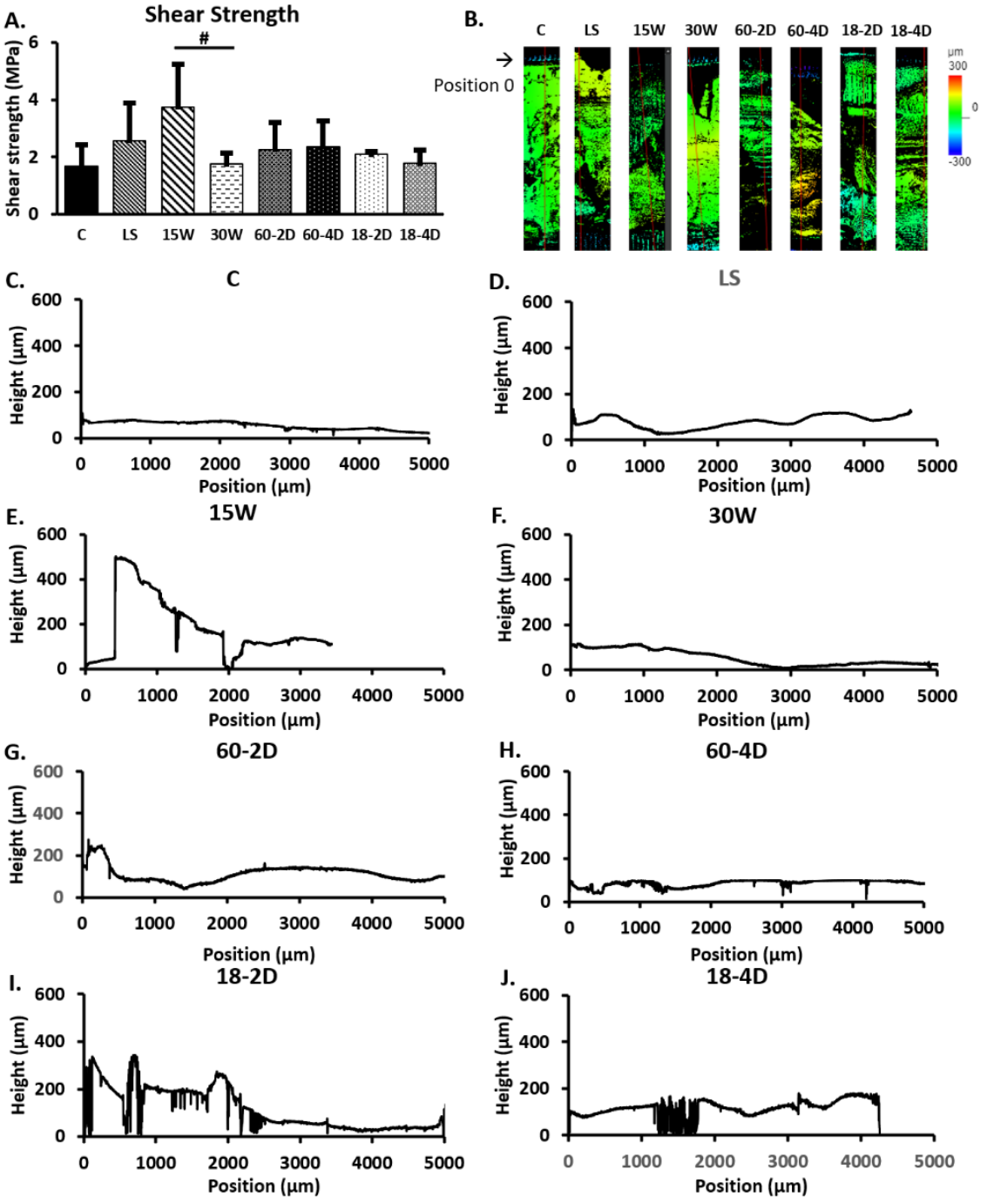

Figure 3.8. Interlayer adhesion analysis using lap shear test. (A) the adhesive strength of groups. 15W had p=0.0571 with respect to the control group, and p=0.0495 with respect to the 30W. (B) height map of the samples after adhesive shear test. (C)-(J) height profile of the samples. * indicates p< 0.05 with respect to control group. # indicates p<0.05 between the groups being compared. n=3 for all groups.

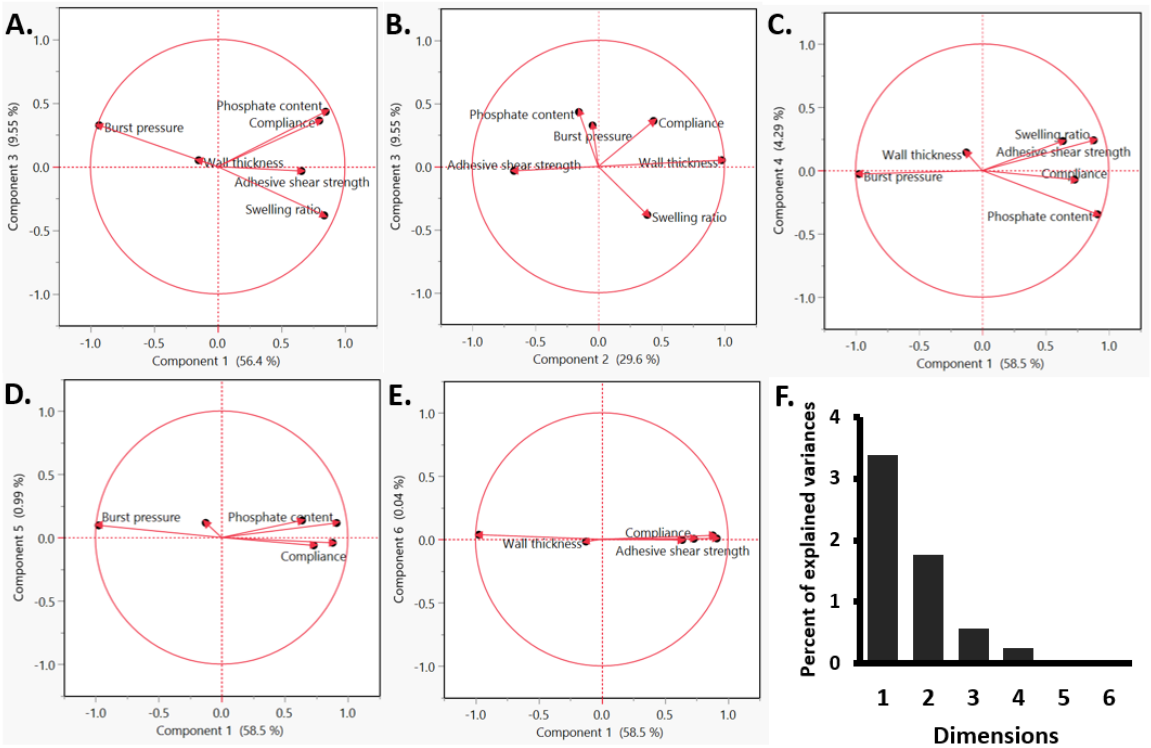

G.	Wall thickness	Compliance	Burst pressure	Adhesive shear strength	Swelling ratio	Phosphate content
Wall thickness	1.0000					
Compliance	0.3471	1.0000				
Burst pressure	0.1260	-0.6165	1.0000			
Adhesive shear strength	-0.7147	0.2859	-0.5454	1.0000		
Swelling ratio	0.2334	0.7009	-0.9220	0.3020	1.0000	
Phosphate content	-0.2849	0.7125	-0.6835	0.5567	0.4849	1.0000

Figure 3.9. Principle component analysis of each component with respect to component 1. (A) PCA plot of component 1 vs. component 3. (B) PCA plot of component 2 vs. component 3. (C) Component 1 vs. Component 4. (D) Component 1 vs. Component 5. (E) Component 1 vs. Component 6. (F) component contribution plot describing the contribution of each of the principal components. (G) shows the correlations between variables. Red = negative correlation, green = positive correlation.

3.5.3 Additional analysis on selected groups

Figure 3.10 shows the additional mechanical properties of selected groups. The groups with the highest and lowest compliance were chosen for the additional analysis. There was no statistical difference between all of the groups for all conditions except for the LS for circumferential elastic modulus (Figure 3.10A-D). The suture retention strength of the groups also did not show any statistical difference (Figure 3.10E).

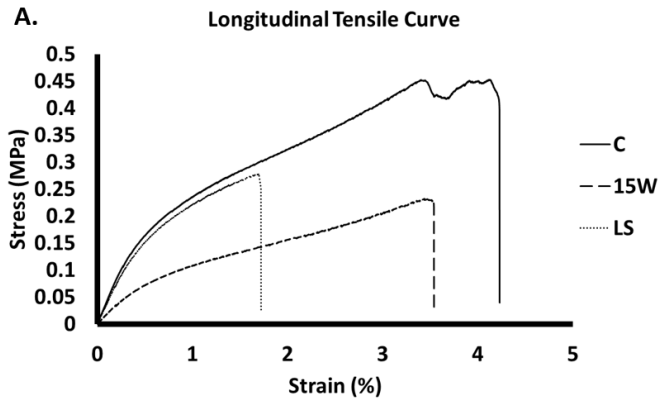

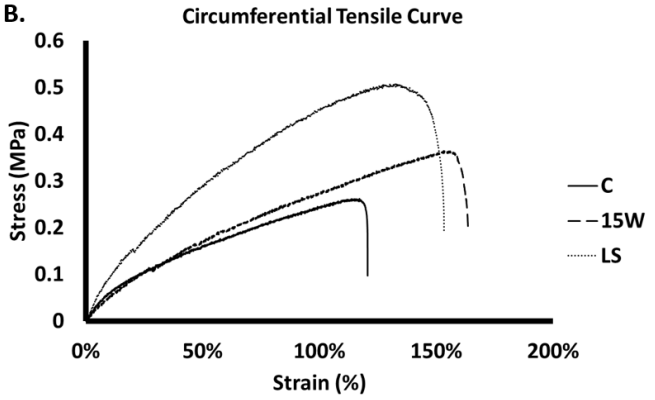

C. Longitudinal Tensile Data

	Ultimate Tensile Stress (MPa)	Elastic Modulus (MPa)
C	0.494 ± 0.132	0.571 ± 0.100
15W	0.511 ± 0.051	0.584 ± 0.119
LS	0.584 ± 0.086	0.802 ± 0.456

D. Circumferential Tensile Data

	Ultimate Tensile Stress (MPa)	Elastic Modulus (MPa)
C	0.306 ± 0.124	0.690 ± 0.136
15W	0.313 ± 0.067	0.674 ± 0.098
LS	0.326 ± 0.105	1.048 ± 0.126*

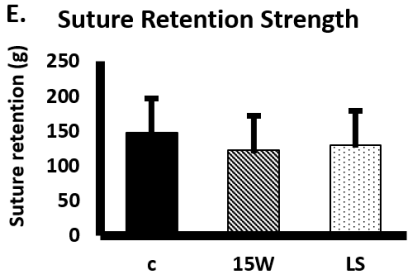

Figure 3.10. Additional bulk mechanical properties of the selected groups. (A) Longitudinal tensile curve. (B) Circumferential tensile curve. (C) Longitudinal ultimate tensile strength and elastic modulus for each groups. (D) Circumferential ultimate tensile stress and elastic modulus. (E) Suture retention strength. n=6 for tensile test results, and n=9 for suture retention strength for all groups. * indicates $p<0.05$ with respect to the control group.

3.6 Discussion

Mechanical failure of vascular grafts can result in clinical catastrophe. To ensure the safety of the patients, vascular grafts were traditionally developed to have high mechanical properties matching the native blood vessel properties [209, 303-311]. Compliance, the elasticity of the blood vessel when

exposed to internal pressure, is one of the important parameters that is being studied in vascular graft engineering to understand the current limitations of small diameter vascular grafts [14, 214]. There are methods to increase the compliance of a material. One of the methods is to reduce the wall thickness [312-314]. However, reducing the wall thickness can negatively affect the burst pressure [291, 315]. Using vascular grafts with low burst pressure could become a critical problem for the patients with the vascular graft implants. Therefore, it is important to understand the effects different parameters have on the burst pressure when increasing the compliance of the vascular grafts. Two parameters that have been found to affect the mechanical properties of hydrogels are interlayer adhesion and crosslinking density [293].

Crosslinking of PVA has been extensively studied. A well-established physical crosslinking method of PVA is freeze-thawing. PVA grafts with freeze-thawing crosslinking are mainly fabricated by bulk molding fabrication. PVA hydrogels crosslinked using freeze-thawing have been shown to have tailored mechanical properties by varying the number of freeze-thawing cycles [90, 316, 317]. The freeze-thawing crosslinking of PVA involves phase separation and crystalline formation. Hydrogen bonds form in the aqueous solution of PVA. During the freezing of PVA solution, ice forms. The formation of ice induces the growth of polymer crystallinity. The growth of polymer crystallinity acts as physical crosslinking points. Subsequently, water-insoluble hydrogels are formed in the later thermal cycles. The abundant hydroxyl groups in the backbones of PVA polymer chains also provide reactive sites for chemical crosslinking of PVA [318]. X-ray photoelectron spectroscopy (XPS) was used in previous literature to test the changes in surface chemistry of PVA. Surface chemistry of the standard method did not show difference without chemical modification [28, 29]. Even though XPS is a sensitive surface characterization method, it is speculated that XPS may not be not sensitive enough to capture the difference crosslinking level. One of the most commonly used crosslinking agent for PVA is glutaraldehyde. It reacts with hydroxyl groups to form an ester bond.

Chaouat *et al.* found that the hydroxyl groups on PVA can also react with STMP to crosslink PVA hydrogels by phosphoesterification [25]. The PVA hydrogels chemically crosslinked with STMP were shown to be capable of achieving a wide range of mechanical properties by altering the fabrication parameters such as humidity and water evaporation [89]. A recent study comparing the hemocompatibility of PVA hydrogels crosslinked by STMP, glutaraldehyde, and freeze-thawing found that crosslinking methods also affect the biological performance of PVA [30].

PVA vascular grafts are fabricated using dip-casting with cylindrical molds [100]. Dip-casting method allows for topographical modification of the PVA grafts, which plays an important role in orientation of the attached cells [232]. Also, different mechanical properties of the PVA vascular grafts can be achieved by altering the number of layers and fabrication parameters. We have observed heterogeneity in transparency between the layers (Figure 3.2A, red arrows) in PVA vascular grafts. The observed heterogeneity can be the result of inconsistencies in crosslinking between the layers [319]. The heterogeneity can also be an indication of a weak interlayer adhesion. A potential method of overcoming the weak interlayer adhesion would be increasing the interlayer crosslinking [320]. With PVA hydrogels, the interlayer crosslinking could occur by having hydrogen bonding between the residual –OH groups of the PVA layers. It was hypothesized that through increasing the interlayer adhesion, the resulting grafts can have high compliance while maintaining burst pressure. Moreover, the heterogeneity suggests that the crosslinking density can be further fine-tuned. We hypothesized that a decrease in the chemical crosslinking density will result in higher compliance and decrease in burst pressure. Furthermore, we hypothesize that post-fabrication processing will affect physical crosslinking, and impact the compliance and burst pressure.

3.6.1 Compliance and burst pressure of the grafts with varying wall thickness

Most often, tensile measurements are made to assess the mechanical properties of the polymers [321, 322]. Additional properties, such as residual stress, rheology, Izod impact measurement, etc. [321, 322], are also tested depending on the application of the polymers. For vascular grafts, burst pressure and compliance are important parameters to measure. Although PVA vascular grafts have been studied previously [25, 289], the relationship between the wall thickness and burst pressure and compliance have not been characterized. Thorough characterization of the compliance and burst pressure of the grafts with different wall thickness was performed first to identify the compliance and burst pressure achieved by different wall thickness. The relationship between the wall thickness and burst pressure (Figure 3.2C) was expected as the structural integrity of tubes is dependent on the wall thickness [291, 315]. The grafts with 6 layers displayed high compliance, but its burst pressure was only 232.7 ± 22.8 mmHg. As systolic blood pressure can rise to 220 mmHg during exercises, PVA grafts with 6 layers were deemed too weak. Grafts with 9 layers have a burst pressure of 485.5 ± 17.9 mmHg, which is at least double the systolic pressure of 220 mmHg. However, the compliance of the grafts with 9 layers was 2.6 ± 0.54% per 40 mmHg. Furthermore, compliance of the PVA grafts with more than 9 layers had compliance less than 2% per 40mmHg. Native blood vessels are reported to

have significantly higher compliance than what was achieved by PVA grafts with 9 layers. A human carotid artery with the diameter of 5.11 ± 0.87mm has compliance of 6.6 ± 1.3% per 100mmHg [209, 303-311]. As shown in Figure 3.4A, the compliance of the PVA grafts with 9 layers are lower than the native blood vessels. However, the compliance of PVA grafts with 9 layers had significantly higher compliance than ePTFE grafts, which are commercially available synthetic vascular graft [209, 303-311]. After assessing the compliance and burst pressure of the groups, the PVA vascular grafts with 9 layers was chosen for further investigation as they had the highest compliance with good burst pressure. Using the PVA grafts with 9 layers, the effect of crosslinking density and interlayer adhesion on the compliance and burst pressure were assessed.

3.6.2 PVA grafts fabricated using different fabrication conditions

The standard fabrication method is described in Figure 1A in detail. The crosslinking of PVA using crosslinker STMP in NaOH solution has been described in the literature numerous times [25, 27, 289, 293]. In brief, the -OH groups on PVA loses the hydrogen atom in the highly basic solution created by NaOH, and becomes reactive. This reactive site then reacts with the STMP. Subsequently, another PVA molecule reacts with the STMP and results in a crosslinked polymer. This process can be modified via changing the PVA concentration, STMP concentration, NaOH concentration, temperature, humidity, and waiting time between the dips [25]. The fabrication conditions were varied to achieve different level of interlayer adhesion and crosslinking density.

The interlayer adhesion occurs when there are crosslinks that spans multiple layers of polymers. The mechanical properties of PVA vascular grafts can be affected by the interlayer adhesion as PVA graft fabrication method is a dip-casting process with waiting periods between dips. The dip-casting process is a type of polymer fabrication method where the mold is dipped multiple times to achieve the desired thickness [321, 323, 324]. Due to the process requiring crosslinking of the layers after each dip, the drying condition of the layers is important to prevent delamination for this fabrication method [321]. One of the easiest parameters to control for dip-casting process is the waiting time between the dips. Waiting time is required to allow for the chemical reactions that crosslinks PVA molecules to occur [25]. Shorter wait time between each dip prevents completion of the reactions, allowing for more partially crosslinked sites for each dip. These partial crosslinking sites can react with the newly applied layer, increasing the interlayer adhesion [320]. Therefore, the drying time

should be kept short for the subsequent layers to be applied before crosslinking of the previous layer is completed to increase the interlayer adhesion.

For the control, the waiting time between the dips is 15 minutes in the first 4 dips, 25 minutes in the fifth to seventh dips, and 30 minutes for the eighth dip and beyond (Figure 3.1A). Instead of increasing the dipping time throughout the fabrication process, the waiting times between dips were kept consistent for the groups comparing the effects of the interlayer adhesion. 15W was fabricated with a flat 15-minute waiting time for all waiting steps instead of the standard protocol. 30W was made using a flat 30-minute waiting time for all waiting steps. The waiting times for 15W and 30W were kept constant so that interlayer adhesion throughout the grafts would remain consistent. There are many methods to make measurements to assess the adhesion between layers [325]. The most standard method of measuring the interlayer adhesion is the adhesive shear test (which is also known as lap shear test) [325].

The crosslinking density and concentration of STMP are positively correlated to the stiffness of the material [293]. As decrease in crosslinking agent can result in lowered crosslinking density, STMP concentration was decreased for one of the experimental groups (LS samples). Also, the concentration of NaOH was reported to be positively related to the crosslinking density [301]. Therefore, 15% w/v NaOH concentration was explored to achieve decreased crosslinking density to assess the effect of low crosslinking density. However, the graft could not be fabricated using the low concentration of NaOH (Table 3.1). We also speculate post-fabrication thermal drying may induce additional physical crosslinking, resulting in higher crosslinking density. To create the PVA grafts with higher crosslinking density, additional groups (60-2D, 60-4D, 18-2D, and 18-4D) were made with extra drying step post-fabrication to encourage additional physical crosslinking.

3.6.3 Effects of interlayer adhesion on PVA graft compliance and burst pressure

As shown in Figure 3.4, 15W had significantly thinner wall than the control group. However, the wall thickness of 30W was not significantly different from the control group. While the 15W and 30W had consistent waiting times between the dips, control group had 15-minute waiting time for the first four dips, 25-minute waiting time for the 5^{th}-7^{th} dips, then 30-minute waiting time for 8^{th} or more dips. The data showed that the longer waiting time is needed and waiting time of the outer layer was related to wall thickness in the outer layer. When the waiting time of the outer later was decreased in 15W, the

thickness was decreased, compared to 30W and control. However, it appears that increasing the early dip waiting time did not significantly affect the thickness.

15W had higher adhesive shear strength than all of the other groups. While not statistically significant against the control group, 15W showed a trend towards significantly higher adhesive shear strength than the control group ($p=0.057$), and a significantly higher adhesive shear strength than 30W ($p<0.05$). This indicates that the 15W had higher adhesion between layers than the other groups, which is in agreement with the height profiles shown in Figure 3.8C-J. As 15W and 30W were fabricated with a flat 15-minute and 30-minute waiting time, respectively, the significant higher shear strength in 15W further demonstrated that the shorter waiting time would increase the interlayer adhesive strength. This could be the result of a larger quantity of partial crosslinking sites available for a shorter waiting time in 15W. The partial crosslinking sites can then work as a bridge between the layers to allow for a larger number of interpenetrating crosslinks [325]. With longer waiting time between layers, the partial crosslinking sites can become crosslinked. This can reduce the crosslinking between the layers. Except for 15W and 30W, all of the samples had variable drying time. For the control group, LS, 60-2D, 60-4D, 18-2D, and 18-4D, the last two layers were applied with 30-minute waiting intervals. This could be the reason these groups did not show statistical difference in the adhesive shear strength.

3.6.4 Effects of chemical crosslinking density on PVA graft compliance and burst pressure

15W had a higher swelling ratio compared to the control group. The partial crosslinking sites could also attribute to the higher swelling ratio. This partial crosslinking sites may have resulted in lower crosslinking density, which could account for the lower burst pressure. However, it is also important to note that the wall thickness of 15W was significantly thinner than the control, indicating that the decrease in burst pressure could also be due to the thinner walls [291]. When the burst pressures were normalized to the wall thickness of the samples, 15W did not show significant difference from the control group (Figure 3.4D). This suggests that the affect from partial crosslinking on burst pressure was less significant than the influence from wall thickness.

The crosslinking of PVA was achieved by phosphoesterification, thus the content of phosphate also reflects the number of chemical crosslinking bonds formed during the fabrication. With lower concentration of STMP added in the reaction solution, it was expected that the resulting PVA grafts

would display lower concentration of phosphate to indicate a lower chemical crosslinking density. However, LS showed higher phosphate content than the control group (Figure 3.6A). The higher phosphate content in conjunction with the lower swelling ratio, LS displayed higher crosslinking density compared to the control group. This is in agreement with the burst pressure normalized to wall thickness (Figure 3.4D). The burst pressure should increase with increase in crosslinking density. A potential explanation for higher crosslinking density is the presence of tighter network due to the multifunctional nature of STMP. As phosphate groups from STMP has 4 potential reactive sites, more than two reactions can occur on a single phosphate group. When less phosphate groups are available, hydroxyl groups have less phosphate groups to react with. Phosphate groups become the limiting reagents, causing multiple phosphoesterification to occur on one phosphate. This results in tighter mesh formation, and therefore tighter crosslinking density. For the PVA crosslinked in abundance of phosphate, more phosphate could react with the hydroxyl groups. The abundance could result in phosphate population that did not react with multiple hydroxyl groups in the polymer network. These unbound phosphate groups then get washed away during the rehydration and storage, effectively resulted in a lower phosphate content in the hydrogels.

The difference in the crosslinking density among 15W, 30W and the control, observed from the phosphate assay (Figure 3.6A), indicated that the waiting time in between different layers affected the chemical crosslinking density. 15W had a significantly higher swelling ratio and significantly lower wall thickness than 30W. Comparing the mechanical properties of 15W and 30W, 30W had significantly lower compliance and significantly higher burst pressure. With a decrease in waiting time from 30 min to 15 min between each dip, more interpenetrating crosslink occurs. The interpenetrating crosslinks contribute to the observation of increased chemical crosslinking density observed from the phosphate assay. Similar to LS, 30W had longer waiting time between each dip, allowing more time for polymer chain to get aligned for hydrogen bonding, which may have contributed to the decreased compliance and increased burst pressure.

3.6.5 Effects of physical crosslinking density on PVA graft compliance and burst pressure

Although the chemical crosslinking density should not change during the additional drying due to extensive washing steps, physical crosslinking may have occurred during 60 °C drying. After the STMP crosslinking of PVA, residual hydroxyl groups remain available for hydrogen bonding

formation. PVA polymer chains display increased mobility at high temperature. The mobile polymer chains have a higher chance to get aligned, bringing the hydroxyl groups close to form hydrogen bonding. This process was achieved through subjecting the fabricated control groups to additional drying.

The extra-drying groups were 60-2D, 60-4D, 18-2D, and 18-4D. 60-2WD and 60-4WD are the two groups that were dried in the 60 ℃ for 2 weeks and 4 weeks, respectively. These two groups had thinner wall thickness than the control groups. 18-2D and 18-4D were the two groups that were dried in the 18 ℃ for 2 weeks and 4 weeks, respectively. The wall thickness of these groups did not differ from that of the control group. The two groups dried at 60 ℃ had lower swelling ratio than the control group regardless of the length of drying, indicating that they may have higher crosslinking density than the control group. Drying in the 18℃ did not alter the swelling ratio of the samples, suggesting that the crosslinking density of the groups dried post-fabrication at 18℃ was not different from that of the control group. The compliance of the 18-2D and 18-4D were comparable to the compliance of 60-2D and 60-4D. All of the post-fabrication drying groups had lower compliance than the control group. 18-2D and 18-4D had similar burst pressure compared to the control group. However, 60-2D and 60-4D had higher burst pressure than the control group. There was no difference observed based on the length of extra drying (2 weeks vs. 4 weeks) for both temperatures. This suggests that the additional physical crosslinking occurred during dehydration rather than the storage.

As the length of drying (2 weeks vs. 4 weeks) did not affect the performance of the grafts, further analysis was performed using 18-2D and 60-2D only. According to the phosphate quantification assay (Fig. 3.6A), 60-2D and 18-2D did not display any difference in total phosphate content within the polymers. FTIR did not also display any difference between the control group and the extra-drying groups (Fig. 3.6B). DSC analysis was performed in addition to assess the degree of crystallinity and overall crosslinking (Fig. 3.7). The DSC results suggested that 18-2D had higher crystallinity and crystallization temperature than the control group, while 60-2D showed a slightly higher fractional crystallinity than the control group. The higher crystallinity, suggesting a higher physical crosslinking, may explain the lower compliance and slight increase in the burst pressure from the post-fabrication drying step. However, while physical crosslinking density can be used to influence compliance and burst pressure, its effect might not be as significant as chemical crosslinking.

3.6.6 Additional mechanical analysis of selected groups

The group that had the highest compliance (15W) and the group that had the lowest compliance (LS) were used to perform additional mechanical property analysis. Both the longitudinal and circumferential tensile data (Figure 3.10A-D) agreed with the compliance data in that the 15W and control group did not show a statistical difference in mechanical behavior. LS had lower compliance than the control group, therefore it was as expected that the group is less elastic than the control group (Figure 3.10D). Suture retention was not affected by the different fabrication conditions. To reiterate, 15W had higher interlayer adhesion but lower crosslinking density than the control group. Therefore, it could be that the increased interlayer adhesion can also increase the suture retention strength. LS also had a thinner wall thickness than the control group. LS had not significantly different interlayer adhesion and higher crosslinking density compared to the control group. This could indicate that higher crosslinking density can increase the suture retention strength as well.

3.7 Conclusion

We investigated the effects of interlayer adhesion and crosslinking density on the compliance of PVA vascular grafts. We found that the higher crosslinking density resulted in higher burst pressure, but resulted in lower compliance. Also, we have found that the increase in interlayer adhesion could increase the burst pressure without sacrificing the compliance. While the findings in this article sheds light on how to improve the performance of the PVA vascular grafts, there are still shortcomings of the PVA crosslinking method utilized here. PVA-STMP crosslinking method using dip-casting is a slow process. This limits the shapes, and therefore applications, of the grafts such fabrication method can produce. Furthermore, PVA tubular grafts are prone to kinking. Kinking could potentially affect the blood flow when the graft is implanted in the patients, resulting in negative clinical outcome. Further research should be performed to improve the fabrication process of PVA-STMP vascular grafts to increase the potential application. Also, the kink resistance of the grafts should be improved to result in better clinical outcome. Lastly, additional methods of increasing interlayer adhesion could be explored to further increase the compliance of PVA grafts. For example, introduction of a layer of aqueous STMP solution between dips could potentially increase the interlayer adhesion by providing additional crosslinkers between layers.

Chapter 4
Consistency of poly(vinyl alcohol) vascular grafts

In this chapter, the need to develop an automated process of fabrication of poly(vinyl alcohol) (PVA) vascular grafts will be addressed. The mechanical properties of PVA grafts made using the manual and automated fabrication method will be compared. Then, the stability of PVA will be examined. Lastly, the parameters that are useful for the application of PVA to arteriovenous graft will be addressed.

4.1 Introduction

While there are successful vascular grafts available for clinical applications, synthetic small diameter vascular grafts (sSDVG) still face limited success due to formation of intimal hyperplasia (IH) [40]. sSDVG is defined as vascular grafts made using synthetic materials to have internal diameter less than 6 mm. These grafts could be used for bypass surgeries as well as for arteriovenous grafts [15, 79]. While there are commercially available vascular grafts, these grafts are often much stiffer than the native blood vessels [14]. The mismatch in the stiffness between the synthetic vascular grafts and the native blood vessels is called compliance mismatch. It can cause disturbances in wall stress and wall shear stress to the cells around the anastomosis because the stiff vascular graft does not expand to alleviate the blood pressure. To overcome the compliance mismatch between the sSDVG and native blood vessels, vascular grafts using compliant biomaterial called poly(vinyl alcohol) (PVA) was developed. PVA grafts have been proposed as a compliant vascular graft since 2008 [25]. Since then, many have tried to study the grafts *in vitro*, *ex vivo*, and *in vivo* experiments to assess whether it would be possible to use PVA grafts in the market [14, 25, 29]. Variable mechanical properties of polyvinyl alcohol (PVA) as well as other beneficial biological properties makes PVA be a good candidate for sSDVG.

However, consistencies of PVA grafts must be improved so that they can be used in clinical application. The fabrication process of PVA vascular grafts is very prone to person-to-person variation. The fabrication of PVA grafts use dip-casting method, where the mold is dipped into crosslinking solution with waiting times between dips [21]. The dip-casting process requires the dipping to be performed with consistent speed to be free of any variation due to shear introduced by the crosslinking solution bath. The process also has to be performed free of air bubbles to minimize

introduction of defects. Also, the molds must be kept vertical between dips so that the crosslinking solution does not aggregate on the surface of the mold. If aggregation of the mold occurs, then wall thickness of the resulting grafts will be highly variable. Also, the benefit of having synthetic vascular graft is that the grafts are readily available off-the-shelf. While PVA hydrogel is chemically crosslinked to be a permanent hydrogel, the stability of the PVA grafts is not studied yet.

In this chapter, the consistency of the PVA grafts made by the automated fabrication process and the manual process was studied. The automation of the fabrication process was used to test whether the consistency in PVA grafts can be improved. Also, the stability of the PVA grafts was studied to assess the consistency of the physical and mechanical properties of the PVA grafts after long incubation time. The hypotheses that will be addressed in this chapter are: (i) the automation process will result in less variation in wall thickness, burst pressure, and compliance compared to the PVA grafts made using the manual fabrication method, and (ii) there will be no more than 5% loss of length, thickness, and dry weight of PVA grafts after 180 days of incubation.

4.2 Materials and methods

4.2.1 Manual fabrication of poly(vinyl alcohol) tubes

Standard PVA crosslinking method was used for graft fabrication as described previously [288]. Briefly, cylindrical molds are dip-cast in the crosslinking solution (10% w/v PVA and 15% STMP w/v as listed below), then dried in controlled environment as shown in Figure 3.1A.

4.2.1.1 PVA crosslinking solution preparation

A 10% aqueous solution of PVA (Sigma-Aldrich, 85-124 kDa, 87-89% hydrolyzed) was mixed with 15% w/v sodium trimetaphosphate (STMP, Sigma-Aldrich) and 30% w/v NaOH at the volumetric ratio of 12:1:0.4, respectively, to create crosslinking solution. PVA grafts were fabricated using base-catalyzed STMP crosslinking. The PVA crosslinking solution was immediately dip-cast on a cylinder mold to form tubular PVA grafts.

4.2.1.2 Dip-casting PVA vascular graft

PVA vascular grafts were cast as previously described (Figure 3.1A) [96]. In short, the molds for the tubular grafts were plasma cleaned, then dipped in PVA crosslinking solution. The coated molds were dried at 20-21℃ and 30% humidity for 15 minutes, before dipping in the crosslinking solution again

for the next layer. For the first four dips, the drying time between dips was 15 minutes, the drying time between dips in the fifth to seventh dip was 25 minutes, and drying time between dips for the eighth dip and higher was 30 minutes. The molds were kept at room temperature at 30% humidity for each waiting period between dips. The molds were inverted every-other dips to ensure even crosslinking throughout the mold. After the dipping completed, the PVA grafts were dried at 18°C and 70-80% humidity for 3 days. PVA hydrogel was rehydrated by submerging in 1x PBS for 2 hours. The rehydrated PVA tubes were stored in 1x PBS until use.

4.2.2 Automatic fabrication of poly(vinyl alcohol) tubes

Automated dip-casting equipment was designed and developed by Fourth-Year Design Project (FYDP) group under the supervision of YeJin Jeong and Dr. Evelyn Yim [326]. In short, the equipment consisted of electrical circuit containing programmable Arduino, three linear actuator, aluminum beams, plastic tubes, and 3D printed parts. The equipment was later revised by the author to increase throughput. Both the original automated dip-casting equipment and the modifications made are shown in Figure 5.1.

The part name for each of the components addressed are listed in Figure 4.1A. The device is constructed so that the cylindrical mold used in dip-casting PVA tubes were held vertically. The linear actuator then brings down the molds into the bath of crosslinking solution prepared as stated in Section 5.2.1.1. The cylindrical molds are then raised back to the starting height, and held for the wait time. The second linear actuator moves the bath holding crosslinking solution out from under the cylindrical molds to ensure the PVA crosslinking solution dripping from the cylindrical mold does not enter the PVA crosslinking solution contained in the bath. For all of the even number of dips, the third linear actuator was used to rotate the rods to change the orientation of the cylindrical molds so that the molds were inverted. The wait time between dips were 15 minutes for 1-4 dips, 25 minutes for 5-7 dips, and 30 minutes for 8 dip and more.

4.2.2.1 Modification to the base automated dip-casting equipment

The holder for the cylindrical molds and the bath for holding PVA crosslinking solution was modified to increase throughput. The modification made to the original dip-casting equipment is shown in Figure 4.1B and Figure 4.1C. The cylindrical mold holder was design in 3D CAD modelling software, then 3D printed. The 3D printed holder was then slid onto the rectangular rod to be mounted

onto the automated dip-casting equipment. The solution bath holding PVA crosslinking solution was also designed in 3D CAD modelling, then 3D printed. Solution bath was covered between dips. For all of the even number of dips, the third linear actuator was used to rotate the rods to change the orientation of the cylindrical molds so that the molds were inverted. The wait time between dips were 15 minutes for 1-4 dips, 25 minutes for 5-7 dips, and 30 minutes for 8 dip and more.

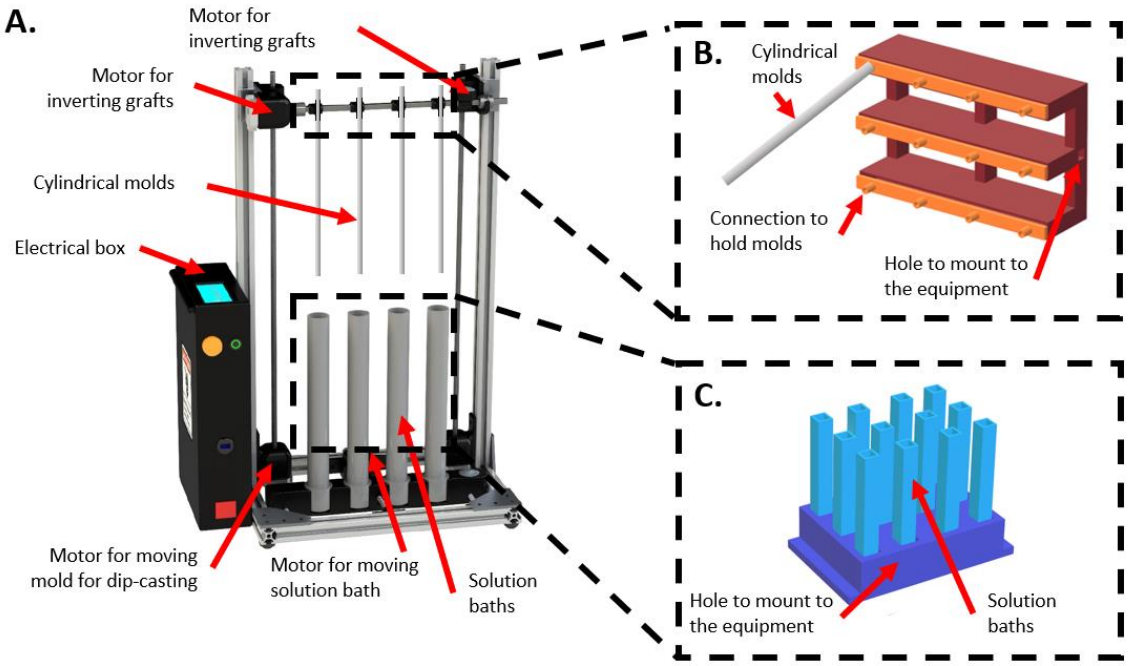

Figure 4.1. Equipment for automated poly(vinyl alcohol) (PVA) vascular graft fabrication process. (A) The equipment for automation of PVA fabrication process developed by the Fourth-Year Design Project group. (B) Computer-assisted design (CAD) model of modified mold holder to improve output. (C) CAD of the solution bath made to match the modified mold holder.

4.2.3 Inner-diameter and wall thickness

2 mm segment rings were cut from the tubular PVA grafts at the ends and at the center of the samples. Images of the 2 mm segments were taken, and the inner diameter and wall thickness of the segments were measured for each segment from the images using MatLab. For each individual sample, the measurements of the inner diameter and the wall thickness from segments at different regions were averaged to yield the average inner diameter and the wall thickness of the sample.

4.2.4 Compliance

3 cm segments of PVA grafts were exposed to 120 mmHg and 80 mmHg of hydrostatic pressure. Images of the grafts were taken at the defined pressures. The outer diameters of the grafts were measured, then the compliances of the grafts were calculated using the following equation [25]:

$$\frac{diameter\ at\ 120m\ mHg - diameter\ at\ 80\ mmHg}{diameter\ at\ 120\ mmHg} * 100 = \%\ compliance\ per\ 40\ mmHg \quad \text{…Equation 1}$$

ePTFE vascular graft (Gore-Tex®, catalog number V04070L) with the inner diameter of 4mm was used to measure the compliance of the ePTFE graft with comparable size using the stated setup.

4.2.5 Burst pressure

Burst pressure measurement was performed following published method [97]. In brief, 4 cm segments of PVA grafts were exposed to internal pressure induced by nitrogen gas at room temperature. The pressure was increased gradually until the graft burst. The burst pressure was recorded at the pressure at which the graft burst. A normalized burst pressure was calculated as burst pressure normalized per unit thickness by dividing the burst pressure of the samples by their wall thickness.

4.2.6 PVA hydrogel stability

PVA tubes fabricated following the procedure described in Section 5.2.1.2 was used for testing the stability of PVA tubes. The schematic for the testing the stability of the PVA hydrogel are shown in Figure 4.2. PVA tubes were cut into 1 cm segments. The segments were washed three times with deionized (DI) water. Cross-sectional and longitudinal images of each section were taken. The wet weight of the PVA segments were measured after thoroughly removing residual liquid with lint-free paper wipes (Kimwipes). The sections were then dried at 60℃ for 72 hours to measure the dry weight. The segments were then submerged in sterilization solution, which comprised of 10% w/v Penicillin-Streptomycin + 1% w/v Amphotericin-B in 1x PBS. The segments submerged in sterilization solution was placed into the incubator for either 3 months or 6 months. The sterilization solution was replaced with fresh sterilization solution every two weeks. After the incubation, they were washed three times with DI water. The segments were then patted dry with lint-free paper wipes, and the wet weight of the segments were measured. The cross-sectional and longitudinal images of the segments were taken. Afterwards, the segments were placed into a 60℃ oven to dry the segments. The dry weights of the segments were measured after 72 hours of drying.

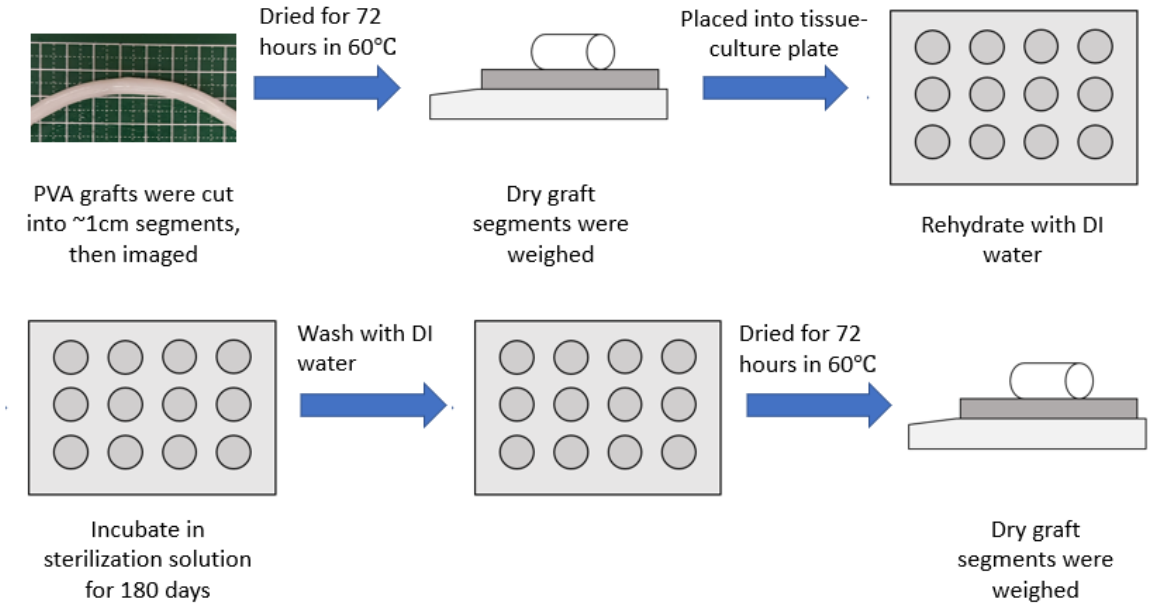

Figure 4.2. Schematic of the stability test performed on PVA graft.

4.2.7 Statistical analysis

Statistical significance was determined using a two-way ANOVA followed by Tukey's multiple comparison analysis with 95% confidence interval using MatLab. The data are presented as mean ± standard deviation. Linear regression was performed to determine the statistical significance between the groups. For the data set displaying the non-linear behavior, the data was revised using logarithmic transformation. For all the presented data, $p<0.05$ is denoted by * unless otherwise specified in the figure caption.

4.3 Results

4.3.1 Comparison between automated and manual fabrication method

Manual fabrication of PVA grafts requires multiple practices due to the fact that the fabrication process is prone for human errors. The FYDP group that developed the base automatic PVA graft fabrication equipment (Fig. 4.1A) tested the equipment by making PVA vascular grafts on their own. The group successfully made PVA grafts, and proved that the equipment can be used to minimize the learning curve required for making PVA grafts. I further modified the equipment to increase the

throughput (Fig. 4.1B and Fig. 4.1C). Furthermore, the design of the crosslinking solution holder was modified to decrease the amount of wasted PVA crosslinking solution. In Table 4.1, the comparison of the throughput and quantity of the required crosslinking solution is stated. The maximum number of grafts that could be made by the equipment increased by three-fold after modification. Also, the quantity of PVA crosslinking solution required decreased after modification to third of the amount required using the base equipment.

Table 4.1. Comparison of productivity per required ingredient between the base and modified equipment.

Equipment made by FYDP group	Max. grafts made per operation	4
	Volume of crosslinking solution needed per graft	150 mL
Equipment made by FYDP group with modification	Max. grafts made per operation	12
	Volume of crosslinking solution needed per graft	40 mL

Figure 4.3 shows the comparison of the physical properties of the PVA grafts made using the manual and automated fabrication methods. The luminal diameter did not show any difference regardless of the number of layers (Fig. 4.3A). The grafts made using the automated fabrication method had significantly lower wall thickness compared to those that were made using the manual fabrication process (Fig. 4.3B). The burst pressure of the grafts made using the automated process was also lower compared to the grafts made using the manual fabrication method (Fig. 4.3C). Since the burst pressure is directly related to the wall thickness, it is to be expected that the graft made from automated process have lower burst pressure than the ones made from manual dip-casting method [327]. The grafts made using the automated method had significantly higher compliance compared to the grafts made using the manual fabrication method (Fig. 4.3D). It was also observed that the grafts made with 6 layers had wide standard deviation. This could be due to the fact that the walls of the grafts were thin.

Figure 4.3E and Figure 4.3F shows the burst pressure and compliance plotted against the wall thickness to inspect the burst pressure and compliance of the grafts with respect to the wall thickness. The plot of burst pressure versus wall thickness shows that there was no statistical difference between the grafts made using different fabrication methods (Fig. 4.3E). Likewise, the plot of compliance versus the wall thickness showed no difference between the two groups. Therefore, it can be concluded that the difference in burst pressure and compliance is due to the wall thickness, rather than alteration in the properties of the hydrogel.

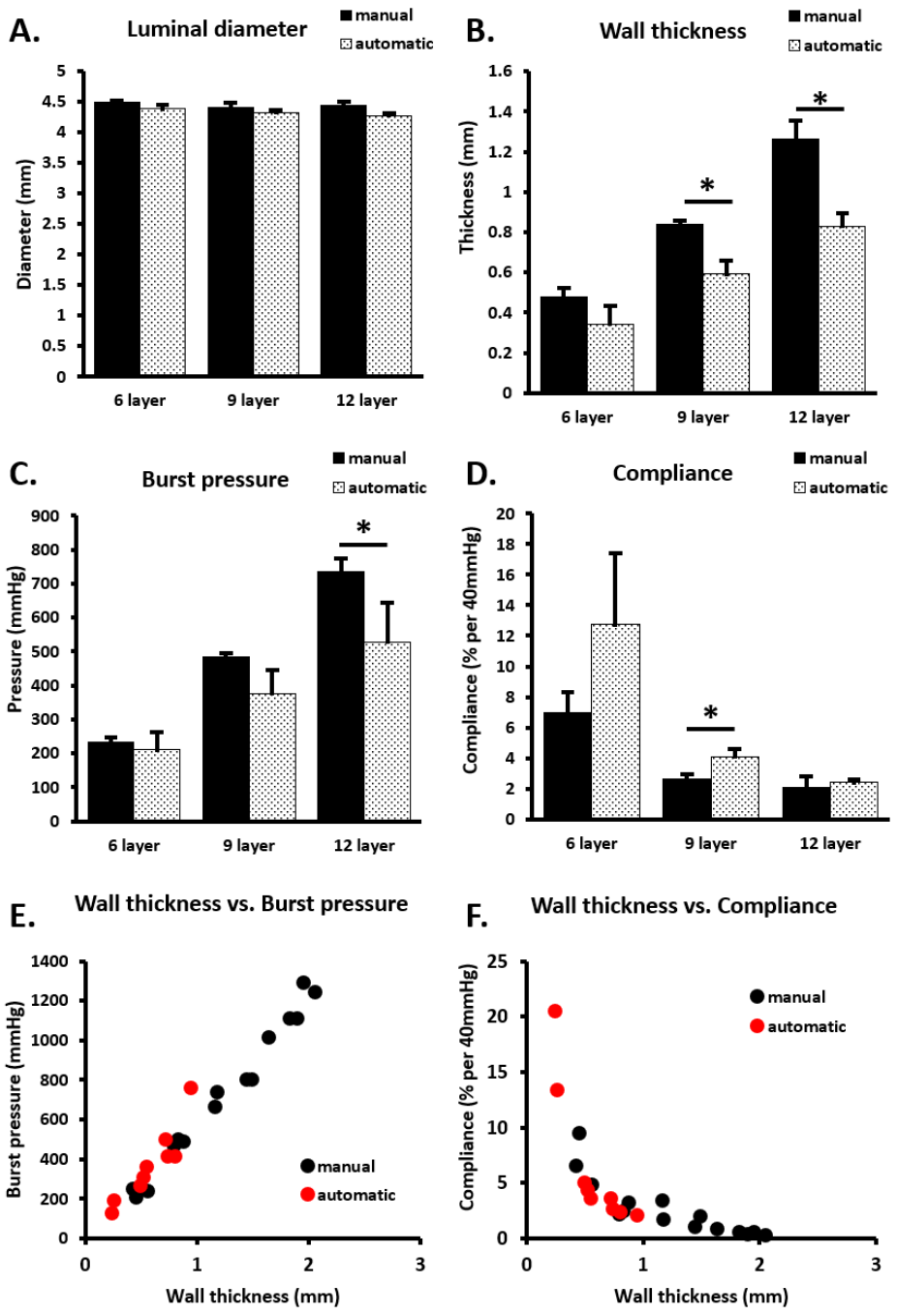

Figure 4.3. Assessment of physical and mechanical properties of the poly(vinyl alcohol) (PVA) grafts made using the manual and automated fabrication process. (A) luminal diameter, (B) wall thickness, (C) Burst pressure), and (D) compliance of the grafts made by the manual (black) and automated (grey) fabrication methods. * indicate statistical difference between the indicated groups with $p<0.05$. (E) plot of wall thickness vs. burst pressure, and (F) plot of wall thickness vs. compliance of the grafts fabricated with manual (black) and automated (red) methods. N = 9 for all groups. Standard deviation used as error bars.

4.3.2 Stability of the PVA vascular grafts

The storage stability of the PVA hydrogel crosslinked with PVA vascular grafts have not been studied. In Figure 4.4, the stability of the PVA grafts after 180 days of incubation is shown. The representative images of the grafts on Day 0 and Day 180 showed that there was no observable change in the segments after the incubation (Fig. 4.4A). The length and wall thickness of the segments were measured, and are shown in Figure 4.4B and Figure 4.4C. No more than 2% average reduction in the length and wall thickness was observed for all groups. Furthermore, the dry weights displayed less than 2% reduction after 180 days of incubation.

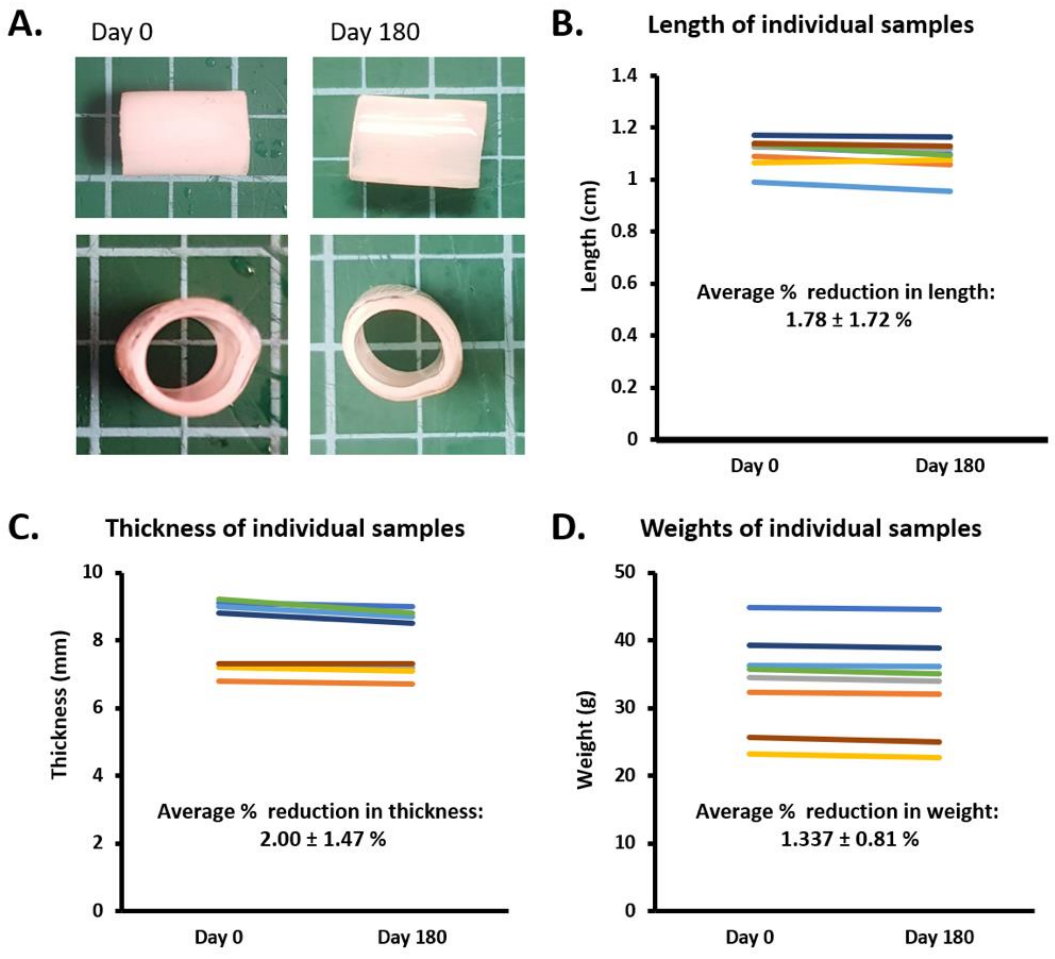

Figure 4.4. Stability of the poly(vinyl alcohol) (PVA) hydrogel. (A) representative images of the graft at day 0 and day 180. (B) lengths, (C) wall thickness, and (D) dry weight of the individual graft segments on day 0 and day 180. Each line represents 1 sample. n=8.

4.4 Discussion

Consistency is important in scientific research – especially so in biomedical engineering. This is due to the fact that there are many sources of error, derivation, and variations. In cell culture, the behaviors of the cells are dependent on the confluence, the composition of the media, the temperature of the incubator, the humidity and carbon dioxide level inside the incubator, and more. In the case of biomaterials used in *in vitro* experiments, the materials can have variations due to derivation in making the bulk solution, and the standard experimental variation in characterization. Materials samples would have to be rejected when errors have been introduced to the process, such as contamination in the solution used make the material, error in fabrication process, as well as potential error in characterization of the material. The scientists perform experiments keeping as many sources of error in mind, and try to keep as many factors as consistent as possible.

Here, the consistency of PVA vascular graft was explored. At an initial glance, PVA vascular graft fabrication process looks easy. It just requires repeated dipping of the mold into the crosslinking solution, with defined waiting time between each dipping [21]. However, the dip-casting must be performed controlled speed or the chance of introducing defects increase. Also, depending on the angle at which the grafts are kept between each dip, the resulting grafts may have skewed wall thickness. Therefore, the grafts will often be made in batches and stored until use. It is possible that the grafts are stored for months before use. Therefore, the stability of the PVA hydrogel can also risk the consistency of the PVA vascular grafts.

4.4.1 Automation of the PVA vascular graft fabrication

Many technologies that are developed in laboratories do not result in translation into clinical settings. This is due to many factors; one of which is the quality control during scale-up [328, 329]. There are active efforts to try and scale-up the processes used in the laboratories. Scale-up of nanofiber manufacturing process for biomedical applications is one of the examples [330]. The publication addressed the use of electrospinning can increase the production of the nanofibers [330]. In semi-conductors, the ability to produce thin layer of graphene sheet is very important due to the conductive and physical properties of graphene [331]. Many research groups developed methods of forming the graphene, which ultimately allowed for large-scale production of graphene [331]. Without the efforts of scale-up, the technologies developed in the laboratories will not be used in real-life applications. However, translation from the lab to the market requires consistency of the resulting product. It is

important that the fabrication process is simplified and controlled so that the process eliminates avoidable error [328]. Variation between batches limits the reliability of the technology, making the product not suitable for use. As a result, methods for good manufacturing practice (GMP) are developed and are actively used in industries for quality control [332].

Variation in the dip-casting process could affect the PVA tubular graft properties. The molds used during the dip-casting must be dipped into the crosslinking solution slowly so that bubbles would not be introduced to the crosslinking solution bath. A bubble can potentially stick to the mold and create a defect, and ultimately cause the graft to fail prematurely at the site of defect [21]. If the mold was not kept vertical during the waiting period between dips, then aggregation of PVA crosslinking solution may form. This could result in varying wall thickness throughout the graft. Furthermore, the molds had to be inverted every-other dip to ensure even wall thickness throughout the graft as well. Therefore, automation of the process was needed to increase the consistency of the PVA vascular grafts made by different individuals. The base automated dip-casting equipment made by FYDP group (Fig. 4.1A) only produced maximum of 4 grafts while requiring 150mL of PVA crosslinking solution per graft. The design was modified to increase the production limit and to decrease waste (Fig. 4.1B and Fig. 4.1C). The resulting modification increased the maximum number of grafts that can be made at once to 12 grafts, while decreasing the volume of PVA crosslinking solution to 40mL per graft (Table 4.1).

The PVA grafts made using the developed automated fabrication process was then tested to ensure batch-to-batch consistency. Figure 4.3 shows the characterization of the physical and mechanical properties of PVA grafts made using manual and automated fabrication process. The lack of improvement in the variation in luminal diameter was expected, as this is determined by the shape of the mold rather than the fabrication process (Fig. 4.3A). On the other hand, the grafts made using the automated process had significantly thinner walls than the grafts made using the manual process with the same number of dips. This could be due to the fact that the dipping speed is controlled for the automated process, but not for the manual process. For automated process, the molds would be removed from the crosslinking solution at a constant rate. However, for the manual dipping process, the speed would vary for each dip. The difference in shear caused by the movement of the mold could result in different amount of crosslinking solution remaining on the molds. The different amount of crosslinking solution would cause different wall thickness for each layer and for each graft. The difference could also be due to the fact that the molds were kept vertical for the automated dip-casting

process, whereas the molds were not kept completely vertical in manual fabrication process. The difference in the angle the molds were held could have played a role in the amount of crosslinking solution that was allowed to drip off from the mold, and result in less of the crosslinking solution remaining on the mold. It was also observed that the standard deviation of the wall thicknesses for the manual dip-casting method was highly variable, while the standard deviation of the grafts fabricated using the automated method was consistent regardless of the number of layers (Fig. 4.3B). This could indicate that the automated fabrication process resulted in more consistent PVA grafts.

The burst pressure, compliance and the variation in / derivation of burst pressure and compliance of the PVA grafts were also compared. It is important that the burst pressure of the PVA grafts be higher than the maximum blood pressure an individual may witness. It has been reported that the highest blood pressure an individual can experience can be 370/360 [333]. This necessitates that the burst pressure of the PVA grafts be higher than at least 400mmHg. The burst pressure of the grafts made using the automated method had much higher variation than the grafts made using the manual dip-casting method (Fig 4.3C). The large variation of the grafts made using the automated method was also observed in compliance measurements (Fig 4.3D). However, it was also observed that the compliance of the grafts made using the automated process are higher than the grafts made using the manual dip-casting process. It is important to note that compliance of the vascular grafts should be matching that of the native blood vessels. Therefore, the compliance of the PVA grafts made with 6 layers may be too high compared to that of the native blood vessels, as they would cause compliance mismatch as well. It was found that rabbit femoral artery had compliance of 5.9±0.5 % per 40mmHg [89], which is similar to the compliance of 9 layer PVA grafts made using automated process. In conclusion, the PVA grafts fabricated using the automated system with 9 layers may be the best candidate when considering both the burst pressure and compliance.

Because both burst pressure and compliance are directly influenced by the wall thickness [291], the relationship between the wall thickness and burst press (Fig. 4.3E), and wall thickness and compliance (Fig. 4.3F) was considered. Using linear regression, it was determined that the two groups did not show significant difference for both the burst pressure and compliance. This indicates that the difference in the burst pressure and compliance may be due to the wall thickness rather than other factors. It is important to note that thinnest PVA grafts made using the manual fabrication process for grafts with 4mm diameter have 6 layers. This is due to the fact that the manual dip-casting method results in introduction of defects. The defects could cause grafts with 6 layers made using manual

fabrication process to fail during compliance measurement. However, the grafts made using the automated fabrication process resulted in PVA grafts with thinner layers that are capable of withstanding the internal pressure required for compliance measurement. This indicates that the grafts made using the automated process could result in grafts with less defects due to having better control of dip-casting process.

4.4.2 Assessing storage stability of PVA grafts

As PVA vascular graft fabrication process requires several days, PVA grafts are made in batches and stored in 1x PBS until use instead of being made as needed [21]. Therefore, the storage stability of PVA hydrogel is important for maintaining consistency between experiments. Figure 4.4 shows the physical changes of PVA grafts after 180 days of incubation in 10% Penicillin-Streptomycin and 1% Amphotericin B solution. There were no observable changes in the appearance of the graft after 180 days (Fig. 4.4A). Detailed measurements were made to accurately compare the samples before and after long-term storage. There were less than 5% reduction in the length (Fig. 4.4B), the wall thickness (Fig. 4.4C), and the dry weight (Fig. 4.4D) of the samples. This is in agreement with the literature, as PVA hydrogels are considered non-degradable [25].

4.5 Conclusion

Here, the consistency of the PVA vascular grafts were studied. Through the development of automated fabrication method, the consistency of the fabricated grafts between each batch was improved. Also, the automated fabrication process allowed for fabrication of PVA grafts with thinner walls by reducing the introduction of defects. This could allow for development of PVA grafts with improved compliance and burst pressure. Lastly, the PVA vascular grafts were incubated for 180 days to test the long-term storage stability of the grafts. It was found that the grafts remained completely intact, with less than 5% loss of the hydrogel.

It was also found, however, that the variability of the grafts resulting from the automated fabrication process can be large. This could be due to an error in the setup of the equipment and should be explored further. For example, the holders for the molds could be misaligned that the molds were tilted during the dip-casting process. Once the variation between grafts is removed by adjusting the setup of the equipment, the process can be used to understand the behaviors of PVA vascular grafts with thinner walls. Also, the automated process can be used to fabricate PVA grafts with higher

compliance, which could be used in clinical setting as a compliant vascular graft. Before reaching clinical application, however, the stability of the graft in exposure to the blood or blood-mimicking fluid should be studied to ensure the safety of the patients.

Chapter 5
Isolated effects of compliance mismatch on vascular smooth muscle cells

In this chapter, novel continuous compliance mismatched poly(vinyl alcohol) (PVA) sample will be described. Detailed procedure of fabrication of continuous compliance mismatch will be explained. Then, the effects of compliance mismatch on vascular smooth muscle cells will be addressed using the fabricated continuous PVA sample.

5.1 Introduction

Cardiovascular disease still remains an active topic of research. Despite much effort, synthetic small-diameter vascular grafts (sSDVG), defined as material-based vascular grafts having less than 6 mm of internal diameter, still face limited success. Success of vascular grafts are determined using patency. Patency is a measure of the luminal opening and is used to determine whether the implanted vascular graft allows for blood flow. Commercially available sSDVG are made using expanded polytetrafluoroethylene (ePTFE) and polyethylene terephthalate (Dacron). These grafts have as low patency as 23% after 2 weeks of implantation for ePTFE [17], and 29% after 7 months for Dacron [18]. There are biological approaches and biomechanical approaches used to study the limited patency. For example, a biological approach to addressing limited patency is endothelialization of the vascular graft wall [29]. A biomechanical approach is through minimizing the discrepancy between the vascular graft and native blood vessels. One of the biomechanical properties that is being studied is compliance.

Compliance in the context of vascular graft engineering refers to the expansion of the graft with exposure to the blood flow [274]. Compliance mismatch refers to the discrepancy in the compliance of the native blood vessel and the implanted vascular graft. The compliance of sSDVG is very low compared to the native blood vessels. For example, an ePTFE graft with 5.4 ± 0.1 mm diameter has compliance of 1.2 ± 0.3% per 100mmHg, whereas human carotid artery with diameter of 5.11 ± 0.87 mm has compliance of 6.6 ± 1.3 % per 100mmHg [14, 306, 308]. The compliance mismatch could result in formation of abnormal wall stress (WS), ultimately affecting the formation of intimal hyperplasia (IH). IH refers to the blockage of the lumen due to the migration and excessive proliferation of vascular smooth muscle cells (VSMC), There are many biological factors that are

found to increase VSMC proliferation and migration [14, 335-337]. It has been observed that platelet-derived growth factor-BB (PDGF-BB) can induce proliferation and migration of VSMCs [335]. Also, nuclear localization of yes-associated protein (YAP) has been found to be involved in proliferation of VSMCs [336], On the contrary, phosphorylated myosin light-chain kinase (pMLCK) has been shown to be responsible for the contraction of VSMCs [337]. The behaviors of these factors are influenced by mechanical stimulation, increasing the complexity of understanding IH.

Numerous studies focused on mechanical stimulation to understand the effects of biomechanical factors, such as wall shear stress (WSS), suture-line stress, and WS, on VSMC and development of IH [14]. The WSS is the shear stress the cells are exposed to due to the blood flow. Abnormal WSS has been found to cause damage to VSMC, and result in causing proliferation of VSMC [35, 151, 282]. Suture-line stress is the localized stress around the anastomosis due to suture. The localized stress of suture-line has been mapped through simulations, and have been correlated with biological observations [23]. The localized stress cause damage to the surrounding VSMC, and result in onset of proliferation of VSMC. WS is the stress that is applied on the substrate the cells are attached. In the case of vascular graft, WS occurs in radial direction because of the expansion of the wall due to internal pressure [273]. The effect of wall stress was assessed with the presence of suture-line [24]. While mechanical stimulation and stiffness of the substrate affecting the cellular behavior is well-understood [273, 321], the effects of compliance mismatch alone is not explored. The effect of compliance mismatch is studied in combination with suture-line stress [23]. The suture-line creates regions with elevated WS, which can affect the biological responses of VSMC [24]. With the development of continuous sample with two distinct regions of stiffness that allows for cellular adhesion, the effects of suture-line and compliance mismatch can be studied independently of each other.

Poly(vinyl alcohol) (PVA) hydrogel has been used in various biological research. PVA displays properties that are required for application to biological research, such as no cytotoxicity, low thrombogenicity, and bio-inertness, [29]. Additionally, PVA allows for easy manipulation of the mechanical properties of the resulting hydrogel [21, 87, 91, 338]. The stiffness of the substrate can be modified using the crosslinking method. For example, the number of freeze-thaw cycle can be used to determine the mechanical properties of the resulting PVA films [91]. Furthermore, Kim et al. showed PVA could be made to have a stiffness gradient by modifying physical crosslinking method in 2015 [87]. Also, PVA hydrogels can be crosslinked using chemical crosslinking method. In 2021,

crosslinking parameters of chemical crosslinking method was altered to study the effects of each parameter on the mechanical properties [21]. While both of the crosslinking method allows for easy manipulation the mechanical properties of PVA hydrogels, it is difficult to achieve a continuous film with the elastic moduli spanning a wide range with a clear transition between the elastic and stiff region.

In this chapter, a hybrid crosslinking method was developed to achieve a continuous PVA film with compliance mismatch. The developed compliance mismatch film was exposed to cyclic strain, and strain map was made to ensure equal application of strain throughout the film. Then, the developed film was used in *in vitro* experiments to assess the impact of compliance mismatch on human umbilical arterial smooth muscle cells (HUASMC) with the application of cyclic strain. The hypotheses of this chapter are: (i) chemical and physical crosslinking can be used simultaneously to achieve a continuous film with compliance mismatch, (ii) HUASMC cultured on compliance mismatch film will result in higher proliferation rate and display phenotypic change to migratory phenotype compared to both compliant and non-compliant films, and (iii) HUASMC cultured on compliance mismatched film would result in higher pMLCK expression, higher PDGF-BB expression, and nuclear localization of YAP.

5.2 Materials and methods

5.2.1 Fabrication of compliance mismatched sample

PVA hydrogels were fabricated using a hybrid of chemically crosslinked PVA hydrogel film and physically crosslinked PVA. The schematic of the PVA sample fabrication is shown in Figure 5.1A through Figure 5.1C. Figure 5.1.A shows an example of end-to-side anastomosis, where the end of the graft is sutured onto the side of the blood vessel. The 3D anastomosis region (black box) is removed, cut, and unraveled to reveal 2D representation of the anastomosis. The 2D representation of the anastomosis is shown in the far right of Figure 5.1A. In Figure 5.1C, the bird-eye-view of the PVA compliance mismatch sample is shown in far right. The schematic of the experimental setup is shown in Figure 5.1D. Note that the samples are placed into the stretcher shown in Figure 5.1D in the same orientation shown in Figure 5.1C. Then, the samples were uniaxially stretched to mimic 1D circumferential stretching experienced by the anastomosis.

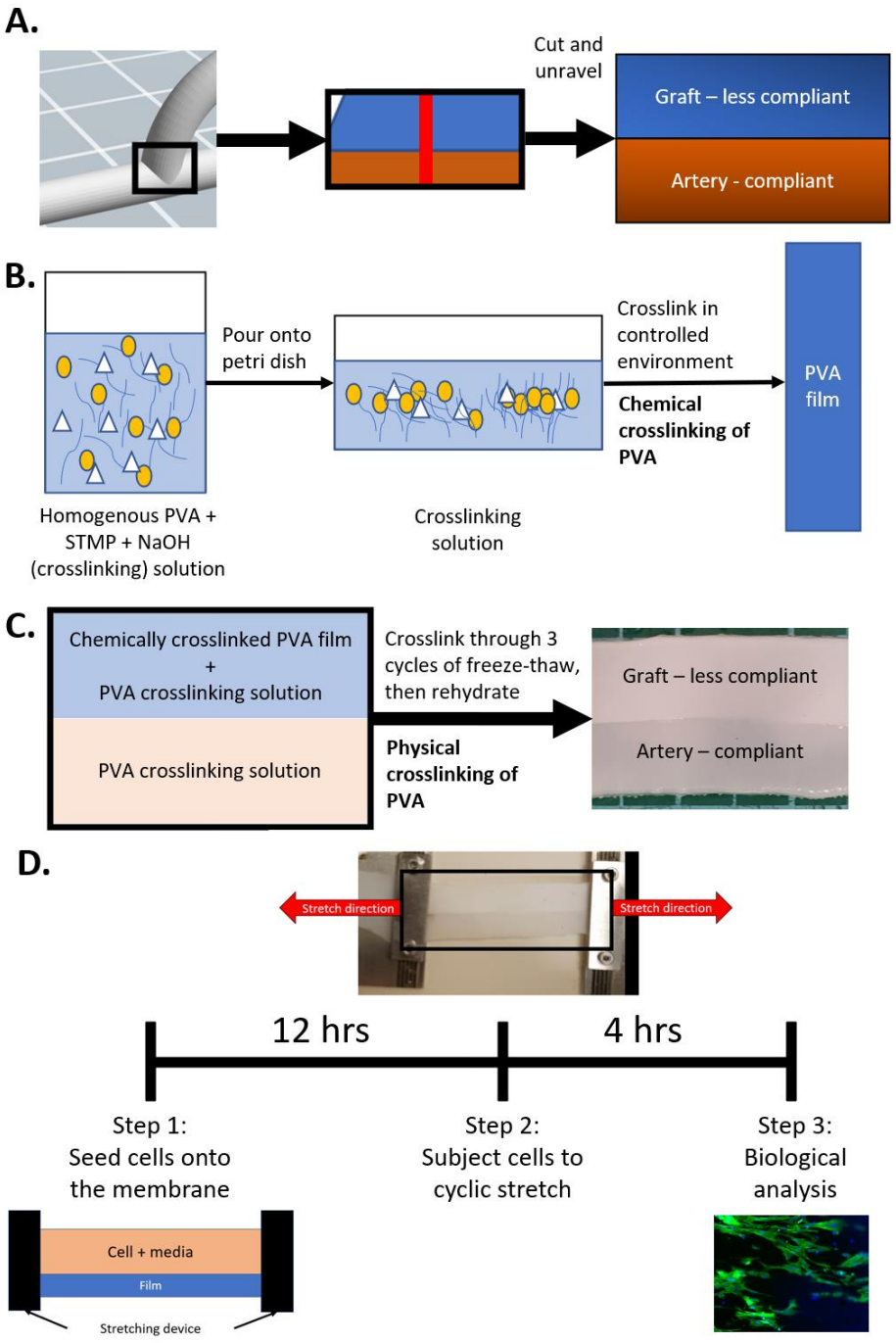

Figure 5.1. Schematic of sample fabrication and experiment. (A) anastomosis unravelled to yield film. (B) chemical corsslinking process of PVA film. (C) physical corsslinking prcoess for making samples. (D) Schematic of the experiment. The cells were seeded onto PVA samples, then incubated overnight to allow for cellular adhesion. The samples were then exposed to cyclis stretching at the strain of 10% for 4 hours. The samples were then used in biological analysis.

5.2.1.1 PVA cast films

PVA films were made using the previously published method [29]. In short, PVA crosslinking solution was prepared by mixing 10% w/v PVA (Sigma-Aldrich, 85-124 kDa, 87-89% hydrolyzed) solution, 15% w/v sodium trimetaphosphate (STMP, Sigma-Aldrich) solution, 30% w/v NaOH solution in 12:1:0.4 ratio. The crosslinking solution was centrifuged at 2500 rpm for 10 minutes to remove any air bubbles within the solution. Afterwards, the crosslinking solution was poured into a square dish so that the height of the solution in the dish was either 1 mm or 2 mm. the dishes were then covered with lid, and placed into a temperature- and humidity-controlled chamber. The crosslinking solution in the dishes were allowed to crosslink in 18℃ with the humidity of 70-80%. After 3 days of crosslinking, the lids were removed. The crosslinking solution were further incubated in the chamber for 4 days. After completion of crosslinking, the PVA films were rehydrated using 1x phosphate-buffered saline (PBS). The films were cut into 2 cm by 8 cm strips, and were stored in 1x PBS until use.

5.2.1.2 PVA compliance mismatched samples

PVA crosslinking solution was prepared using the same composition as above. Customized molds were made to have internal dimensions of 2 cm of height, 4 cm of width, and 8 cm of length. PVA crosslinking solution was poured into the customized molds so that approximately half of the height of the mold was filled with the crosslinking solution. The strips of PVA films prepared in Section 5.2.1.1 were placed into the molds. Additional PVA crosslinking solution was poured on top of the PVA films. The molds were then covered with the lid, letting out excess PVA crosslinking solutions in the process. Once the molds were completely closed, they were placed into the freezer for at least 12 hours (freeze cycle). Then, the molds were removed from the freezer and were stored in room temperature for at least 12 hours (thaw cycle). The molds went through a total of three freeze-thaw cycle. Afterwards, PVA samples were cut into 1 cm by 8cm strips.

The sample made using only the physically crosslinked PVA was labelled as compliant (C). The samples that had two sides: one side physically crosslinked only and other side had hybrid of physically crosslinked PVA and 1 mm chemically crosslinked PVA film = was labeled as mismatched (M). The samples consisting of hybrid of physically crosslinked PVA and 1 mm chemically crosslinked PVA film was labelled not compliant (NC). To study more physiologically relevant compliance mismatch [29], samples with higher compliance mismatch were made. The

higher compliance mismatch (2M) samples that had two sides, one side physically crosslinked only and other side had hybrid of physically crosslinked PVA and 2 mm chemically crosslinked PVA film. The samples consisting of hybrid of physically crosslinked PVA and 2 mm chemically crosslinked PVA film was labelled higher not compliant (2NC). The samples were then washed in deionized water (DIW) for 24 hours using magnetic stir bar. PVA samples were modified with gelatin immediately after the wash.

5.2.1.3 Gelatin modification

Surface modification of PVA using gelatin was performed following previously published protocol [28]. 2% w/v gelatin (Sigma-Aldrich, Gelatin from bovine skin, Type B) solution was made prior to gelatin modification of PVA samples. For the 2% gelatin solution, gelatin crystals were added to the correct volume DIW. The gelatin crystals were dissolved by autoclaving. The gelatin solution was stored in the fridge until use. The samples were dried in a 60℃ oven. The samples were dried for either 3 days or 7 days. Carbonyldiimidazole (CDI) was dissolved in dimethyl sulfoxide (DMSO) at the concentration of 100 mg/ml. The resulting solution was referred to as CDI-DMSO solution and was made 24 hours prior to use. Once the samples were dried for the designated time, they were removed from the oven and were immediately submerged in CDI-DMSO solution. The samples submerged in CDI-DMSO solution were placed on a rocker at 120rpm and were rocked for either 1 hour or 3 hours. While CDI reaction was taking place, 2% w/v gelatin solution was removed from the fridge and warmed up to 37℃. After the gelatin solution became liquid completely, the gelatin solution was diluted using DIW to make 1% w/v gelatin solution. After the CDI reaction, the samples were washed with equivalent volume of 1x PBS three times. After the wash, the samples were submerged in 1% w/v gelatin solution. The samples were kept in the incubator overnight to allow for CDI-gelatin reaction to occur. The samples were washed with equivalent volume of 1x PBS three times. The samples were sterilized immediately after the wash.

5.2.1.4 Sterilization of PVA samples

10% w/v Penicillin-Streptomycin (Gibco, Penicillin-Streptomycin 10,000U/mL solution) + 1% Amphotericin B (Corning, Amphotericin B 250μg/mL solution) solution was made using sterile DIW. Sterilization solution was made prior to usage, and were stored at 4 deg C until use. If the sterilization solution was not used within two weeks of preparation, then the solution was kept frozen at -20 deg C, and was thawed immediately prior to use. The samples that were washed after gelatin modification

were kept under UV light inside biosafety cabinet for 45 minutes. The samples were partially covered with 1x PBS during the 45 minutes. After UV treatment, the samples were completely submerged in the sterilization solution for 30 minutes. The samples were then washed three times with equivalent volume of sterile 1x PBS. After the wash, the samples were again submerged in the sterilization solution for at least 1 hour. The samples were washed three times with equivalent volume of sterile 1x PBS. The samples were kept in sterile 1x PBS solution until use.

5.2.1.5 PVA compliance mismatched samples for strain mapping

Some samples were fabricated with black glitter for the purpose of strain mapping. Just prior to freeze-thaw cycle, black glitter (LET'S RESIN, B08NJW18J2, approx. 0.5mm x 0.5mm in dimension), was sprinkled on top of the PVA crosslinking solution inside the customized molds. Afterwards, the samples went through freeze-thaw cycle as stated in Section 4.2.1.2. The resulting PVA samples underwent the gelatin modification process described in Section 4.2.1.3 and Sterilization of PVA samples stated in Section 4.2.1.4. The resulting samples were washed by submerging in 1x PBS and stirred with magnetic stir bar overnight to remove any loose glitter. Afterwards, the samples were stored in 1x PBS until use.

5.2.2 Elastic modulus measurement

The thicknesses of the samples were measured using the caliper. The prepared samples were loaded onto the Uniaxial material tester (UMT; AGSX Shimadzu, Japan) so that the long edge of the sample was perpendicular to the clamp of the UMT. The samples were placed so that the gauge lengths of 2 cm. The samples were then stretched at a rate of 25 mm/min until the tensile failure of the sample. The thicknesses of the samples were input to the software of the UMT prior to making the measurements. The software was used to calculate the elastic moduli.

5.2.3 Strain mapping throughout the sample

Cyclic stretching was performed using MechanoCulture (CellScale Uniaxial stimulation of 2 parallel specimens; discontinued). The device was programmed to have 10% strain; the initial length of the sample being 40mm, and the length after stretch was 44mm. the cyclic stretching was performed at 1Hz for 4 hours unless stated otherwise. The strain map of the PVA samples were made to ensure even strain throughout the sample during stretching. Then, PVA samples cultured with HUASMC were loaded onto MechanoCulture to be exposed to cyclic stretching.

Strain-mapping throughout the sample was done using the code developed by Dr. Keng Hwee Chiam and the members of his lab from A*STAR Bioinformatics Institute, Singapore. The samples were prepared as stated in Section 4.2.1.4. The samples were loaded onto MechanoCulture. The surface of PVA samples were dried by wiping with low-dust wipes. Then, black glitter was sprinkled on top of the samples. A camera was placed so that it was directly on top of the sample, looking down at the sample from vertical position. Any solution remaining on the PVA sample was removed to remove unwanted reflection. The camera was used to record a video clip of the samples during cyclic stretching.

5.2.4 Cell culture

Human umbilical arterial smooth muscle cell (HUASMC; VWR, catalog # CA10064-266; lot # 458z025.2) was purchased from Lonza. Cells were cultured in Maintenance culture media during cell passage and maintenance. Cells were cultured in experiment culture media during experiment. Maintenance media was made by revising the commercially available composition [339]. Per 100 ml of maintenance media, the composition of media used in this chapter was: 90 ml of Dulbecco's Modified Eagle Medium/Nutrient Mixture-F-12 (DMEM/F-12) with L-glutamine and 15 mM 4-(2-hydroxyethyl)-1-piperazineethanesulfonic acid (HEPES) (CORNING), 5ml of fetal bovine serum (FBS) (Avantor), 3.75ml of Glutamax^{TM}-I (100x) (Gibco), 1ml of Penicillin-streptomycin (Pen-Strep) (10,000µg/ml), 125µl of 40% Glucose, 2.5µl of epithelial growth factor, and 0.5µl of fibroblast growth factor. HUASMC with passage between 4 to 7 was used for the experiments. The composition of maintenance media was revised to make experiment media. Per 100ml, the composition of experiment media was: 94ml of DMEM/F-12 with L-glutamine and 15mM HEPES, 5ml of FBS, and 1ml of Pen-Strep.

5.2.4.1 Maintenance cell culture

Cryopreserved HUASMC was purchased at passage 2 from Lonza. The HUASMC were thawed and immediately submerged in maintenance media with the volume equivalent to 2x the volume of the cryoprotectant. The cell solution was transferred to conical tube and centrifuged at 1000 rpm for 5 min. The supernatant was removed, leaving the pellet in the conical tube. The cell pellet was resuspended in maintenance media, and seeded on cell-culture treated T25 flask. Cells were allowed to proliferate to 90-95% confluence. After reaching the target confluence, cells were suspended from the T25 flask surface using 0.05% Trypsin-EDTA. The suspended cells were diluted in maintenance

media. Afterwards, cell suspension was transferred to conical tube, then centrifuged at 1000 rpm for 5 min. The maintenance media and trypsin were aspirated out, and cell pellet was resuspended in maintenance media. The resuspended cells were used to seed the subsequent cell culture flasks.

5.2.4.2 PVA sample cell adhesion test in 24-well plate

Fabricated PVA samples (from Section 4.2.1.4) were cut into small pieces and placed into 24-well plate well. Silastic tube was cut into rings with 1cm in height. The PVA samples were clamped down using silastic tube. Cells were seeded onto the film at the seeding density of 20,000 cells/cm^2. The cells were cultured in experiment media overnight to allow for cell adhesion. Cells were washed with 1x PBS three times, then fixed by submerging in 4% paraformaldehyde (PFA) solution for 15 minutes. After fixing, 4% PFA solution was aspirated out. The samples were washed with 1x PBS for three times prior to immunofluorescence (IF) staining.

5.2.4.3 Cell culture on PVA sample strips

Seeding protocol developed to ensure consistent seeding onto PVA samples is shown in Figure 4.2. Customized seeding mold was made to for the purpose of seeding HUASMCs onto PVA samples strips. Poly(dimethyl siloxane) PDMS (Dow Corning, Syglard 184) crosslinking solution was made using 1:10 ratio of curing agent to base, mixed thoroughly, then centrifuged to remove air bubbles. The customized seeding mold was 3D printed. The seeding mold was coated with PDMS by dipping the seeding mold into PDMS, then letting the excess drip off. The customized seeding mold that was dipped in PDMS crosslinking solution was covered and was left in room temperature for two days.

PVA samples strips were loaded onto customized seeding mold. HUASMC were then seeded onto the PVA sample strips at the seeding density of 20,000 cells/cm^2, 30,000 cells/cm^2, or 40,000 cells/cm^2. The cells were allowed to adhere onto the PVA samples by incubating overnight cultured in experimental media. After overnight incubation, the experimental media was aspirated out. The samples were washed with 1x PBS three times. The samples were then fixed by submerging in 4% PFA for 15 minutes. After fixing, the samples were washed with 1x PBS three times prior to IF staining. The samples with different seeding density were stained with IF markers immediately after fixation.

For cyclic stretching, HUASMC were seeded onto PVA samples at the seeding density of 20,000 cells/cm^2. Four PVA samples were seeded per experiment. The cells were incubated in experimental

media, and allowed to adhere to the PVA samples overnight. The two strips of samples were then loaded into the MechanoCulture and submerged in experimental media. The remaining two strips of PVA samples seeded with HUASMC were removed from the seeding mold and were cut into four pieces per strip. Each piece was placed into a 24-well plate well. The pieces were then submerged in experimental media. The PVA samples loaded in MechanoCulture were stretched with 10% strain at 1 Hz for 4 hours. The samples were washed with 1x PBS three times after the cyclic stretching. After the mechanical stimulation, the samples were either fixed in 4% PFA for 15 minutes, or processed in the steps specified in Section 4.2.7 for western blot. The samples that were fixed were washed three times, then moved to 24-well plate wells, then used for the immunofluorescence staining stated in Section 4.2.5 and Section 4.2.6.

5.2.5 Proliferation assay

EdU assay (LifeTech) was performed following commercially available protocol [340]. In summary, 10 μM EdU solution (sterile-filtered 2-mercaptoethanol 10mM solution) was made in experiment media. The cells were incubated with EdU solution for 4 hours during the application of cyclic strain. EdU solution was also added to the control group for 4 hours of incubation concurrently. The samples were fixed and transferred to 24-well plate as stated in Section 4.2.4.3. Then, the cells were blocked by submerging in blocking buffer for at least 1 hour in room temperature. The blocking buffer was made using 10% goat serum + 0.03% Triton^{TM} X-100 (Sigma-Aldrich; for molecular biology) in 1x PBS. After blocking, the samples were washed three times with 1x PBS.

The samples were then stained by submerging in the staining solution for 1 hour at room temperature. The staining solution consisted of 676.5 μl of 1x PBS, 108.5 μl of 0.93M Tris-buffer, 10 μl of 100 mM CuSO4, 5 μl of 2 mM Alexa Fluor 488 azide (Thermo Fisher Scientific), and 200 μl of 0.5M ascorbic acid per 1 mL of staining solution. The plate containing the samples were wrapped with aluminum foil directly after adding the staining solution. Then, the samples were washed with 1x PBS three times. The samples were submerged in DAPI staining solution for 30 minutes. The dilution and description of the DAPI staining solution is shown in Table 4.2. The samples were washed with 1x PBS three times then were imaged using fluorescent microscope.

5.2.6 Immunofluorescence staining

5.2.6.1 Blocking

Samples were fixed and transferred into 24-well plate wells as described in Section 4.2.4.3. The cells were then blocked by submerging in blocking buffer for at least 1 hour at room temperature. The blocking buffer was made using 10% goat serum + 0.03% Triton™ X-100 in 1x PBS. After blocking, the samples were washed three times with 1x PBS.

5.2.6.2 Primary antibody

The cells were then incubated with primary antibodies overnight at 4°C. The primary antibodies that were used are: rabbit Desmin primary antibody (Life Technologies, ab32362; dilution from stock 1:50), mouse Vimentin primary antibody (Life Technologies, V2258-2ML; dilution from stock 1:200), rabbit PDGF-BB primary antibody (Thermo Fisher Scientific, bs-1316R; dilution from stock 1:100), mouse YAP primary antibody (Proteintech®, 66900-1-Ig; dilution from stock 1:100), and rabbit pMLCK primary antibody (Invitrogen, PA5-17726; dilution from stock 1:100). Desmin and Vimentin were co-stained, PDGF-BB and YAP were co-stained, and pMLCK was stained alone. The stock solution used for dilution was made following the protocol provided by the supplier.

5.2.6.3 Secondary antibody staining

The samples were washed with 1x PBS three times, then were stained using secondary antibodies for 30 minutes at room temperature. The secondary antibodies used were as follows: goat anti-mouse Alexa Fluor 488 (Thermo Fisher Scientific; dilution from stock 1:1000), goat anti-rabbit Alexa Fluor 488 (Thermo Fisher Scientific; dilution from stock 1:1000), goat anti-mouse Alexa Fluor 546 (Thermo Fisher Scientific; dilution from stock 1:1000), and goat anti-rabbit Alexa Fluor 546 (Thermo Fisher Scientific; dilution from stock 1:1000). The secondary staining solution was made so that it consisted of either goat anti-mouse Alexa Fluor 488 and goat anti-rabbit Alexa Fluor 546, or goat anti-mouse Alexa Fluor 546 and goat anti-rabbit Alexa Fluor 488. The plates containing the samples were covered using aluminum foil with the addition of secondary antibody solution. The secondary antibody solution was removed, and the samples were washed three times with 1x PBS. Lastly, the samples were stained with DAPI (Sigma Aldrich; dilution from stock 1:5000) and Alexa Fluor Phalloidin 647 (Invitrogen; dilution from stock 1:200).

5.2.6.4 Fluorescence imaging

Fluorescence images were acquired using Zeiss Microscope. Acquired fluorescence images were used for quantification of the signals. For EdU staining, positive nuclei was counted. The percent of positive nuclei were then calculated by dividing by the total number of cells counted. Fluorescence intensity of pMLCK signals and PDGF-BB were calculated by using ImageJ. The number of cells with concentrated PDGF-BB was quantified by counting the cells with spheres of high intensity of PDGF-BB. The concentrated PDGF-BB signal was defined as regions with PDGF-BB intensity that was 1.5 times higher than the adjacent regions. YAP nuclear localization was quantified by dividing the average intensity of the nucleus by the average intensity of the cytoplasm.

5.2.7 Western blot

Western blot was performed following the protocol by the Bio-Rad [341]. The modifications to the protocol were made to accommodate for the cyclic stretching system used in the experiments. The modifications are stated in this section.

5.2.7.1 Protein purification from HUASMCs seeded on PVA samples

Just before the completion of the cyclic stretching, Halt™ Protease & Phosphatase inhibitor cocktail (100x) (Thermo Scientific) was added to 1mL of Pierce™ RIPA buffer (Thermo Scientific) to make lysis cocktail. The lysis cocktail was placed onto ice until use. After 4 hours of cyclic stretching, the experiment media was aspirated out. The samples inside the MechanoCulture were washed three times with 1x PBS. 10 mL of 1x PBS was used for each wash, with the used 1x PBS aspirated out each time. The cells were scraped from the PVA sample, then pipetted into an Eppendorf tube. 100uL of lysis cocktail was added to the Eppendorf tubes. The cells were mixed with the lysis solution using pipet. The Eppendorf tubes were placed in ice, and were rocked for 30 minutes. The Eppendorf tubes were then centrifuged at 5000g for 1 hour. The supernatants were transferred to fresh Eppendorf tubes and were kept frozen until use.

5.2.7.2 Protein quantification

Protein concentration of the samples were quantified prior to performing western blot. The samples were thawed immediately prior to protein quantification. Protein extracted from Section 4.2.7.1 was quantified using Pierce™ BCA Protein assay Kit (Thermo Scientific) following the protocol provided by the manufacturer [342]. The standard for the working range of 20-2,000 μg/ml was made.

Working reagent (WR) was prepared by mixing BCA Reagent A with BCA Reagent B in 50:1 ratio. The protein quantification was performed using microplate. 10uL of each unknown sample and standards were pipetted into each well. Each sample and standard consisted of triplicates. WR was added to each well so that the sample to WR ratio was 1:20. After addition of WR, the plate was mixed by placing on the shaker for 30 seconds. The plate was covered, and incubated at 37℃ for 30 minutes. The plate was cooled to room temperature, then the absorbance was measured at 562nm on a plate reader. The average absorbance of the blank standard was subtracted from other measurements. Afterwards, the average absorbance of each standard and each sample were calculated. The standard curve was plotted in EXCEL. The concentration of the proteins of the samples were determined by using the created standard curve.

5.2.7.3 Gel electrophoresis

Electrophoresis buffer (EB) was made by diluting 10x Tris/Glucine/SDS Buffer (Bio-Rad) in DI water. 4x Laemmli Sample Buffer (Bio-Rad) was used to dilute the samples. Blank sample buffer dilution was also made using ultra-pure DI water and sample buffer. The diluted sample solution was activated at 90℃ for 5 minutes. The samples were allowed to cool down enough so that they were safe to touch. Then, Mini-PROTEAN TGX Stain-Free Gels 4-15%, 10-well comb, 30uL (Mini Gel; Bio-Rad) was unwrapped and placed into the gel electrophoresis clamp. The clamp was placed into the gel electrophoresis chamber. The EB was poured into the clamp enough so that the buffer overflowed. The buffer level was observed intermittently for 10 minutes to ensure no leakage. When there was no leakage, EB was poured into the gel electrophoresis chamber to indicated level. The wells in Mini Gel were cleared of any potential air bubbles or debris by pipetting in each well gently using micropipette. Then, samples were loaded into the wells so that 1mg/ml of protein was loaded in each well. 5 µl of Precision Plus Protein Unstained Standards* (Bio-Rad) was loaded in one of the wells. The blank was also loaded in one of the wells. The lid of the gel electrophoresis chamber was closed to complete the circuit. The protein migration was allowed to occur at the voltage of 200 V at 1.5 A for 15 minutes, or until the sample buffer migrated just beyond the indicated line at the bottom of the Mini Gel. The Mini Gel was removed from the holder by using the key. The Mini Gel was imaged using ChemiDoc (ChemiDoc™ MP Imaging System; Bio-Rad) to ensure even protein migration. If the protein migration was deemed good, then the gel was used to transfer the protein onto the transfer membrane.

5.2.7.4 Protein transfer onto transfer membrane

Trans-Blot Turbo 5x Transfer Buffer (Bio-Rad) was diluted using DI water prior to used. The diluted transfer buffer was stored in the fridge in long enough advance to cool the solution to 4℃. The TransBlot® Turbo™ Mini-size LF PVDF Membrane, 7.1cm x 8.5 cm (transfer membrane; Bio-Rad) was wetted with methanol for at least 30 minutes prior to wetting in transfer buffer. The Western Blotting Filter Paper, 7cm x 8.4cm, thickness 0.83mm (filter paper; Thermo Scientific) were wetted with transfer buffer along with the transfer membrane. The transfer sandwich was made so that the order was filter paper, gel, transfer membrane, and filter paper starting from cathode (- end) to anode (+ end). The gel was transferred at 20V, with maximum amperage of 1 Amps, for 1 hour. The gel and the transfer membrane were imaged using ChemiDoc to ensure good transfer. The gel was discarded if there was complete protein transfer.

5.2.7.5 Immunoblotting

The transfer membrane was placed in SuperBlock™ Blocking Bugger in TBS (blocking buffer; Thermo Fisher Scientific) and were blocked with agitation for at least 2 hours at room temperature. The blocking buffer was discarded. Then, the membrane was blocked using the blocking buffer for 2 additional hours. The transfer membrane was then submerged in primary antibody solution made using the anti-rabbit PDGF-BB antibody (Invitrogen; dilution from stock 1:1000) in blocking buffer. The transfer membrane was stored with agitation in the primary antibody solution for at least 2 hours at room temperature. The primary antibody solution was removed, and the transfer membrane was washed with 1x PBS. Each wash consisted of 10 minutes of agitation in 1x PBS at room temperature. The secondary antibody solution was made using goat anti-rabbit Alexa Fluor 488 (Invitrogen; dilution from stock 1:2,000). The transfer membrane was then submerged in secondary antibody solution and were incubated with agitation for 1 hour at room temperature. The secondary antibody solution was diluted according to the suggestions of the manufacturer. The secondary antibody was removed after the 1hr incubation and was washed three times with 1x PBS. The transfer membrane was then imaged using ChemiDoc.

5.2.7.6 Quantification of protein

The immunofluorescence protein signal was quantified using ImageJ. Total protein was used as the control for normalization of the data. The values of the IF signal of the target protein were divided by

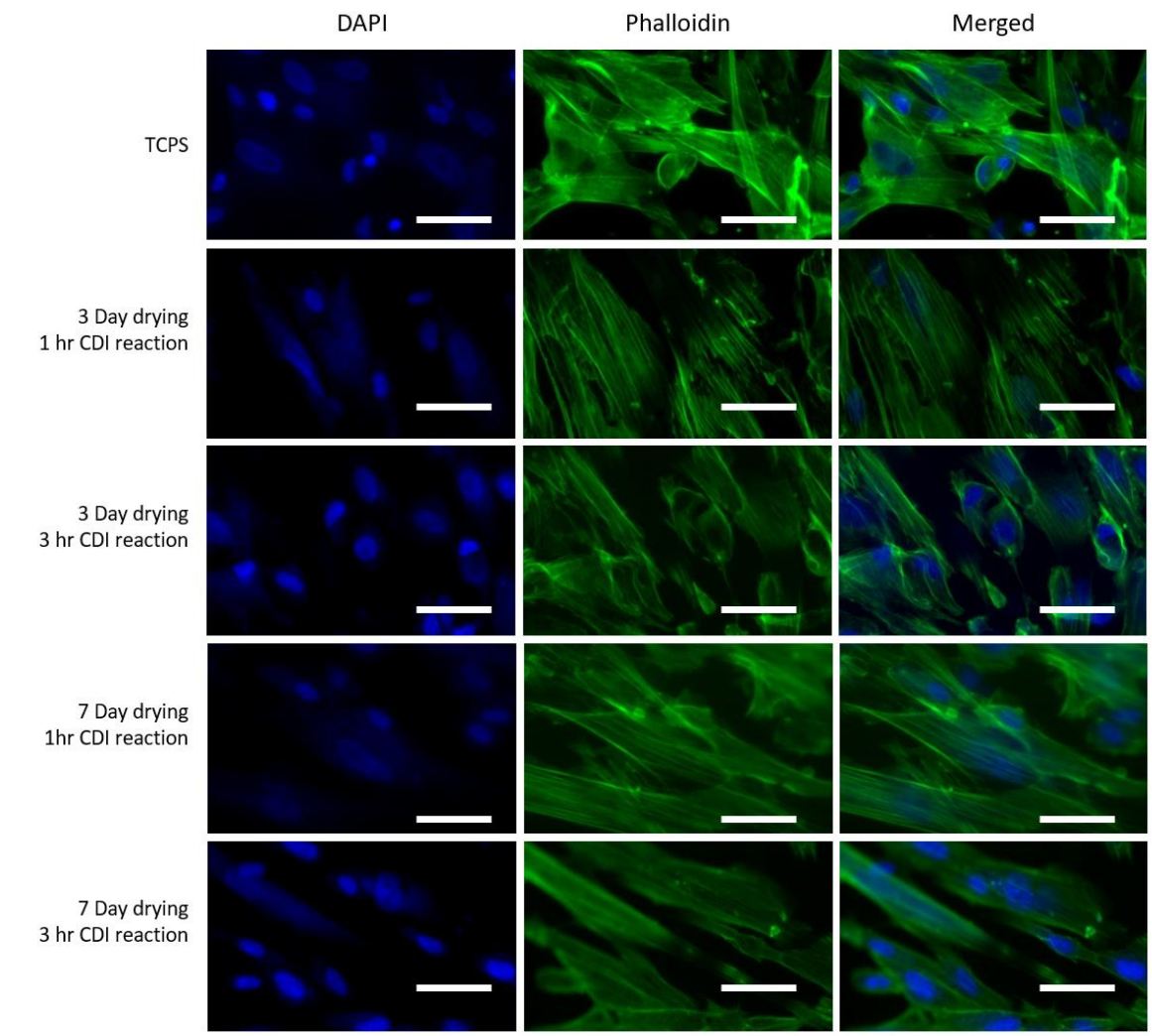

Figure 5.2. PVA-CDIg modification and verification of cell adhesion on PVA fabricated with different gelatin immobilization conditions. PVA – poly(vinyl alcohol), CDI – Carbonyldiimidazole, and g – gelatin. Scale bar shown is 50µm.

the normalized control value to achieve relative expression of the target protein. Statistical analysis was performed on the relative expression of the target protein after the normalization.

5.2.8 Statistical analysis

Statistical significance was determined using a two-way ANOVA followed by Tukey's multiple comparison analysis with 95% confidence interval using MatLab. The data are presented as mean ± standard deviation. For all the presented data, $p<0.05$ is denoted by * unless otherwise specified in the figure caption.

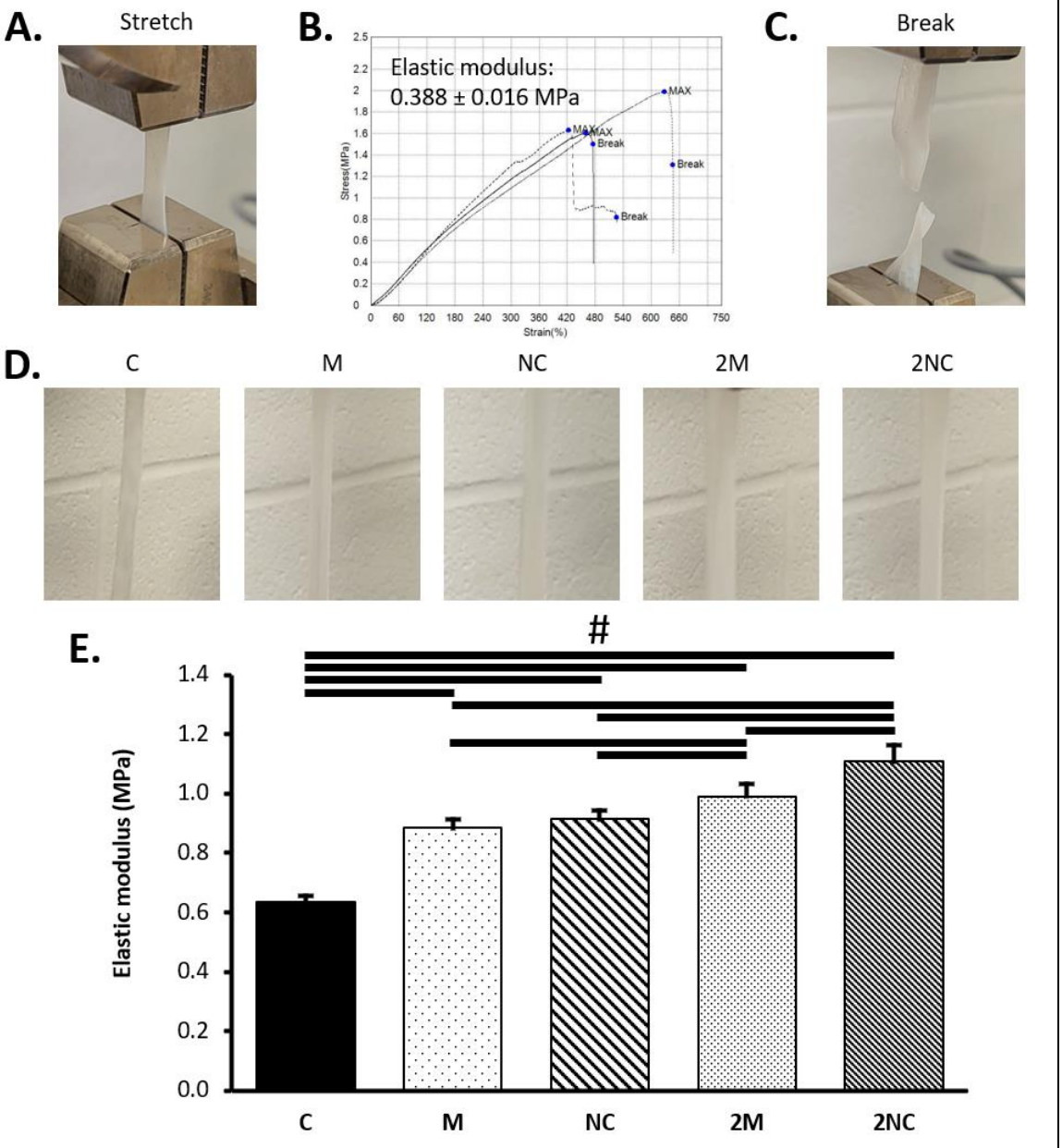

Figure 5.3. Characterization of PVA samples. (A) Image of the sample in tensile test. The film is oriented so that the mismatch line was perpendicular to the stretch direction. (B) the stress-strain curve of the mismatched sample from tensile test shown in (A). (C) image of a break during tensile test while the mismatch line was parallel to the stretch direction. (D) Images of the samples during tensile test. C-Compliant, M – compliance mismatch, NC – not compliant, 2M – higher compliance mismatch, and 2NC – higher not compliant. The tensile tests for M and 2M were performed with the mismatch line parallel to the direction of stretch. (E) Elastic moduli of the groups. N=3 for each group. * indicates statistical significance between indicated groups with $p<0.05$. Two-way ANOVA used for statistical analysis.

5.3 Results

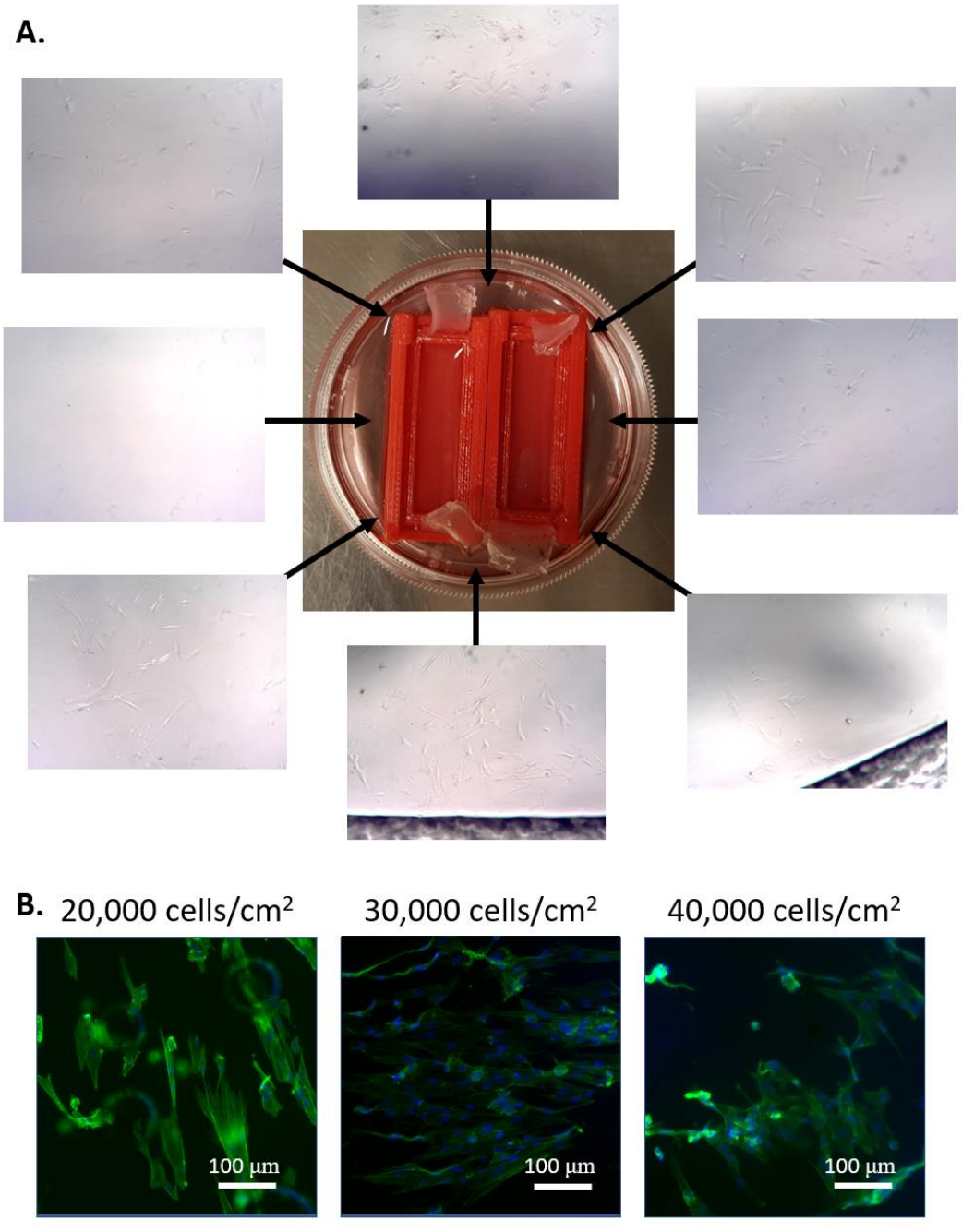

Figure 5.4. Verification of cell seeding protocol. (A) Image of the seeding molds in use and surrounding surface after overnight of incubation. (B) F-actin immunofluorescence staining of HUASMCs seeded with defined seeding density.

5.3.1 Verification of sample properties

5.3.1.1 Cellular adhesion

PVA hydrogel does not support cellular adhesion without chemical modification. Therefore, the protocol had to be modified to ensure proper incorporation of gelatin on PVA surface using CDI reaction. As CDI is highly reactive with water, PVA-CDI reaction must occur in anhydrous condition [343]. Two different drying times were tried to identify the level of dryness required for PVA-CDI reaction of the hydrogel with desired dimensions. Also, the length of CDI-gelatin reaction required for the immobilization of gelatin was explored. Figure 5.2 shows the different reaction times used for each step. The VSMCs cultured on PVA hydrogels that were dried for 3 days displayed lack of uniform cellular adhesion regardless of the CDI-gelatin reaction time. The PVA samples with 7 days of drying resulted in good cellular adhesion regardless of the CDI-gelatin reaction time. Therefore, PVA samples with 7 days of drying and 1 hour of CDI reaction was labeled and referred to as PVA-CDIg, and were used in subsequent experiments.

5.3.1.2 Physical properties

Elastic modulus was measured for each sample to measure the stiffness of each of sample. Also, the published chemical modification of PVA using CDI reaction requires drying of the PVA hydrogel [28]. It is known that the drying of PVA hydrogel could cause changes in the stiffness of the hydrogel [21]. Therefore, the stiffness of the PVA samples were measured after CDI-gelatin modification.

To ensure the continuity of the samples, tensile test was performed so that the compliance mismatch line was perpendicular to the direction of stretch. The samples remained intact and displayed linear relationship in stress vs. strain graph until at least 360% strain (Fig 5.3A and fig. 5.3B). Furthermore, the tensile test was performed so that the compliance mismatch line was parallel to the stretch direction (Fig. 5.3 C-E). The samples displayed clean break throughout the sample when the compliance mismatched line was parallel to the direction of stretch (Fig 5.3C). Therefore, the samples were concluded to have good integration of the chemically crosslinked PVA film in physically crosslinked PVA sample.

Figure 5.3E shows the elastic modulus of each of the sample groups. C represents the PVA samples with elastic modulus similar to the native blood vessels. C showed elastic modulus of 0.636±0.021 MPa, which is similar to the reported elastic modulus of the native blood vessels of 0.683±0.147

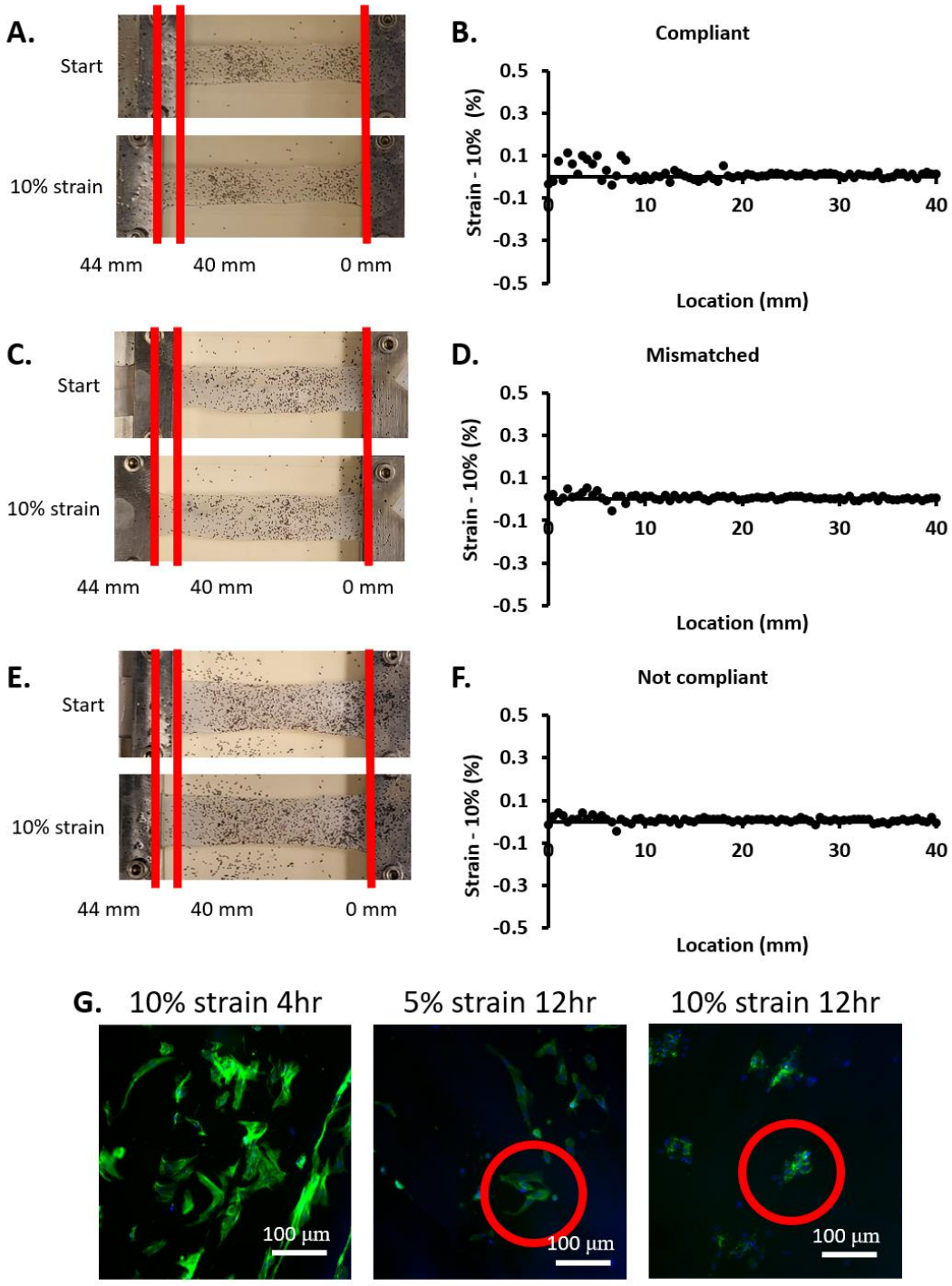

Figure 5.5. Verification of strain and cell confluence after cyclic strain. (A) Image at initial length and at 10% strain of compliant sample. (B) Strain deviation from 10% strain for compliant samples. (C) Image at initial length and at 10% strain of mismatched sample. (D) Strain deviation from 10% strain for mismatched samples. (E) Image at initial length and at 10% strain of not compliant sample. (F) Strain deviation from 10% strain for not compliant samples. (G) F-actin immunofluorescence staining of HUASMCs seeded on compliant samples after exposure to cyclic stretching of defined strain and duration.

[102, 304].NC is a sample that is stiff throughout the entire sample with the elastic modulus of 0.915±0.042 MPA throughout the sample. M is the compliance mismatch samples with compliant region having the elastic modulus of C and not compliant region having the elastic modulus of NC in a continuous film. 2NC had elastic modulus were 1.109±0.055MPa. Lastly, 2M samples are compliance mismatched samples with elastic modulus of C sample in the compliant region and elastic modulus of 2NC sample in the not compliant region in a continuous film. The elastic modulus of the stiff regions in 2M samples were comparable to the circumferential elastic modulus of the PVA grafts, which were 1.08±0.03 MPa, published in the literature [29], while being significantly lower compared to the elastic modulus of ePTFE is 42.9±2.6MPa [311]. Therefore, while 2M samples cannot be used to estimate the compliance mismatch between the native blood vessels and ePTFE graft, 2M can be used to reflect the compliance mismatching between the native blood vessels and PVA grafts, which had thicker wall thickness without optimization to achieve compliance matching.

5.3.2 Verification of cell seeding procedure

Figure 5.4A shows the custom-made seeding molds being used for the seeding of HUASMC on PVA samples. The images of the cells that leaked from the seeding mold are shown as well. Different seeding densities were tried in order to identify the ideal seeding density to achieve confluence of 50-60%. In Figure 5.4B, the samples seeded with different seeding density are shown. The samples seeded with 20,000 cells/cm^2 and 40,000 cell/cm^2 had confluence of 50-60%. The samples seeded with 30,000 cells/cm^2 resulted in confluence of 80-90%. It was observed that the samples seeded with the seeding density of 40,000 cells/cm^2 resulted in formation of cell clusters and areas with no cells. Therefore, the following experiments were performed with the seeding density of 20,000 cells/cm^2.

5.3.3 Verification of uniform strain throughout the sample during cyclic loading

For experiments exposing the cells to cyclic stretching, it is important that the sample does not have localization of strain. The formation of localized variation in strain was additionally of concern as the PVA-CDIg samples have two regions with different elasticity. Therefore, strain map was made to ensure there was uniform strain throughout the sample. Figure 5.5A is a representative image from the video used for particle tracking for assessing the strain on compliant sample. The resulting strain is plotted in Figure 5.5B. The strain map revealed that the samples were being subjected to uniaxial stretching with 10% strain, resulting in 1D stretching in y-direction. No movement of the particles were observed in the direction perpendicular to the stretch direction (x-direction). Figure 5.5C is a

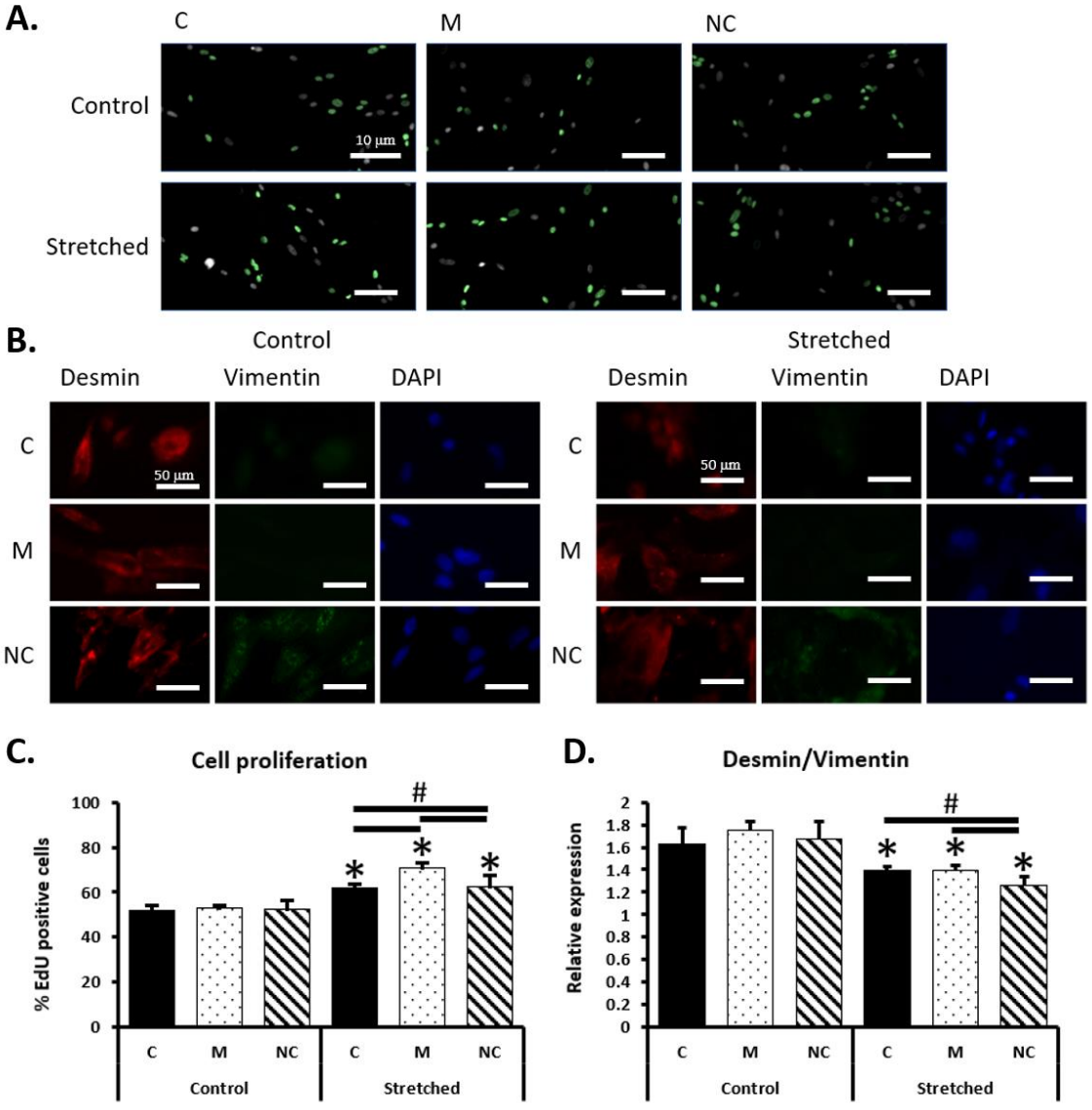

Figure 5.6. Cell proliferation and phenotypic analysis of HUASMC. (A) Representative images of EdU assay. (B) Representative immunofluorescence (IF) image of each sample for Desmin, Vimentin, and DAPI staining. Samples seeded with human umbilical arterial smooth muscle cells (HUASMC) were exposed to 10% strain for 4 hours before IF stain. C-compliant, M-mismatched, and NC-not compliant. Scalebar=50μm. (C) cell proliferation quantified using EdU assay. (D) Ratio of IF signal intensity of Desmin to Vimentin. * indicates statistical significance between indicated groups to their respective control group with $p<0.05$. # indicates statistically significant difference between the indicated groups with $p<0.05$. Two-way ANOVA used for statistical analysis. N=6. Number of cells per sample=100.

representative image of compliant mismatched sample used for stain mapping. The resulting strain is plotted in Figure 5.5D. Figure 5.5E is a representative image of the compliant sample. The resulting strain is plotted in Figure 5.5F. Note that the plots are centered around 10% strain to visualize the deviation from the 10% strain. It was found that the deviation from 10% strain was less than 0.1%

throughout the samples for all samples. Therefore, the platform was deemed as suitable for the cyclic stretch study.

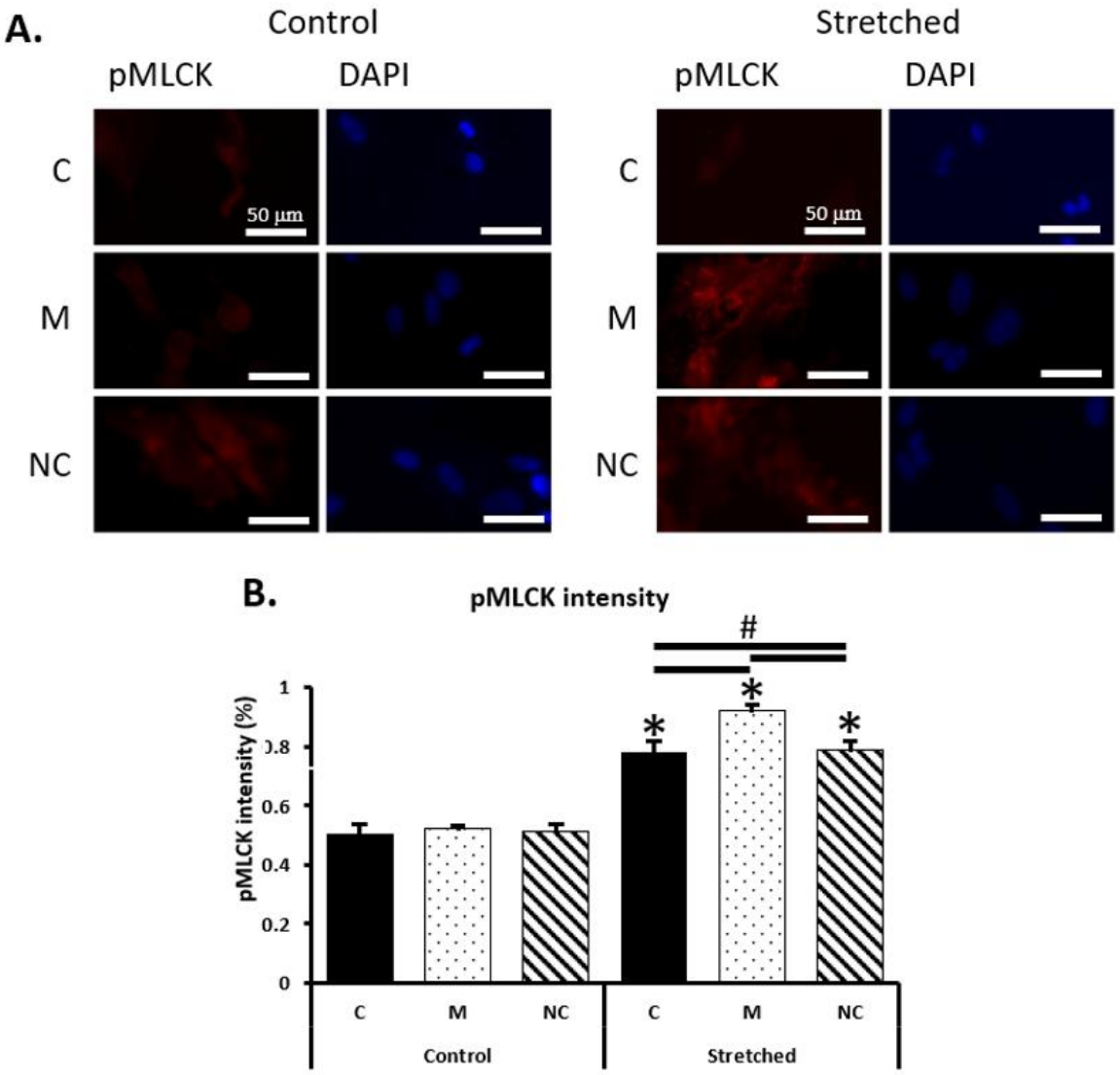

Figure 5.7. Expression of pMLCK in HUASMC. (A) Representative immunofluorescence (IF) stain of pMLCK. pMLCK – phosphorylated Myosin light-chain kinase. Samples seeded with human umbilical arterial smooth muscle cells (HUASMC) were exposed to 10% strain for 4 hours before IF stain. C-compliant, M-mismatched, and NC-not compliant. Scalebar=50μm. (A) Quantification of pMLCK intensity from IF stain. * indicates statistical significance between indicated groups to their respective control group with $p<0.05$. # indicates statistically significant difference between the indicated groups with $p<0.05$. Two-way ANOVA used for statistical analysis. N=6. Number of cells per sample=100.

Afterwards, the strain and duration of cyclic stretching was tested to identify the experimental setup (Figure 5.5G). The duration and magnitude of the cyclic stretching needed to be identified as they are important factors in mechanical stimulation experiments. Compliant samples were used to test the

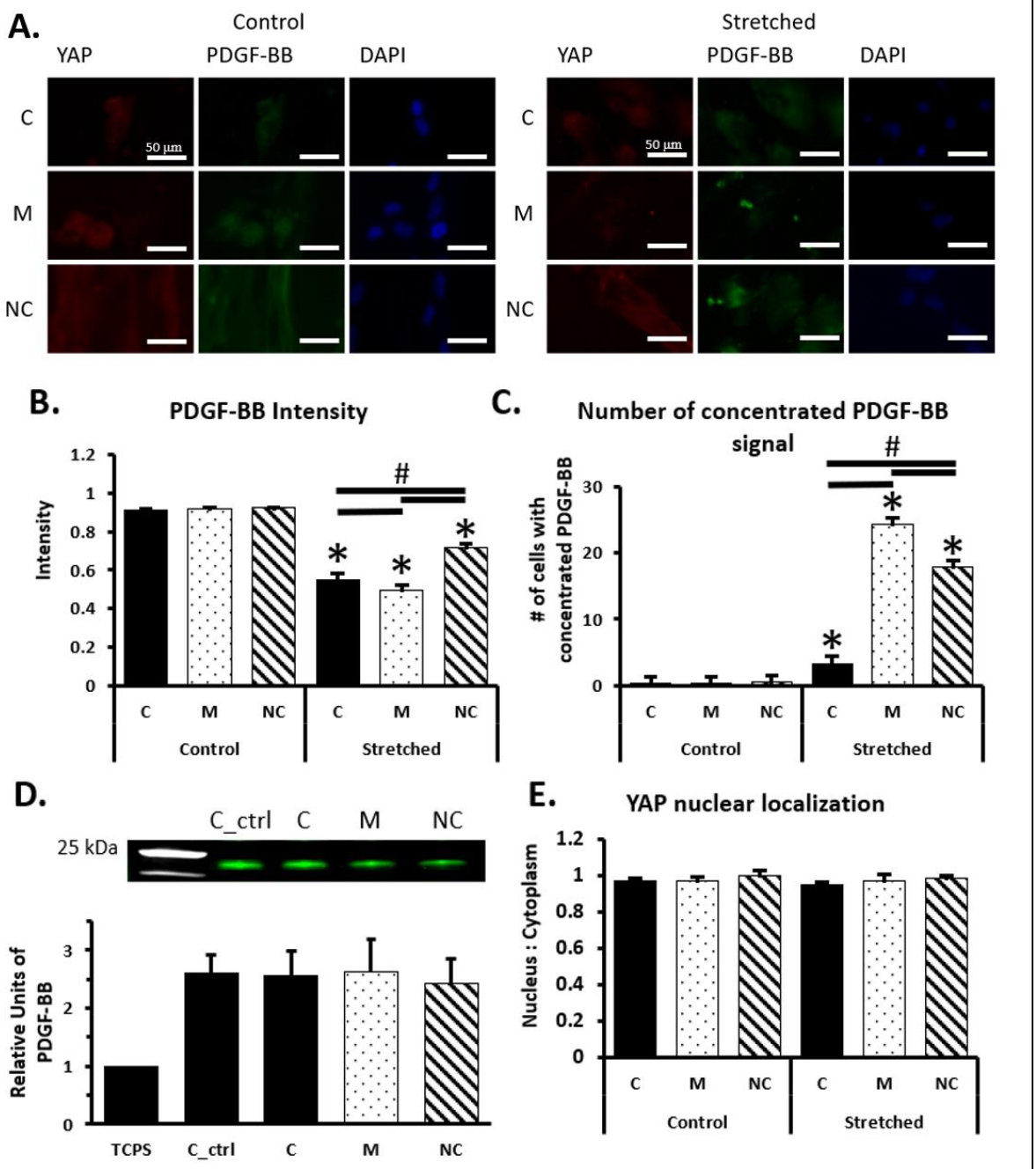

Figure 5.8. Distribution of PDGF-BB and YAP within HUASMC. (A) Representative immunofluorescence (IF) stain of PDGF-BB and YAP. PDGF-BB – platelet derived growth factor-BB, and YAP – yes-associated protein. Samples seeded with human umbilical arterial smooth muscle cells (HUASMC) were exposed to 10% strain for 4 hours before IF stain. C-compliant, M-mismatched, and NC-not compliant. Scalebar=50μm. (B) Quantification of intensity of PDGF-BB. (C) Number of cells with concentrated PDGF-BB signal. (D) Western blot of HUASMCs for PDGF-BB. C_ctrl = compliant sample without exposure to cyclic stretching. (E) Ratio of nuclear to cytoplasmic YAP. * indicates statistical significance between indicated groups to their respective control group with $p<0.05$. # indicates statistically significant difference between the indicated groups with $p<0.05$. Two-way ANOVA used for statistical analysis. N=6. Number of cells per sample=100.

following conditions: 10% strain for 4 hours, 5% strain for 12 hours, and 10% strain for 12 hours. Both of the 12 hr stretching resulted in samples with low cell density after stretch, and observation of cell clusters. The cell clusters were not visible in samples that were stretched for 4 hrs with 10% strain. The cells cultured on samples stretched for 4 hrs with 10% strain also displayed good cell adhesion. Therefore, the following experiments were decided to have 10% cyclic strain for 4 hours.

5.3.4 Effects of compliance mismatch on HUASMC

HUASMCs were stained with various biomarkers to visualize the cellular responses to the mechanical stimulation. The cells were stained with Desmin, Vimentin, PDGF-BB, YAP, and pMLCK along with DAPI and F-actin. For understanding the role of compliance mismatch in development of IH, proliferation and migration must be assessed. EdU assay is a DNA proliferation assay, where EdU binds with the replicating DNA. The assay displayed that the cells had higher proliferation after mechanical stimulations (Figure 5.6A and Figure 5.6C). Among the groups, HUASMC cultured on mismatched films displayed highest proliferation. Desmin and Vimentin staining is used to determine the phenotype of VSMCs [344-346]. Figure 5.6B shows the IF images of the cells that were stained with Desmin, Vimentin, and DAPI, and the quantification is shown in Figure 5.6D in terms of Desmin to Vimentin ratio. The decrease in desmin to vimentin ratio observed in Figure 5.6D after exposure to cyclic stretching indicates that the cells displayed migratory phenotype [346]. The ratio of desmin to vimentin was lowest for the not compliant group exposed to cyclic stretching.

Increase in expression of pMLCK is observed in VSMC with contractile phenotype [347]. Figure 5.7A shows IF stain images of pMLCK and DAPI with and without exposure to cyclic stretching. The IF signal was quantified and plotted as shown in Figure 5.7B. It was found that all of the groups exposed to the cyclic stretching resulted in higher expression of pMLCK compared to the control groups. Among the stretched group, mismatched groups displayed significantly higher expression of pMLCK.

Both PDGF-BB and YAP are known to be influenced by the stiffness of the substrate as well as the presence of mechanical stimulation [335, 348]. Both PDGF-BB and YAP are associated with increase in SMC proliferation [336, 349]. PDGF-BB is known to bind with PDGF receptor to start proliferation cascade [264]. YAP stays scattered throughout the cells normally, then undergoes nuclear localization when the cells become proliferative phenotype [336]. Figure 5.8A shows the IF staining of PDGF-BB, YAP, and DAPI. The overall intensity was quantified, and shown in Figure

5.8B. It was found that the overall expression of PDGF-BB was lower for the group exposed to the mechanical stimulation, with mismatched sample having the lowest intensity. However, pockets with high intensity of PDGF-BB were observed in M and NC after exposure to cyclic stretching. Therefore, the number of cells with the concentrated PDGF-BB signal was quantified (Fig. 5.8C). The groups exposed to cyclic stretching resulted in higher number of cells with concentrated PDGF-

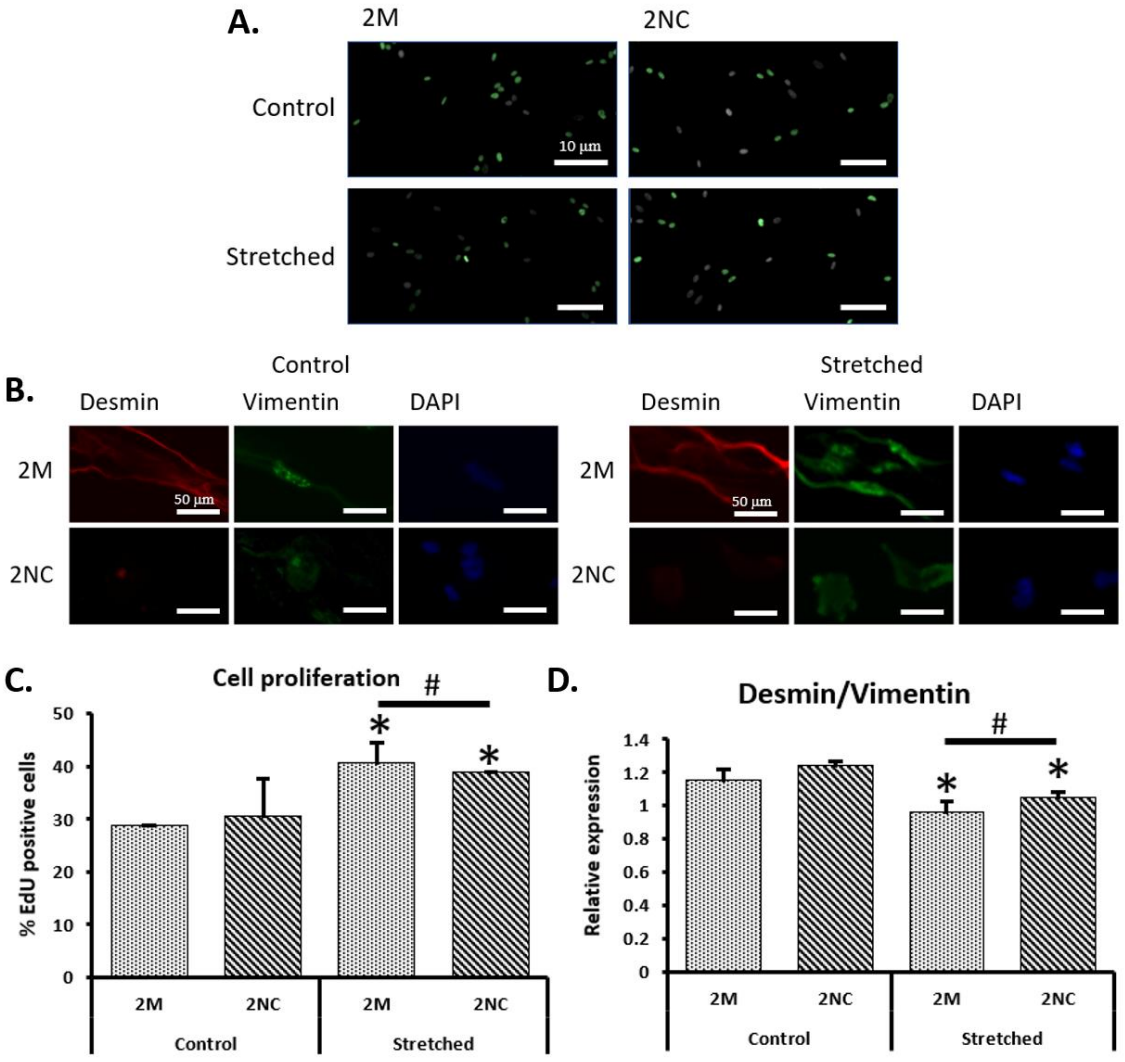

Figure 5.9. Proliferation and phenotypic changes on HUASMC cultured on higher compliance mismatch with and without cyclic stretch. (A) Representative images of EdU Assay. (B) Immunofluorescence (IF) stain of Desmin and Vimentin. Samples seeded with human umbilical arterial smooth muscle cells (HUASMC) were exposed to 10% strain for 4 hours before IF stain for stretched group. 2M – higher compliance mismatch. Scalebar=50µm. (C) cell proliferation quantified using EdU assay. (D) Ratio of IF signal intensity of Desmin to Vimentin. # indicates statistically significant difference between the indicated groups with $p<0.05$. Two-way ANOVA used for statistical analysis. N=6. Number of cells per sample=50.

BB signal. To assess whether there was difference in total expression of PDGF-BB, western blot was performed on the samples exposed to cyclic stretching (Fig. 5.8D). There was no difference in PDGF-BB expression. Lastly, YAP nuclear localization was quantified and shown in Figure 5.8E. No differences were observed among the samples.

5.3.5 Effects of higher compliance mismatch on HUASMC

Additional samples were made to test the effects of the higher compliance mismatch. 2M and 2NC samples were exposed to cyclic stretching with the sample parameters as the previous groups. Representative images of EdU assay are shown in Figure 5.9A. EdU assay was used to determine the proliferation of the cells, and the quantification are shown in Figure 5.9C. There was significant increase in the number of proliferative cells after exposure to the mechanical stimulation. Representative IF images of Desmin and Vimentin staining are shown in Figure 5.9B. The ratio of the IF intensity of Desmin and Vimentin were calculated and shown in Figure 5.9D. The ratio of Desmin to Vimentin was higher for the control group compared to the stretched group. Therefore, it can be concluded that HUASMC displayed proliferative and migratory phenotype after exposure to stretch on higher compliance mismatched film. C are the compliant samples with elastic modulus of 0.636±0.021 MPa, which is comparable to the reported elastic modulus of the native blood vessels of 0.683±0.147 [102, 304]. NC is a sample that is stiff throughout the entire sample with the elastic modulus of 0.915±0.042 MPA throughout the sample. M is the compliance mismatch samples with compliant region having the elastic modulus of C and not compliant region having the elastic modulus of NC in a continuous film. In addition to M and NC, 2M and 2NC were developed to test whether different severity of compliance mismatch could also affect VSMC. 2NC are uniform samples with the elastic modulus of 1.109±0.055MPa, which is similar to the reported elastic modulus of 1.08±0.03 MPa for PVA grafts [29]. 2M is the compliance mismatched samples comprised of region with elastic modulus of compliant samples on one side, and region with elastic modulus of not compliant samples on the other side. PVA from PVA fucoidan is not compliance matching and close to 2NC without optimization. Although 2NC is still far from ePTFE, it would still be one step physiologically closer to determining the effects of compliance mismatch. 2M displayed higher cell proliferation and lower Desmin to Vimentin ratio compared to 2NC. This could indicate that VSMC proliferation and migration could be increased when using PVA grafts in vascular bypass.

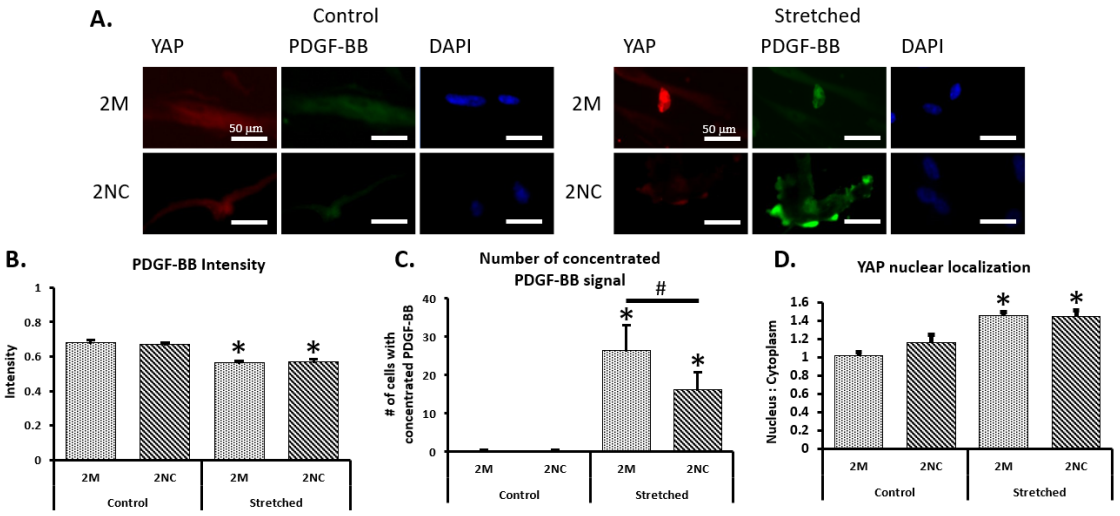

Figure 5.10. Comparison of YAP and PDGF-BB with HUASMCs cultured on 2M with and without cyclic stretch. (A) Representative immunofluorescence (IF) stain of PDGF-BB and YAP. PDGF-BB – platelet derived growth factor-BB, and YAP – yes-associated protein. Samples seeded with human umbilical arterial smooth muscle cells (HUASMC) were exposed to 10% strain for 4 hours before IF stain for stretched group. 2M – higher compliance mismatch. Scalebar=50μm. (B) Intensity of PDGF-BB. (C) Number of cells with concentrated PDGF-BB signals. (D) Ratio of nuclear to cytoplasmic YAP. # indicates statistically significant difference between the indicated groups with $p<0.05$. Two-way ANOVA used for statistical analysis. N=6. Number of cells per sample=50.

The experiments were repeated with 2M samples, then stained with YAP and PDGF-BB antibodies to test the effects of higher compliance mismatch. The IF staining of YAP and PDGF-BB is shown in Figure 5.10A. The PDGF-BB intensity was lower (Fig. 5.10B), while the number of cells with concentrated PDGF-BB signal was higher for the stretched group (Fig. 5.10C). 2M had higher number of cells with concentrated PDGF-BB signal compared to 2NC. Also, it was observed that the location of the concentrated PDGF-BB signal overlapped with the DAPI signal, indicating that the PDGF-BB could have migrated into the nucleus. Lastly, the YAP nuclear localization was observed for the higher compliance mismatch (Fig. 5.10D). 2NC displayed comparable amount of nuclear localization compared to 2M.

5.4 Discussion

Currently available sSDVG face low patency due to intimal hyperplasia (IH). IH refers to stiffening of the vascular wall due to migration and excessive proliferation of VSMC. It is known to develop near the heel, toe, and floor of distal anastomosis [14]. There are multiple factors that affects development of IH. It can be triggered due to biomechanical factors, material incompatibility of the graft, WS, as well as WSS [14]. The detailed review on factors contributing to the onset and development of IH was published in 2020 [14]. One of the biomechanical factors that is hypothesized

to influence onset and development of IH is compliance mismatch [23, 41, 45, 114, 273]. Despite many efforts, the exact extent of the effects of compliance mismatch on IH, and therefore on the failure of sSDVG, is still not fully understood.

The mechanical properties of the surroundings affecting the cellular behavior is a well-observed phenomenon. In stem cells, mechanical cues are shown to cause the differentiation as well as self-renewal [87]. In the study published by Bandaru et al. in 2020, they addressed the effects of mechanical elasticity on angiogenesis by human mesenchymal stem cells [350]. In osteoblasts, substrate stiffness is shown to influence the functional maturation [351]. Basal epithelial cells have displayed varying level of nuclear localization of YAP depending on the stiffness of the substrate [348]. Additionally, PDGF-BB has been known to influence the proliferation of VSMCs [335], and has been found to be upregulated in cells exposed to WS [157]. Behaviors of VSMC are also affected by mechanical stimulation. For example, VSMC exposed to mechanical injury resulted in increased expression of vimentin and decreased expression of desmin [352]. Studies have found that exposure to cyclic strain causes VSMC to release PDGF-BB, triggering [268] cell proliferation and migration.

5.4.1 Development of continuous compliance mismatched samples

There are many difficulties in understanding the effects of compliance mismatch on IH. One of the difficulties is to decouple the mechanical factors. WS, WSS, suture-line, and compliance mismatch are all factors that can contribute to the development of IH. These factors are difficult to parse as they occur concurrently *in vivo*. In order for a vascular graft to be implanted, it has to be sutured onto the native blood vessels. Implantation can cause disturbance on the blood vessel wall leading to development of abnormal WS around the anastomosis. Also, the suture-line causes localized high stress to occur around the sutures [24]. The angle and size of the anastomosis and the shape of the graft contribute to the development of abnormal WSS. Lastly, compliance mismatch can contribute to development of both abnormal WS and abnormal WSS. While the effects of suture-line, WS, and WSS on VSMC have been studied, the decoupled effect of compliance mismatch has not been studied yet. The benefit of having a continuous compliance mismatched film is that it can simplify the analysis by removing the suture-line. It is inevitable that suture-line will be formed in *in vivo* experiments, as a vascular graft has to be implanted. Therefore, it is important to develop an *in vitro* model with continuous compliance mismatch film that can be used to study the isolated effects of compliance mismatch.

PVA used in literature are crosslinked primarily through physical crosslinking method using freeze-thaw cycle or chemical crosslinking method using STMP. The number of freeze-thaw cycles can be used to vary the elastic modulus of the resulting PVA hydrogel to be in the 50-250 kPa range [353]. The polymer concentration can be further changed to achieve higher elastic modulus ranging between 40-90 MPa [90]. PVA hydrogel chemically crosslinked with STMP have been reported to have the elastic modulus of 200 kPa [25]. Furthermore, making continuous hydrogel with different stiffness can be achieved by PVA. For example, methods to make continuous PVA hydrogels with varying stiffness has been studied [87]. In the study published in 2015, stiffness gradient was achieved by varying the freeze-thaw cycle to study the stem cell differentiation in response to the stiffness of the substrate [87].

While achieving stiffness gradient in a continuous hydrogel can be useful, it cannot be used to study the effects of compliance mismatch. For compliance mismatch, a continuous film with two sections having distinctively different stiffness is required (Fig. 5.1A). By combining the chemical and physical crosslinking method (Fig. 5.1B-D), a continuous PVA hydrogel with compliant and not compliant sides were made as shown in Figure 5.1C. However, the gel had to be modified further as PVA without biochemical modification does not support cell adhesion. The dehydration step required for CDI-gelatin modification can alter the stiffness of the resulting PVA hydrogels [28]. Therefore, it was important to measure the elastic modulus of the samples after the CDI-gelatin modification was performed. Figure 5.2 shows the different reaction times used for PVA-CDI-gelatin reaction. It was found that 3-day drying of the PVA hydrogels resulted in inconsistent HUASMC attachment regardless of the length of the CDI-gelatin reaction time. Both 7-day drying and 1-hour CDI-gelatin reaction as well as 3hour of reaction resulted in uniform cellular attachment. Therefore, the biochemical modification step of 7 days of drying and 1 hour of CDI-gelatin reaction was used for the samples for the subsequent experiments.

After determining the procedures for the fabrication of PVA compliance mismatched samples, tensile tests were performed to quantify the elastic modulus of each sample. As shown in Figure 5.3A-C, the compliance mismatched PVA samples had good integration of physically and chemically crosslinked PVA. Compliance in vascular graft is a measure of strain when the graft is exposed to a specified internal pressure. Therefore, measuring compliance of a film is difficult due to the geometric limitation. Here, the compliance of the PVA samples were estimated using the elastic modulus, which is a measurement describing the relationship between strain and stress of the film.

The elastic modulus of the native blood vessels have been reported to vary from 0.3 - 5.5 MPa [354]. Therefore, the elastic moduli of the samples fall within the range of the elastic modulus possible by native blood vessels. Also, elastic moduli of C, M, NC, 2M, and 2NC displayed significant difference between each other with exception of M and NC. M used for the experiments consisted of the compliance side with the elastic modulus of 0.636 ± 0.021 MPa and not compliant side consisting of 0.915 ± 0.029 MPa. As shown in Figure 5.3E, the 2M samples consisted of the compliant side same elastic modulus as compliant side of M and not compliant side with the elastic modulus of 1.109 ± 0.055 MPa. The 2M samples displayed elastic modulus value that is comparable to reported value of circumferential elastic modulus of small-diameter PVA graft [29], and therefore was used to study more physiologically relevant compliance mismatch. It was concluded that the physical and chemical crosslinking of PVA hydrogel resulted in continuous compliance mismatched sample with physiologically relevant elastic modulus.

The dimension and seeding density needed to be identified prior to performing *in vitro* experiments for reliable results. The samples have to be 1 cm by 6 cm in dimensions in order to be loaded onto MechanoCulture to be exposed to cyclic stretching. To ensure even seeding, customized seeding mold was made (Fig. 5.4A). The seeding method using the custom-made mold resulted in leakage of the cells along the shorter edges of the seeding mold. However, there were no cells observed along the long edges of the seeding molds, and the samples resulted in consistent seeding. The second consideration is the seeding density. VSMC is one of the cell types that display contact inhibition [355, 356]. To maximize the understanding of proliferation and migration of the VSMC, confluence of 50-60% was chosen to avoid contact inhibition. After trying different seeding densities, 20,000 cells/cm^2 yielded 50-60% seeding density (Fig. 5.4B).

Because the developed sample contained two distinct sections with different stiffness, the strain-map had to be made in order to verify uniform strain throughout the samples. Strain mapping tracks the movement of the particles in 2D direction. As shown in Figure 5.5A through Figure 5.5F, uniform uniaxial strain (in y-direction) was observed throughout the PVA samples regardless of the sample type. There were no movement of the particles in the x-direction. This is thought to be that the samples were not undergoing enough strain to cause displacement of the particles in both x- and y-direction. The setup was then used to identify the strain and duration of cyclic stretching to which HUASMC could be exposed. Atlan et al. showed that the PVA grafts displayed that the mechanical properties of the PVA grafts changed after exposure to cyclic stretching for 1 hour at 50-60% strain

[334]. It was speculated that the PVA grafts would not undergo such change in mechanical properties under 10% strain. Colombo et al. observed that different level of strain could affect the proliferation and migration of VSMC. In their study, they observed that VSMC proliferation was increased *in vitro* after exposure to 10% strain [242]. Therefore, 5% and 10% strain were used in studying the effects of cyclic stretching in HUASMC. As shown in Figure 5.5G, significant number of cells detached when exposed to 12 hours of cyclic stretching regardless of the strain. This could be due to the cells being in culture for too long, and become confluent to form cell clusters (Fig. 5.5G, red circles). This could be a promising explanation as cell clusters were observed with the samples that were seeded with 40,000 cells/cm^2 seeding density (Fig. 5.4B, red circles). Therefore, 10% strain for 4 hours was concluded to be the ideal time to be used in the following experiments.

5.4.2 Application of the continuous compliance mismatched samples *in vitro*

The effects of cyclic stretching on VSMCs are well-studied [22, 157, 357]. It has been found that the extent of strain applied to the cells can influence the proliferation and migration of the cells [122, 358]. Alterations in the strain have also been found to induce inflammatory responses [155, 156]. Also, some stretch experiments tried various lengths of exposure to cyclic strain to study the acute responses as well as long-term responses of VSMC [256]. However, these responses used a substrate with single stiffness, and could not be used to understand the effects of compliance mismatch.

With the development of the cyclic stretching system with continuous compliance mismatch, the independent effects of compliance mismatch on VSMCs can be studied *in vitro*. It has been found already that the compliance mismatch may have additional effects on top of suture-line around the anastomosis in development of IH [154]. Suture-line forms localized stress around the sutures. The stress that are experienced around the anastomosis depends on the suture type, the gauge of the suture needed, and the flow through the anastomosis [24, 154]. Having the platform to study the effects of compliance mismatch alone will allow for simplification needed to understand the effects of individual factors.

5.4.2.1 Effect of compliance mismatch on VSMC exposed to cyclic stretch

The developed compliance mismatch sample was used to expose HUASMCs to cyclic stretching with the strain of 10% for 4 hours, then were analyzed using IF staining to assess their biological responses (Fig. 5.6 through Fig. 5.8). EdU assay is a proliferative assay that quantifies the proliferating cells by

binding to the replicating DNA. The assay showed that the proliferation was significantly increased with compliance mismatched samples after application of cyclic stretching (Fig. 5.6C). Then, the phenotypic change of the VSMC was studied using desmin and vimentin [344, 345, 359]. The ratio of desmin to vimentin was significantly decreased in the groups that were exposed to cyclic stretching (Fig. 5.6D). This is in agreement with published literature as higher expression of vimentin have been observed in VSMC with migratory phenotype [346]. In combination with the increased Vimentin expression, it could be concluded that the exposure to cyclic stretching resulted in cellular responses towards arterial remodeling. Also, it can be concluded that compliance mismatch influenced the cells to have higher proliferation.

It has been found in literature that pMLCK can influence the contractility of VSMCs [337], and regulate migration and proliferation of VSMC through mitogen-activated protein kinase cascade [337]. IF signals of pMLCK shown in Figure 5.7A is quantified in Figure 5.7B. The expression of pMLCK was increased in compliance mismatch sample compared to the other groups when exposed to cyclic stretching. It can be concluded that while exposure to cyclic stretching caused significant increase, compliance mismatch also played a role in increasing the expression of pMLCK.

PDGF-BB is another biomolecules known to regulate the proliferation and migration of VSMC [267, 349]. The overall intensity of PDGF-BB was lower for the compliance mismatched group (Fig. 5.8B). This is opposite to the findings in the literature, as increase in PDGF-BB has been found to increase proliferation and migration of VSMCs [360]. However, areas of high intensity signal of PDGF-BB were observed (Fig. 5.8A). Therefore, the cells with the areas of high intensity of PDGF-BB was quantified (Fig. 5.8C). It was found that there was significantly higher number of cells with concentrated PDGF-BB signal for compliance mismatched samples and not compliant samples. This could be that the PDGF-BB in those cells were binding to PDGF receptors to trigger the subsequent biological reactions. Also, western blot was performed to quantify the amount of endogenous PDGF-BB (Figure 5.8D). It was found that the expression level of PDGF-BB was not significantly different between all of the stretched groups. Therefore, it was concluded that the PDGF-BB did not change in the expression level, but were redistributed. PDGF-BB could be packed into exosome to be secreted out of the cells. This is in correspondence with the literature as secretion of PDGF-BB is observed in proliferating VSMC [267].

YAP nuclear localization is observed to inhibit apoptosis [272]. Furthermore, YAP is known to contribute to HUASMC changing to proliferative phenotype when exposed to cyclic stretching [271]. Therefore, YAP nuclear localization was also studied here. The quantification of IF signal shown in Figure 5.8A indicated that there was no nuclear localization observed regardless of the exposure to cyclic stretching, of the stiffness of the substrate (Fig. 5.8E). This could be due to the fact that the stretch duration is too short for YAP translocation to occur.

5.4.2.2 VSMC response to higher compliance mismatch

In order to assess the effects of compliance mismatch further, samples with higher compliance mismatch were used. The cell proliferation (Fig 5.9C) increased with the exposure to cyclic stretching on higher mismatch sample. Also, decrease in desmin to vimentin ratio was observed (Fig. 5.9D). The PDGF-BB signal intensity (Fig. 5.10B) decreased as it did in the compliance mismatched model (Fig. 5.8B). Furthermore, it was observed that cell proliferation and change to migratory phenotype was more pronounced in 2M compared to 2NC. These findings were in correspondence with the earlier data shown in Figure 5.6.

The regions with high intensity of PDGF-BB signal were also observed with samples with higher compliance mismatch after exposure to cyclic stretching (Fig. 5.10C). 2NC also had lower number of cells with concentrated PDGF-BB signal, which is in agreement with the data shown in Figure 5.8. Unlike in earlier data, however, it was clear that the PDGF-BB signals were localized at the nucleus (Fig. 5.10A). It could be that the localization of PDGF-BB to the nucleus promotes further expression of PDGF-BB, leading to increase in PDGF around the nucleus. YAP localization was also observed with higher compliance mismatch samples exposed to cyclic stretching. In the first compliance mismatch model, no nuclear localization of YAP was observed (Fig. 5.8A). However, statistically significant amounts of cells displayed nuclear localization of YAP when exposed to cyclic stretching on higher compliance mismatch samples (Fig. 5.10D). It is important to note that the HUASMC cultured on 2NC also displayed nuclear localization of YAP after exposure to cyclic stretching. 2M and 2NC displayed statistically similar level of nuclear localization, indicating that the nuclear localization occurred due to higher stiffness, but not necessarily due to compliance mismatch. Therefore, it can be concluded that the extent of compliance mismatched samples influenced the behavior of PDGF-BB and YAP differently. The difference in biological response due to higher compliance mismatch indicate potential increase in the proliferation and migration of HUASMC.

5.5 Conclusion

In order to study the isolated effects of compliance mismatch on VSMCs, continuous PVA hydrogel with two distinct sections with different elastic modulus was developed. The continuous PVA hydrogel could allow for removal of suture-line stress localization so that the effects of the compliance mismatch between the implanted graft and the native artery can be studied independently. The continuous PVA hydrogel with compliance mismatch was made by using both physical and chemical crosslinking method. The resulting hydrogel displayed good integration between the two different types of crosslinking methods. Also, protocols for biochemical modification to enhance cellular adhesion and cell seeding on strips of PVA hydrogels were developed. The strain-maps of the samples were made to ensure uniform strain throughout the samples.

The developed PVA compliance mismatched samples were used in experiments to assess the effects of compliance mismatch on HUASMCs with exposure to cyclic stretching. The samples with compliance mismatch resulted in higher proliferation as well as higher pMLCK intensity after exposure to cyclic stretching. Additionally, pockets of high concentrations of PDGF-BB signal were observed from the compliance mismatched samples. The concentration of PDGF-BB signal was more pronounced in higher compliance mismatched samples. Furthermore, nuclear localization was observed with higher compliance mismatched samples. Therefore, it can be concluded that different level of compliance mismatch can have varying effects on HUASMC.

The compliance mismatch PVA films can be used to further study the effects of compliance mismatch on IH. For example, cellular responses to cyclic stretching while on compliance mismatched substrate in the presence of PDGF-BB inhibitor could be studied. VSMC proliferation is promoted when the cells were cultured in the presence of PDGF-BB [349]. By using the developed compliance mismatched films, it will be possible to study the mechanistic effects of PDGF-BB in IH. Also, the experiments performed in this study focused on the spatial distribution of intrinsic PDGF-BB. External spatial distributions of growth factors are actively being studied [186, 361]. The In 2018, Tannenberg et al. found that extracellular retention of PDGF-B played an important role in hypoxia-induced pulmonary hypertension. Since the surface of PVA can be easily modified with biochemical molecules, it is a promising platform to be used to study the spatial distribution of different growth factors and the effects of stiffness concurrently.

Chapter 6
Conclusion and future directions

In this chapter, the conclusion and suggestions for future directions for each chapter will be addressed.

6.1 Conclusion

Researchers are actively studying to understand and overcome the failures of synthetic small-diameter vascular grafts (sSDVG). One of the identified hurdles in overcoming the limitations of sSDVG intimal hyperplasia (IH), which refers to the thickening of the blood vessel wall due to excessive proliferation and migration of vascular smooth muscle cells (VSMC). It was found that the proliferation and migration of VSMCs are influenced by mechanical stimulation. Therefore, it was hypothesized that compliance mismatch, which is the mismatch in stiffness between the native blood vessels and the implanted sSDVG, could cause the abnormal proliferation and migration of VSMC.

Poly(vinyl alcohol) (PVA) was proposed as a potential candidate to be a compliant sSDVG [25]. PVA is a bio-inert, low-thrombogenic, and low-cytotoxic hydrogel with adjustable mechanical properties. In this thesis, the effects of crosslinking density and interlayer adhesion on the compliance of PVA vascular grafts was studied. It was found that higher interlayer adhesion resulted in increase in the burst pressure of the resulting tubes. However, the compliance of the resulting grafts were lower than the grafts with lower interlayer adhesion. Therefore, the posed hypothesis that the increase in interlayer adhesion will allow for higher compliance and higher burst pressure when the grafts have the same wall thickness was proven to be false. The increase in crosslinking density resulted in improvement in the burst pressure but decreased compliance of the grafts, indicating that the hypothesis posed was correct. Lastly, the post-fabrication modification did display changes in crosslinking density, and resulted in grafts with increased burst pressure and decreased compliance. Therefore, it can be concluded that the last hypothesis posed for the chapter was proved to be true.

In Chapter 4, automated PVA fabrication process was developed to decrease variation due to fabrication process. It was determined that the process allowed for Fourth-Year Design Project (FYDP) group to fabricate PVA grafts with consistency. The equipment was further modified to increase the throughput while decreasing the wasted crosslinking solution. It was found that automated fabrication resulted in decrease in wall thickness and burst pressure. This could be because

the consistency in dipping process reduced error during dip-casting process. Therefore, it can be concluded that the first hypothesis posed comparing the variation of the two fabrication methods was true. Also, the assessment stability of PVA graft concluded that PVA grafts lost less than 2% of its physical content over 180 days of incubation. The second hypothesis that was posed in the chapter was also proven as true.

Lastly, a continuous compliance mismatched PVA film was developed to test the effects of compliance mismatch on human umbilical arterial smooth muscle cells (HUASMC) in a simplified system. In Chapter 5, first hypothesis of chemical and physical crosslinking can be used simultaneously to achieve a continuous film with compliance mismatch was tested. The resulting samples displayed continuity while having distinct regions with different stiffness, proving that the hypothesis was true. The samples were then used in *in vitro* experiments to assess the effects of compliance mismatch on VSMCs with the exposure to cyclic stretching to test the hypothesis that HUASMC cultured on compliance mismatch film will result in higher proliferation rate compared to both compliant and non-compliant films. It was found that compliance mismatch resulted in higher cell proliferation. Also, the phenotypic change to migratory phenotype was observed. This can indicate that compliance mismatch without suture-line can cause migration and proliferation of VSMCs. The last hypothesis that was tested in this chapter was that HUASMC cultured on compliance mismatched film would result in higher phosphorylated myosin light-chain kinase (pMLCK) expression, higher platelet-derived growth factor-BB (PDGF-BB) expression, and nuclear localization of yes-associated protein (YAP). Immunofluorescence staining of PDGF-BB also showed concentration of PDGF-BB and increased pMLCK expression for compliance mismatched model. The concentration of PDGF-BB overlapped with the location of nuclei in higher compliance mismatch sample. Furthermore, nuclear localization of YAP was observed in samples with higher compliance mismatch, whereas the compliance mismatch did not show any YAP nuclear localization. Therefore, it can be concluded that not only does compliance mismatch result in higher expression of pMLCK, in localization of PDGF-BB, and nuclear translocation of YAP, but also the degree of compliance mismatch also plays a role in the extent of biological responses.

6.2 Future directions

6.2.1 Mechanical properties of poly(vinyl alcohol) tubes for vascular graft application

The relationship between the compliance and interlayer adhesion, and compliance and crosslinking density was explored. It was found that both the interlayer adhesion and crosslinking density play a vital role in the mechanical properties of the PVA tubes. The findings can be used fabricate PVA grafts with desired mechanical properties by manipulating the interlayer adhesion and crosslinking density. Based on the data presented in this thesis, adjustment of the interlayer adhesion may be interesting to explore to further improve the compliance. For example, the standard method that have been used for fabrication of PVA grafts used differing waiting times between each dip as shown in Figure 3.1A. Instead of increasing the time between each dip to 30 minutes, keeping the time between dip at flat 15 minutes. Then, number of dips can be increased to reach desired wall thickness to ensure burst pressure that would be safe for clinical use. Dynamic mechanical analysis (DMA) could be used to further identify the mechanical properties of PVA grafts. DMA is an equipment that could characterize a material's properties using temperature, stress, and frequency. Therefore, DMA could be used to determine the frequency-dependent behavior of PVA hydrogels. Lastly, the preliminary simulation study shown in Appendix A could be modified to reflect the elastic modulus of the grafts that are fabricated with desired compliance and burst pressure. The simulation could allow for understanding of the hemodynamics required prior to performing the experiments *in vitro* or *in vivo*.

6.2.2 Consistency of poly(vinyl alcohol) vascular grafts

It was found that the automated fabrication process can allow for fabrication of PVA vascular grafts with thinner walls. This means the platform can be used to fabricate grafts with higher compliance. However, the grafts made using automated process had higher variation in both burst pressure as well as compliance. It will be important to identify the source of error for the automated dip-casting equipment in order to decrease the variation between grafts. For example, the variation could come from the fact that the molds were not kept completely vertical during each waiting period. It would also be due to the fact that the crosslinking solution was not changed capped during the fabrication process. For manual dip-casting method, the crosslinking solution is prevented from crosslinking by keeping the crosslinking solution in a sealed container. The automated fabrication process, however, does not allow for the crosslinking solution to be stored in a sealed container. This could allow for partial crosslinking of PVA inside the crosslinking solution bath, resulting in different coating of the

mold as the process continues. Therefore, it could be worthwhile to try further modifying the automated dip-casting equipment to try sealing the solution baths between dips. Also, the stability of PVA grafts showed little degradation of the hydrogel after 180 days of incubation. While the experiment showed that the physical properties of the grafts did not change, the mechanical properties of the grafts were not assessed. The stability experiment should be repeated using the full-length PVA grafts to test different mechanical properties of the grafts. Also, while the stability of the 1x phosphate buffered saline with 10% penicillin-streptomycin and 1% Amphotericin B tested the long-term storage, it could not test the stability of the graft in working condition. Therefore, the stability of PVA grafts in blood-mimicking fluid or in the presence of whole blood should be tested. If the grafts were to be used in clinical setting, then they would be exposed to blood long-term.

6.2.3 Isolated effects of compliance mismatch on vascular smooth muscle cells

Arterial stiffening can occur due to diseases such as diabetes, hypertension, pseudixanthoma elasticum, and Marfan syndrome [362]. Also, many lifestyle factors can contribute to the arterial stiffening. Such factors include smoking, sedentary lifestyle, aging, and sleep disturbance [362]. The altered stiffness of the blood vessel walls can lead to lethal medical conditions such as aneurysms, stroke, kidney diseases, and heart failure [362]. In Chapter 5, the platform for exposing continuous compliance mismatch samples with two distinct regions having different stiffness was explored. The platform allowed for application of uniform cyclic stretching *in vitro* to understand the effects of compliance mismatch on VSMC. The hybrid crosslinking method of PVA hydrogels can be modified to become an *in vitro* platform to study the arterial stiffening in difference diseases. For example, the hybrid PVA crosslinking process can be modified so that the resulting sample mimics the shape of different stages of arterial stiffening due to thrombosis. Thrombosis occurs due to deposition of plaque on the arterial wall, which may not result in uniform stiffening of the arterial wall. Therefore, chemically crosslinked PVA film with varying wall thickness could be made to study whether the localized wall stiffness would result in exacerbating the progression of thrombogenesis. This could allow for understanding the extent at which the arterial stiffening can affect onset and propagation of atherosclerosis as well.

The compliance mismatched samples could also be used with different cells types to study the effect of different stiffness in conjunction with mechanical stimulation. For example, stem cells are known to either differentiate or not differentiate depending the stiffness of the substrate [87]. The

differentiation of stem cells could be further studied to test whether the presence of different stiffness along with mechanical stimulation could also affect the cell fate of stem cells. In the case of osteocytes, the compliance mismatch could be used to study whether the difference in stiffness could result in different lacunae formation.

The effect of compliance mismatch should also be further studied. The experiments studied the proliferation and phenotypic expression of VSMC to identify that they are displaying proliferative and migratory phenotype. However, the actual migration of the cells was not observed. Therefore, cell migration study using the platform should be performed. This experiment could elucidate whether the migration of the VSMC differs in regions with different compliance, or if the cellular migration occurs uniformly throughout the sample as long as there is compliance mismatch present in the samples. Furthermore, the experiments performed in this thesis studied the cellular responses to the mechanical stimulation without the presence of foreign biomolecules. The presence of exogenous PDGF-BB on VSMC proliferation is well-known phenomena [267]. Therefore, repeating the experiments with the addition of PDGF-BB could also lead to the understanding of whether the presence of exogenous PDGF-BB could further increase the proliferation and migration of VSMC. This is especially important as the experiments that were performed did not account for exogenous growth factors that are available *in vivo*. The cell migration study could also be performed concurrently with the presence of exogenous growth factors to study the combined effects of compliance mismatch and different growth factors. Furthermore, the suppressive effects of proteins in VSMC proliferation can be studied as well. For example, adenosine monophosphate-activated protein kinase is known to suppress VSMC proliferation [363]. The compliance mismatch experiments could be repeated to study whether the increased proliferation due to compliance mismatch and mechanical stimulation could be countered by the presence of the proteins that are known to suppress the proliferation or migration of VSMC.

Furthermore, the platform should be used in inhibition studies to identify the potential therapeutic targets for decreasing the formation of intimal hyperplasia in vascular grafts. The platform allows for experiments mimicking the compliance mismatch between the native blood vessels and vascular grafts to occur *in vitro*. This indicates that the platform can be used to address physiologically relevant VSMC behaviors in gene expression and protein expression. In the experiments presented, gene expression of the cells was not studied. Also, while the western blot was used to quantify the expression of PDGF-BB, other proteins that are associated with proliferation and migration of VSMC

were not studied. For example, p53 gene was found to be a potential target to inhibit VSMC proliferation [364]. A study in 2009 found that miR-221 and miR-222 could also promote development of intimal hyperplasia through increasing VSMC proliferation [365]. Also, increase in matrix metalloproteinase is known to increase the proliferation of VSMC [366]. These studies could be repeated using the developed compliance mismatch platform to study the effects of the gene expressions on intimal hyperplasia.

Lastly, the effects of suture-line stress can be directly compared to the effects of compliance mismatch using the developed continuous compliance mismatched samples. Suture-line can be made along the compliance mismatch line, and be directly compared to the group without suture. The sutures with different gauge could be made along the compliance mismatch line to study the effects of different suture thickness on the behaviors of VSMC. Also, the effects of different suture techniques resulting in cell damage around the anastomosis was studied [367]. Different suture techniques could be used to study whether there are synergistic effects of the suture method and compliance mismatch. The compliance mismatch platform would allow for physiologically relevant understanding of the effects of different suture techniques on VSMC in vascular grafts.

References

1. *Cadiovascular diseases*. 2022; Available from: https://www.who.int/health-topics/cardiovascular-diseases#tab=tab_1.
2. Vaidya, S.R. and N.R. Aeddula, *Chronic renal failure*, in *StatPearls [Internet]*. 2021, StatPearls Publishing.
3. Castellani, R.J., R.K. Rolston, and M.A. Smith, *Alzheimer disease.* Disease-a-month: DM, 2010. **56**(9): p. 484.
4. Sun, Y.-S., et al., *Risk factors and preventions of breast cancer.* International journal of biological sciences, 2017. **13**(11): p. 1387.
5. Bostwick, D.G., et al., *Human prostate cancer risk factors.* Cancer: Interdisciplinary International Journal of the American Cancer Society, 2004. **101**(S10): p. 2371-2490.
6. Osta, W.A., et al., *EpCAM is overexpressed in breast cancer and is a potential target for breast cancer gene therapy.* Cancer research, 2004. **64**(16): p. 5818-5824.
7. Yiannopoulou, K.G. and S.G. Papageorgiou, *Current and future treatments for Alzheimer's disease.* Therapeutic advances in neurological disorders, 2013. **6**(1): p. 19-33.
8. Peter Arno Stonebridge, J.B.C.D., John Graeme Houston, Robert Gordon Hood, *Vascular graft*, U.S. Patent, Editor. 30 Jun 2015, Vascular Flow Technologies Limited: United States.
9. *Hemodialysis*. 2022; Available from: https://www.niddk.nih.gov/health-information/kidney-disease/kidney-failure/hemodialysis#:~:text=Hemodialysis%20is%20a%20treatment%20to,and%20calcium%2C%20in%20your%20blood.
10. Control, C.f.D. and Prevention, *About underlying cause of death, 1999-2020.* On CDC's National Center for Health Statistics WONDER online database. Accessed at http://wonder. cdc. gov/ucd-icd10. html on Mar, 2020. **27**: p. 2022.
11. Creager, M.A. and J. Loscalzo, *Arterial Diseases of the Extremities*, in *Harrison's Principles of Internal Medicine, 20e*, J.L. Jameson, et al., Editors. 2018, McGraw-Hill Education: New York, NY.
12. Stone, G.W., et al., *Five-year outcomes after PCI or CABG for left main coronary disease.* New England Journal of Medicine, 2019. **381**(19): p. 1820-1830.
13. Deutsch, M., et al., *Clinical autologous in vitro endothelialization of infrainguinal ePTFE grafts in 100 patients: a 9-year experience.* Surgery, 1999. **126**(5): p. 847-855.
14. Jeong, Y., Y. Yao, and E.K. Yim, *Current understanding of intimal hyperplasia and effect of compliance in synthetic small diameter vascular grafts.* Biomaterials Science, 2020.
15. Duque, J.C., et al., *Dialysis arteriovenous fistula failure and angioplasty: intimal hyperplasia and other causes of access failure.* American Journal of Kidney Diseases, 2017. **69**(1): p. 147-151.
16. Williams, D., et al., *Tailoring of arteriovenous graft-to-vein anastomosis angle to attenuate pathological flow fields.* Scientific reports, 2021. **11**(1): p. 1-10.
17. Lidman, D.H., B. Faibisoff, and R.K. Daniel, *Expanded polytetrafluoroethylene as a microvascular graft: An experimental study.* Microsurgery, 1980. **1**(6): p. 447-456.
18. Allen, B.T., et al., *Influence of endothelial cell seeding on platelet deposition and patency in small-diameter Dacron arterial grafts.* Journal of vascular surgery, 1984. **1**(1): p. 224-233.
19. Sottiurai, V., *Distal anastomotic intimal hyperplasia: Histocytomorphology, pathophysiology, etiology, and prevention.* International Journal of Angiology, 2011. **8**: p. 1-10.

20. Lehmann, E.D., K.D. Hopkins, and R.G. Gosling, *Aortic compliance measurements using Doppler ultrasound: in vivo biochemical correlates.* Ultrasound in medicine & biology, 1993. **19**: p. 683-710.
21. Jeong, Y., et al., *Changing compliance of poly (vinyl alcohol) vascular grafts through modifying interlayer adhesion and crosslinking density.* Frontiers in Materials, 2021. **7**: p. 456.
22. Thacher, T., R.F. Da Silva, and N. Stergiopulos, *Differential effects of reduced cyclic stretch and perturbed shear stress within the arterial wall and on smooth muscle function.* American journal of hypertension, 2009. **22**(12): p. 1250-1257.
23. Ballyk, P.D., et al., *Compliance mismatch may promote graft–artery intimal hyperplasia by altering suture-line stresses.* Journal of biomechanics, 1997. **31**(3): p. 229-237.
24. Roussis, P.C., A. Giannakopoulos, and H. Charalambous, *Suture line response of end-to-side anastomosis: A stress concentration methodology.* Cardiovascular engineering and technology, 2015. **6**(1): p. 36-48.
25. Chaouat, M., et al., *A novel cross-linked poly (vinyl alcohol)(PVA) for vascular grafts.* Advanced Functional Materials, 2008. **18**(19): p. 2855-2861.
26. Cutiongco, M.F., et al., *In vitro and ex vivo hemocompatibility of off-the-shelf modified poly (vinyl alcohol) vascular grafts.* Acta biomaterialia, 2015. **25**: p. 97-108.
27. Ino, J.M., et al., *Evaluation of hemocompatibility and endothelialization of hybrid poly (vinyl alcohol)(PVA)/gelatin polymer films.* Journal of Biomedical Materials Research Part B: Applied Biomaterials, 2013. **101**(8): p. 1549-1559.
28. Rizwan, M., et al., *One-Pot Covalent Grafting of Gelatin on Poly (Vinyl Alcohol) Hydrogel to Enhance Endothelialization and Hemocompatibility for Synthetic Vascular Graft Applications.* ACS Applied Bio Materials, 2019. **3**(1): p. 693-703.
29. Yao, Y., et al., *Fucoidan functionalization on poly (vinyl alcohol) hydrogels for improved endothelialization and hemocompatibility.* Biomaterials, 2020: p. 120011.
30. Bates, N.M., et al., *Evaluation of the Effect of Crosslinking Method of Poly (Vinyl Alcohol) Hydrogels on Thrombogenicity.* Cardiovascular Engineering and Technology, 2020: p. 1-8.
31. Bates, N.M., et al., *Bioconjugation of a collagen-mimicking peptide onto poly (vinyl alcohol) encourages endothelialization while minimizing thrombosis.* Frontiers in Bioengineering and Biotechnology, 2020. **8**: p. 621768.
32. Brown, T.D., *Techniques for mechanical stimulation of cells in vitro: a review.* Journal of biomechanics, 2000. **33**(1): p. 3-14.
33. van Oers, R.F., H. Wang, and R.G. Bacabac, *Osteocyte shape and mechanical loading.* Current osteoporosis reports, 2015. **13**(2): p. 61-66.
34. Kim, S.A., et al., *Laminar shear stress suppresses vascular smooth muscle cell proliferation through nitric oxide-AMPK pathway.* Biochemical and biophysical research communications, 2017. **490**(4): p. 1369-1374.
35. Zhang, H., et al., *Wall shear stress promotes intimal hyperplasia through the paracrine H2O2-mediated NOX-AKT-SVV axis.* Life sciences, 2018. **207**: p. 61-71.
36. *MechanoCulture T6* Available from: https://www.cellscale.com/products/mct6/.
37. Go, A.S., et al., *Heart disease and stroke statistics—2013 update: a report from the American Heart Association.* Circulation, 2013. **127**(1): p. e6-e245.
38. Ravi, S. and E.L. Chaikof, *Biomaterials for vascular tissue engineering.* Regenerative medicine, 2010. **5**(1): p. 107-120.
39. Walpoth, B.H., et al., *Improvement of patency rate in heparin-coated small synthetic vascular grafts.* Circulation, 1998. **98**: p. II-319.

40. Enomoto, S., et al., *Long-term patency of small-diameter vascular graft made from fibroin, a silk-based biodegradable material.* Journal of vascular surgery, 2010. **51**(1): p. 155-164.
41. Abbott, W.M., et al., *Effect of compliance mismatch on vascular graft patency.* Journal of vascular surgery, 1987. **5**(2): p. 376-382.
42. Lemson, M., et al., *Intimal hyperplasia in vascular grafts.* European Journal of Vascular and Endovascular Surgery, 2000. **19**(4): p. 336-350.
43. Sottiurai, V.S., et al., *Distal anastomotic intimal hyperplasia: biogenesis and etiology.* European journal of vascular surgery, 1988. **2**: p. 245-56.
44. Hong-De Wu, M., et al., *The direct effect of graft compliance mismatch per se on development of host arterial intimal hyperplasia at the anastomotic interface.* Annals of Vascular Surgery, 1993. **7**(2): p. 156-168.
45. Post, A., et al., *Elucidating the role of graft compliance mismatch on intimal hyperplasia using an ex vivo organ culture model.* Acta biomaterialia, 2019. **89**: p. 84-94.
46. Albers, F.J., *Causes of hemodialysis access failure.* Advances in renal replacement therapy, 1994. **1**(2): p. 107-118.
47. Mousa, A.Y., et al., *Patency in arteriovenous grafts in hemodialysis patients.* Vascular and endovascular surgery, 2013. **47**(6): p. 438-443.
48. Organization, W.-W.H. *Cardiovascular diseases (CVDs)*. 2017; Available from: https://www.who.int/en/news-room/fact-sheets/detail/cardiovascular-diseases-(cvds).
49. England, N. *Cardiovascular disease*. 2022; Available from: https://www.nhs.uk/conditions/cardiovascular-disease/.
50. *Angina*. 2022; Available from: https://www.mayoclinic.org/diseases-conditions/angina/symptoms-causes/syc-20369373#:~:text=Angina%20(an%2DJIE%2Dnuh,or%20pain%20in%20the%20chest.
51. *Heart attack*. 2022; Available from: https://www.mayoclinic.org/diseases-conditions/heart-attack/symptoms-causes/syc-20373106.
52. *Stroke*. 2022; Available from: https://www.mayoclinic.org/diseases-conditions/stroke/symptoms-causes/syc-20350113.
53. *Peripheral Arterial Disease (PAD)*. 2022; Available from: https://www.cdc.gov/heartdisease/PAD.htm#:~:text=Peripheral%20arterial%20disease%20(PAD)%20in,arteries%2C%20which%20is%20called%20atherosclerosis.
54. *Heart failure - Also called congestive heart failure*. 2022; Available from: https://www.heartandstroke.ca/heart-disease/conditions/heart-failure#:~:text=Heart%20failure%20is%20a%20chronic,from%20fluid%20in%20the%20lungs.
55. *Coronary Heart Disease*. 2022; Available from: https://www.hopkinsmedicine.org/health/conditions-and-diseases/coronary-heart-disease#:~:text=The%20left%20main%20coronary%20artery,left%20side%20of%20the%20heart.
56. Lorbeer, R., et al., *Reference values of vessel diameters, stenosis prevalence, and arterial variations of the lower limb arteries in a male population sample using contrast-enhanced MR angiography.* PLoS One, 2018. **13**(6): p. e0197559.
57. Park, K.-H., et al., *Suitability of endovascular repair with current stent grafts for abdominal aortic aneurysm in Korean patients.* Journal of Korean Medical Science, 2011. **26**(8): p. 1047-1051.
58. *Femoral Artery*. 2022; Available from: https://my.clevelandclinic.org/health/body/21645-femoral-

artery#:~:text=The%20diameter%20of%20the%20artery,access%20point%20for%20endovascular%20procedures.
59. Wolf, Y.G., Z. Kobzantsev, and L. Zelmanovich, *Size of normal and aneurysmal popliteal arteries: a duplex ultrasound study.* Journal of vascular surgery, 2006. **43**(3): p. 488-492.
60. Brownstein, A.J., et al., *Natural history of aneurysmal aortic arch branch vessels in a single tertiary referral center.* Journal of Vascular Surgery, 2018. **68**(6): p. 1631-1639. e1.
61. Cheney, A.E. and J.M. McCabe, *Alternative percutaneous access for large bore devices.* Circulation: Cardiovascular Interventions, 2019. **12**(6): p. e007707.
62. Holubkov, R., et al., *Large brachial artery diameter is associated with angiographic coronary artery disease in women.* American heart journal, 2002. **143**(5): p. 802-807.
63. Beniwal, S., K. Bhargava, and S.K. Kausik, *Size of distal radial and distal ulnar arteries in adults of southern Rajasthan and their implications for percutaneous coronary interventions.* Indian heart journal, 2014. **66**(5): p. 506-509.
64. NIH - National Heart, L., and Blood Institue *Peripheral Artery Disease* 2020; Available from: https://www.nhlbi.nih.gov/health-topics/peripheral-artery-disease.
65. Virani, S.S., et al., *Heart disease and stroke statistics—2021 update: a report from the American Heart Association.* Circulation, 2021. **143**(8): p. e254-e743.
66. *Chronic kidney disease*. 2022; Available from: https://www.mayoclinic.org/diseases-conditions/chronic-kidney-disease/symptoms-causes/syc-20354521.
67. Outcomes, K.D.I.G., *Chapter 1: definition and classification of CKD.* Kidney Int Suppl, 2013. **3**(1): p. 19-62.
68. *Peritoneal Dialysis* Available from: https://www.niddk.nih.gov/health-information/kidney-disease/kidney-failure/peritoneal-dialysis#:~:text=Peritoneal%20dialysis%20is%20a%20treatment,a%20catheter%2C%20in%20your%20belly.
69. Ghantous, W., et al., *Limitations of peritoneal dialysis (PD) in the treatment of ESRD patients.* ASAIO Journal, 1979. **25**(1): p. 100-103.
70. Htay, H., et al., *Multicenter registry analysis of center characteristics associated with technique failure in patients on incident peritoneal dialysis.* Clinical Journal of the American Society of Nephrology, 2017. **12**(7): p. 1090-1099.
71. Steve A. Herweck, T.K., Paul Martakos, *self-sealing implantable vascular graft*, U.S. Patent, Editor. 9 Mar 1993, Atrium Medical Corp: United States
72. Esmon, C., *Inflammation and thrombosis.* Journal of Thrombosis and haemostasis, 2003. **1**(7): p. 1343-1348.
73. Ross, R., *Atherosclerosis — An Inflammatory Disease.* New England Journal of Medicine, 1999. **340**: p. 115-126.
74. Kyrle, P.A. and S. Eichinger, *Deep vein thrombosis.* The Lancet, 2005. **365**(9465): p. 1163-1174.
75. LaPelusa, A. and H.D. Dave, *Physiology, Hemostasis.* 2019.
76. Stevens, D.U., et al., *Cardiovascular and thrombogenic risk of decidual vasculopathy in preeclampsia.* American journal of obstetrics and gynecology, 2014. **210**(6): p. 545. e1-545. e6.
77. Henke, P.K., et al., *Fibrotic injury after experimental deep vein thrombosis is determined by the mechanism of thrombogenesis.* Thrombosis and haemostasis, 2007. **98**(11): p. 1045-1055.
78. Towne, J.B., *Role of fibrointimal hyperplasia in vein graft failure: Research initiatives in vascular surgery.* Journal of Vascular Surgery, 1989. **10**(5): p. 583-585.

79. Adhikari, K.R., B.S. Tucker, and V. Thomas, *Tissue engineering of small-diameter vascular grafts*, in *Biointegration of Medical Implant Materials*. 2020, Elsevier. p. 79-100.
80. Caliskan, E., et al., *Saphenous vein grafts in contemporary coronary artery bypass graft surgery.* Nature Reviews Cardiology, 2020. **17**(3): p. 155-169.
81. Bellon, J., et al., *Arterial autografts and PTFE vascular microprostheses: similarities in the healing process.* European Journal of Vascular Surgery, 1994. **8**(6): p. 694-702.
82. Seifu, D.G., et al., *Small-diameter vascular tissue engineering.* Nature Reviews Cardiology, 2013. **10**(7): p. 410-421.
83. Falk, A., *Maintenance and salvage of arteriovenous fistulas.* Journal of Vascular and Interventional Radiology, 2006. **17**(5): p. 807-813.
84. Siddiqui, M.A., S. Ashraff, and T. Carline, *Maturation of arteriovenous fistula: analysis of key factors.* Kidney research and clinical practice, 2017. **36**(4): p. 318.
85. Baker, M.I., et al., *A review of polyvinyl alcohol and its uses in cartilage and orthopedic applications.* Journal of Biomedical Materials Research Part B: Applied Biomaterials, 2012. **100**(5): p. 1451-1457.
86. Gu, Z.Q., J.M. Xiao, and X.H. Zhang, *The development of artificial articular cartilage–PVA-hydrogel.* Bio-Medical Materials and Engineering, 1998. **8**(2): p. 75-81.
87. Kim, T.H., et al., *Creating stiffness gradient polyvinyl alcohol hydrogel using a simple gradual freezing–thawing method to investigate stem cell differentiation behaviors.* Biomaterials, 2015. **40**: p. 51-60.
88. Morandim-Giannetti, A.d.A., et al., *Conditions for obtaining polyvinyl alcohol/trisodium trimetaphosphate hydrogels as vitreous humor substitute.* Journal of Biomedical Materials Research Part B: Applied Biomaterials, 2016. **104**(7): p. 1386-1395.
89. Cutiongco, M.F., et al., *Submillimeter diameter poly (vinyl alcohol) vascular graft patency in rabbit model.* Frontiers in bioengineering and biotechnology, 2016. **4**: p. 44.
90. Gupta, S., S. Goswami, and A. Sinha, *A combined effect of freeze--thaw cycles and polymer concentration on the structure and mechanical properties of transparent PVA gels.* Biomedical Materials, 2012. **7**(1): p. 015006.
91. Fukumori, T. and T. Nakaoki, *Significant improvement of mechanical properties for polyvinyl alcohol film prepared from freeze/thaw cycled gel.* Open Journal of Organic Polymer Materials, 2013. **2013**.
92. Kim, K.-J., S.-B. Lee, and N.-W. Han, *Kinetics of crosslinking reaction of PVA membrane with glutaraldehyde.* Korean Journal of Chemical Engineering, 1994. **11**(1): p. 41-47.
93. Darabi, M.A., et al., *An alkaline based method for generating crystalline, strong, and shape memory polyvinyl alcohol biomaterials.* Advanced Science, 2020. **7**(21): p. 1902740.
94. do Nascimento, F.C., et al., *Formulation and characterization of crosslinked polyvinyl alcohol (PVA) membranes: effects of the crosslinking agents.* Polymer Bulletin, 2021. **78**(2): p. 917-929.
95. Bo, J., *Study on PVA hydrogel crosslinked by epichlorohydrin.* Journal of applied polymer science, 1992. **46**(5): p. 783-786.
96. Pohan, G., et al., *Luminal Plasma Treatment for Small Diameter Polyvinyl Alcohol Tubular Scaffolds.* Frontiers in bioengineering and biotechnology, 2019. **7**: p. 117.
97. Pohan, G., et al., *Effect of Ethylene Oxide Sterilization on Polyvinyl Alcohol Hydrogel Compared with Gamma Radiation.* Tissue Engineering Part A, 2020. **26**(19-20): p. 1077-1090.

98. Rizwan, M., et al., *One-pot covalent grafting of gelatin on polyvinyl alcohol hydrogel to enhance endothelialization and hemocompatibility for synthetic vascular graft applications.* ACS Applied Bio Materials, 2019.
99. Maitra, J. and V.K. Shukla, *Cross-linking in hydrogels-a review.* Am. J. Polym. Sci, 2014. **4**(2): p. 25-31.
100. Cutiongco, M.F., et al., *Planar and tubular patterning of micro and nano-topographies on poly (vinyl alcohol) hydrogel for improved endothelial cell responses.* Biomaterials, 2016. **84**: p. 184-195.
101. Miyashita, H., et al., *Collagen-immobilized poly (vinyl alcohol) as an artificial cornea scaffold that supports a stratified corneal epithelium.* Journal of Biomedical Materials Research Part B: Applied Biomaterials: An Official Journal of The Society for Biomaterials, The Japanese Society for Biomaterials, and The Australian Society for Biomaterials and the Korean Society for Biomaterials, 2006. **76**(1): p. 56-63.
102. Pashneh-Tala, S., S. MacNeil, and F. Claeyssens, *The tissue-engineered vascular graft—past, present, and future.* Tissue Engineering Part B: Reviews, 2016. **22**(1): p. 68-100.
103. Al Shakarchi, J., G. Houston, and N. Inston, *Early cannulation grafts for haemodialysis: a systematic review.* The Journal of Vascular Access, 2015. **16**(6): p. 493-497.
104. Dantzer, R., et al., *From inflammation to sickness and depression: when the immune system subjugates the brain.* Nature reviews neuroscience, 2008. **9**(1): p. 46-56.
105. Barker, R.A. and H. Widner, *Immune problems in central nervous system cell therapy.* NeuroRx, 2004. **1**(4): p. 472-481.
106. J. Gordon Betts, P.D., Eddie Johnson, Jody E. Johnson, Oksana Korol, Dean Kruse, Brandon Poe, James A. Wise, Mark Womble, Kelly A. Young, *Anatomy and Physiology*. 2017, Rice University Rice University
107. Mills, B., T. Robb, and D. Larson, *Intimal hyperplasia: slow but deadly.* Perfusion, 2012. **27**(6): p. 520-528.
108. Chen, D., et al., *Inhibition of Thrombin Receptor Signaling on α-Smooth Muscle Actin+ CD34+ Progenitors Leads to Repair After Murine Immune Vascular Injury.* Arteriosclerosis, thrombosis, and vascular biology, 2012. **32**(1): p. 42-49.
109. Allaire, E. and A.W. Clowes, *Endothelial cell injury in cardiovascular surgery: the intimal hyperplastic response.* The Annals of thoracic surgery, 1997. **63**(2): p. 582-591.
110. Sterpetti, A.V., et al., *Progression and regression of myointimal hyperplasia in experimental vein grafts depends on platelet-derived growth factor and basic fibroblastic growth factor production.* Journal of vascular surgery, 1996. **23**(4): p. 568-575.
111. Lyman, D., et al., *Compliance as a factor effecting the patency of a copolyurethane vascular graft.* Journal of biomedical materials research, 1978. **12**(3): p. 337-345.
112. Roberts, G., et al., *The role of physical and chemical characteristics in assessing the performance of a new biological vascular graft.* Journal of biomedical materials research, 1989. **23**(4): p. 443-450.
113. Brossollet, L., *Mechanical issues in vascular grafting: a review*. 1992, SAGE Publications Sage UK: London, England.
114. Surovtsova, I., *Effects of compliance mismatch on blood flow in an artery with endovascular prosthesis.* Journal of biomechanics, 2005. **38**(10): p. 2078-2086.
115. Stewart, S.F. and D.J. Lyman, *Effects of an artery/vascular graft compliance mismatch on protein transport: a numerical study.* Annals of biomedical engineering, 2004. **32**(7): p. 991-1006.

116. di Luca, M., et al., *The Dichotomy of Vascular Smooth Muscle Differentiation/De-Differentiation in Health and Disease*, in *Muscle Cell and Tissue-Current Status of Research Field*. 2018, IntechOpen.
117. Haudenschild, C.C., *Morphology of intimal hyperplasia: Research initiatives in vascular surgery.* Journal of Vascular Surgery, 1989. **10**(5): p. 591-592.
118. Tennant, M. and J.K. McGeachie, *Blood vessel structure and function: a brief update on recent advances.* Australian and New Zealand Journal of Surgery, 1990. **60**(10): p. 747-753.
119. Huynh, T., et al., *Remodeling of an acellular collagen graft into a physiologically responsive neovessel.* Nature biotechnology, 1999. **17**(11): p. 1083-1086.
120. Radomski, M.W., R.M.J. Palmer, and S. Moncada, *The anti-aggregating properties of vascular endothelium: interactions between prostacyclin and nitric oxide.* British Journal of Pharmacology, 1987. **92**: p. 639-646.
121. Castellot, J., et al., *Cultured endothelial cells produce heparinlike inhibitor of smooth muscle cell growth.* The Journal of Cell Biology, 1981. **90**: p. 372-379.
122. Cirillo, P., et al., *Activated platelets and leucocytes cooperatively stimulate smooth muscle cell proliferation and proto-oncogene expression via release of soluble growth factors.* Cardiovascular research, 1999. **43**: p. 210-8.
123. Cirillo, P., et al., *Activated platelets stimulate tissue factor expression in smooth muscle cells.* Thrombosis Research, 2003. **112**: p. 51-57.
124. Weber, A.-A. and K. Schror, *The significance of platelet-derived growth factors for proliferation of vascular smooth muscle cells.* Platelets, 1999. **10**: p. 77-96.
125. Li, G., et al., *Direct In Vivo Evidence Demonstrating Neointimal Migration of Adventitial Fibroblasts After Balloon Injury of Rat Carotid Arteries.* Circulation, 2000. **101**: p. 1362-1365.
126. Siow, R.C.M., C.M. Mallawaarachchi, and P.L. Weissberg, *Migration of adventitial myofibroblasts following vascular balloon injury: insights from in vivo gene transfer to rat carotid arteries.* Cardiovascular research, 2003. **59**: p. 212-21.
127. Spaet, T.H., et al., *Intimal injury and regrowth in the rabbit aorta; medial smooth muscle cells as a source of neointima.* Circulation research, 1975. **36**: p. 58-70.
128. Li, L., et al., *Neointimal hyperplasia associated with synthetic hemodialysis grafts.* Kidney International, 2008. **74**: p. 1247-1261.
129. Costa, R.d.F.B.d., et al., *Effects of external gamma radiation on femoral artery reimplantation in rats: morphometrical analyzes.* Acta Cirurgica Brasileira, 2003. **18**(2): p. 86-96.
130. Scott, N.A., et al., *Identification of a Potential Role for the Adventitia in Vascular Lesion Formation After Balloon Overstretch Injury of Porcine Coronary Arteries.* Circulation, 1996. **93**: p. 2178-2187.
131. Shi, Y., et al., *Adventitial myofibroblasts contribute to neointimal formation in injured porcine coronary arteries.* Circulation, 1996. **94**: p. 1655-64.
132. Oparil, S., et al., *Estrogen attenuates the adventitial contribution to neointima formation in injured rat carotid arteries.* Cardiovascular Research, 1999. **44**(3): p. 608-614.
133. Bassiouny, H.S., et al., *Anastomotic intimal hyperplasia: mechanical injury or flow induced.* Journal of vascular surgery, 1992. **15**: p. 708-16; discussion 716-7.
134. Sottiurai, *Distal Anastomotic Intimal Hyperplasia: Histocytomorphology, Pathophysiology, Etiology, and Prevention.* The International journal of angiology : official publication of the International College of Angiology, Inc, 1999. **8**: p. 1-10.

135. LoGerfo, F.W., et al., *Downstream anastomotic hyperplasia. A mechanism of failure in Dacron arterial grafts.* Annals of surgery, 1983. **197**: p. 479-83.
136. Tordoir, J.H.M., et al., *Early experience with stretch polytetrafluoroethylene grafts for haemodialysis access surgery: Results of a prospective randomised study.* European Journal of Vascular and Endovascular Surgery, 1995. **9**: p. 305-309.
137. Fillinger, M.F., et al., *Graft geometry and venous intimal-medial hyperplasia in arteriovenous loop grafts.* Journal of vascular surgery, 1990. **11**: p. 556-66.
138. Haruguchi, H. and S. Teraoka, *Intimal hyperplasia and hemodynamic factors in arterial bypass and arteriovenous grafts: a review.* Journal of Artificial Organs, 2003. **6**: p. 227-235.
139. Kornowski, R., et al., *In-stent restenosis: contributions of inflammatory responses and arterial injury to neointimal hyperplasia.* Journal of the American College of Cardiology, 1998. **31**: p. 224-30.
140. Roy-Chaudhury, P., et al., *Venous neointimal hyperplasia in polytetrafluoroethylene dialysis grafts.* Kidney International, 2001. **59**: p. 2325-2334.
141. Hoch, J.R., et al., *Macrophage depletion alters vein graft intimal hyperplasia.* Surgery, 1999. **126**: p. 428-37.
142. Newby, A.C. and A.B. Zaltsman, *Molecular mechanisms in intimal hyperplasia.* The Journal of Pathology, 2000. **190**: p. 300-309.
143. Goetze, S., et al., *TNF-α–Induced Migration of Vascular Smooth Muscle Cells Is MAPK Dependent.* Hypertension, 1999. **33**: p. 183-189.
144. Kanthou, C., et al., *Thrombin receptor activating peptide (TRAP) stimulates mitogenesis, c-fos and PDGF-A gene expression in human vascular smooth muscle cells.* Thrombosis and haemostasis, 1995. **74**: p. 1340-7.
145. Nakajima, T., et al., *Involvement of NF-κB Activation in Thrombin-Induced Human Vascular Smooth Muscle Cell Proliferation.* Biochemical and Biophysical Research Communications, 1994. **204**: p. 950-955.
146. McNamara, C.A., et al., *Thrombin stimulates proliferation of cultured rat aortic smooth muscle cells by a proteolytically activated receptor.* Journal of Clinical Investigation, 1993. **91**: p. 94-98.
147. Chistiakov, D.A., A.N. Orekhov, and Y.V. Bobryshev, *Effects of shear stress on endothelial cells: go with the flow.* Acta physiologica, 2017. **219**(2): p. 382-408.
148. Ballermann, B.J., et al., *Shear stress and the endothelium.* Kidney international. Supplement, 1998. **67**: p. S100-8.
149. Malek, A.M., S.L. Alper, and S. Izumo, *Hemodynamic Shear Stress and Its Role in Atherosclerosis.* JAMA, 1999. **282**: p. 2035.
150. Nadaud, S., et al., *Sustained increase in aortic endothelial nitric oxide synthase expression in vivo in a model of chronic high blood flow.* Circulation research, 1996. **79**: p. 857-63.
151. Ojha, M., *Wall shear stress temporal gradient and anastomotic intimal hyperplasia.* Circulation research, 1994. **74**: p. 1227-31.
152. Walpola, P.L., A.I. Gotlieb, and B.L. Langille, *Monocyte adhesion and changes in endothelial cell number, morphology, and F-actin distribution elicited by low shear stress in vivo.* The American journal of pathology, 1993. **142**: p. 1392-400.
153. Rana, A., et al., *Shear-dependent platelet aggregation: mechanisms and therapeutic opportunities.* Frontiers in cardiovascular medicine, 2019. **6**.
154. Ballyk, P.D., et al., *Compliance mismatch may promote graft-artery intimal hyperplasia by altering suture-line stresses.* Journal of biomechanics, 1998. **31**: p. 229-37.

155. Southgate, K.M., et al., *Increased Secretion of Basement Membrane–Degrading Metalloproteinases in Pig Saphenous Vein Into Carotid Artery Interposition Grafts.* Arteriosclerosis, Thrombosis, and Vascular Biology, 1999. **19**: p. 1640-1649.
156. MAYR, M., et al., *Mechanical stress-induced DNA damage and rac-p38MAPK signal pathways mediate p53-dependent apoptosis in vascular smooth muscle cells.* The FASEB Journal, 2002. **16**: p. 1423-1425.
157. Haga, J.H., Y.-S.J. Li, and S. Chien, *Molecular basis of the effects of mechanical stretch on vascular smooth muscle cells.* Journal of biomechanics, 2007. **40**(5): p. 947-960.
158. Predel, H.G., et al., *Implications of pulsatile stretch on growth of saphenous vein and mammary artery smooth muscle.* Lancet (London, England), 1992. **340**: p. 878-9.
159. Reininger, A.J., et al., *Flow mediated fibrin thrombus formation in an endothelium-lined model of arterial branching.* Thrombosis Research, 1994. **74**: p. 629-641.
160. Macarie, R.D., et al., *The expression of MMP-1 and MMP-9 is up-regulated by smooth muscle cells after their cross-talk with macrophages in high glucose conditions.* Journal of cellular and molecular medicine, 2018. **22**(9): p. 4366-4376.
161. Baird, R.N. and W.M. Abbott, *Pulsatile blood-flow in arterial grafts.* Lancet (London, England), 1976. **2**: p. 948-50.
162. Baird, R.N., et al., *Dynamic compliance of arterial grafts.* American Journal of Physiology-Heart and Circulatory Physiology, 1977. **233**: p. H568-H572.
163. DePaola, N., et al., *Vascular endothelium responds to fluid shear stress gradients.* Arteriosclerosis and thrombosis : a journal of vascular biology, 1992. **12**: p. 1254-7.
164. Bao, X., C. Lu, and J.A. Frangos, *Temporal gradient in shear but not steady shear stress induces PDGF-A and MCP-1 expression in endothelial cells: role of NO, NF kappa B, and egr-1.* Arteriosclerosis, thrombosis, and vascular biology, 1999. **19**: p. 996-1003.
165. Liu, S.Q., et al., *Pattern formation of vascular smooth muscle cells subject to nonuniform fluid shear stress: role of PDGF-β receptor and Src.* American Journal of Physiology-Heart and Circulatory Physiology, 2003. **285**: p. H1081-H1090.
166. Ho, R.X.-Y., et al., *The cell adhesion molecule IGPR-1 is activated by, and regulates responses of endothelial cells to shear stress.* The Journal of biological chemistry, 2019: p. jbc.RA119.008548.
167. Tone, E.I.V., *The Vicious Cycle of Arterial Stiffness and Arterial Media Calcification.* 2019.
168. Mack, J.J., et al., *NOTCH1 is a mechanosensor in adult arteries.* Nature Communications, 2017. **8**: p. 1620.
169. Sterpetti, A.V., et al., *Shear stress modulates the proliferation rate, protein synthesis, and mitogenic activity of arterial smooth muscle cells.* Surgery, 1993. **113**: p. 691-9.
170. Kraiss, L.W., et al., *Shear stress regulates smooth muscle proliferation and neointimal thickening in porous polytetrafluoroethylene grafts.* Arteriosclerosis and Thrombosis: A Journal of Vascular Biology, 1991. **11**: p. 1844-1852.
171. Sterpetti, A.V., et al., *Modulation of arterial smooth muscle cell growth by haemodynamic forces.* European Journal of Vascular Surgery, 1992. **6**: p. 16-20.
172. Meyerson, S.L., et al., *The effects of extremely low shear stress on cellular proliferation and neointimal thickening in the failing bypass graft.* Journal of Vascular Surgery, 2001. **34**: p. 90-97.
173. Haga, M., et al., *Oscillatory shear stress increases smooth muscle cell proliferation and akt phosphorylation.* Journal of Vascular Surgery, 2003. **37**: p. 1277-1284.
174. Zwolak, R.M., M.C. Adams, and A.W. Clowes, *Kinetics of vein graft hyperplasia: association with tangential stress.* Journal of vascular surgery, 1987. **5**: p. 126-36.

175. Haga, J.H., Y.-S.J. Li, and S. Chien, *Molecular basis of the effects of mechanical stretch on vascular smooth muscle cells.* Journal of Biomechanics, 2007. **40**: p. 947-960.
176. Wilson, E., et al., *Strain-Responsive Regions in the Platelet-Derived Growth Factor-A Gene Promoter.* Hypertension, 1998. **31**: p. 170-175.
177. Pannier, B.M., et al., *Methods and devices for measuring arterial compliance in humans.* American journal of hypertension, 2002. **15**: p. 743-53.
178. Schwenger, V., et al., *Color Doppler Indices of Renal Allografts Depend on Vascular Stiffness of the Transplant Recipients.* American Journal of Transplantation, 2006. **6**: p. 2721-2724.
179. V., R.K., et al., *Brachial artery stiffness estimation using ARTSENS*, in *2017 39th Annual International Conference of the IEEE Engineering in Medicine and Biology Society (EMBC)*. 2017, IEEE. p. 262-265.
180. Joseph, J., et al., *Technical Validation of ARTSENS-An Image Free Device for Evaluation of Vascular Stiffness.* IEEE journal of translational engineering in health and medicine, 2015. **3**: p. 1900213.
181. Joseph, J., et al., *ARTSENSTouch - A portable device for evaluation of carotid artery stiffness*, in *2015 37th Annual International Conference of the IEEE Engineering in Medicine and Biology Society (EMBC)*. 2015, IEEE. p. 3755-3758.
182. Joseph, J., et al., *Arterial compliance probe for cuffless evaluation of carotid pulse pressure.* PLOS ONE, 2018. **13**: p. e0202480.
183. Joseph, J., M.I. Shah, and M. Sivaprakasam, *ARTSENS® Pen: A portable, image-free device for automated evaluation of vascular stiffness*, in *2016 IEEE International Symposium on Medical Measurements and Applications (MeMeA)*. 2016, IEEE. p. 1-6.
184. Sahani, A.K., J. Joseph, and M. Sivaprakasam, *Evaluation of the algorithm for automatic identification of the common carotid artery in ARTSENS.* Physiological Measurement, 2014. **35**: p. 1299-1317.
185. Joseph, J., et al., *ARTSENS® Pen—portable easy-to-use device for carotid stiffness measurement: technology validation and clinical-utility assessment.* Biomedical Physics & Engineering Express, 2020. **6**(2): p. 025013.
186. Haller, M.J., et al., *Radial Artery Tonometry Demonstrates Arterial Stiffness in Children With Type 1 Diabetes.* Diabetes Care, 2004. **27**: p. 2911-2917.
187. London, G.M. and B. Pannier, *Arterial functions: how to interpret the complex physiology.* Nephrology Dialysis Transplantation, 2010. **25**: p. 3815-3823.
188. Wilkinson, I.B., et al., *The influence of heart rate on augmentation index and central arterial pressure in humans.* The Journal of physiology, 2000. **525**(1): p. 263-270.
189. Močnik, M., S. Nikolić, and N.M. Varda, *Arterial compliance measurement in overweight and hypertensive children.* The Indian Journal of Pediatrics, 2016. **83**(6): p. 510-516.
190. Laurent, S., et al., *Expert consensus document on arterial stiffness: methodological issues and clinical applications.* European Heart Journal, 2006. **27**: p. 2588-2605.
191. Knutsen, R.H., et al., *Minoxidil improves vascular compliance, restores cerebral blood flow, and alters extracellular matrix gene expression in a model of chronic vascular stiffness.* American Journal of Physiology-Heart and Circulatory Physiology, 2018. **315**(1): p. H18-H32.
192. Rivera-Rivera, L.A., et al., *Assessment of vascular stiffness in the internal carotid artery proximal to the carotid canal in Alzheimer's disease using pulse wave velocity from low rank reconstructed 4D flow MRI.* Journal of Cerebral Blood Flow & Metabolism, 2020: p. 0271678X20910302.

193. Pattinson, K., G. Wynne-Jones, and C.H. Imray, *Monitoring intracranial pressure, perfusion and metabolism.* Continuing Education in Anaesthesia Critical Care & Pain, 2005. **5**: p. 130-133.
194. Bude, R.O. and J.M. Rubin, *Relationship between the Resistive Index and Vascular Compliance and Resistance.* Radiology, 1999. **211**: p. 411-417.
195. Lee, W.-J., et al., *Progression of cerebral white matter hyperintensities and the associated sonographic index.* Radiology, 2017. **284**(3): p. 824-833.
196. Calabia, J., et al., *Doppler ultrasound in the measurement of pulse wave velocity: agreement with the Complior method.* Cardiovascular Ultrasound, 2011. **9**: p. 13.
197. Weber, T., et al., *Noninvasive determination of carotid–femoral pulse wave velocity depends critically on assessment of travel distance: a comparison with invasive measurement.* Journal of Hypertension, 2009. **27**: p. 1624-1630.
198. Joseph, J., et al., *Arterial compliance probe for cuffless evaluation of carotid pulse pressure.* PloS one, 2018. **13**(8): p. e0202480.
199. Nabeel, P., J. Joseph, and M. Sivaprakasam. *Arterial compliance probe for local blood pulse wave velocity measurement*. in *2015 37th Annual International Conference of the IEEE Engineering in Medicine and Biology Society (EMBC)*. 2015. IEEE.
200. Vappou, J., J. Luo, and E.E. Konofagou, *Pulse wave imaging for noninvasive and quantitative measurement of arterial stiffness in vivo.* American journal of hypertension, 2010. **23**(4): p. 393-398.
201. Vardoulis, O., T.G. Papaioannou, and N. Stergiopulos, *On the estimation of total arterial compliance from aortic pulse wave velocity.* Annals of biomedical engineering, 2012. **40**(12): p. 2619-2626.
202. Liberson, A.S., et al., *A physics based approach to the pulse wave velocity prediction in compliant arterial segments.* Journal of biomechanics, 2016. **49**(14): p. 3460-3466.
203. Qiang, Y., et al., *Evaluation of the Impact of Passive Smoke on Arterial Elasticity via Echo-Tracking Technology in a Rabbit Model.* Journal of Ultrasound in Medicine, 2014. **33**(11): p. 1949-1956.
204. McGarry, M., et al., *In vivo repeatability of the pulse wave inverse problem in human carotid arteries.* Journal of biomechanics, 2017. **64**: p. 136-144.
205. Vanden Eynden, F., et al., *Measuring pulmonary arterial compliance: mission impossible? Insights from a novel in vivo continuous-flow based experimental model.* Pulmonary circulation, 2018. **8**(2): p. 2045894018776882.
206. Haluska, B.A., et al., *Influence of cardiovascular risk factors on total arterial compliance.* Journal of the American Society of Echocardiography, 2008. **21**(2): p. 123-128.
207. Haluska, B.A., et al., *Measurement of arterial distensibility and compliance to assess prognosis.* Atherosclerosis, 2010. **209**(2): p. 474-480.
208. Talts, J., R. Raamat, and K. Jagomägi, *Influence of pulse pressure variation on the results of local arterial compliance measurement: A computer simulation study.* Computers in biology and medicine, 2009. **39**(8): p. 707-712.
209. Tai, N., et al., *Compliance properties of conduits used in vascular reconstruction.* British Journal of Surgery, 2000. **87**(11): p. 1516-1524.
210. Abbott, W.M., et al., *Effect of compliance mismatch on vascular graft patency.* Journal of vascular surgery, 1987. **5**: p. 376-82.
211. He, F., L. Hua, and L.-j. Gao, *A Computational Model for Biomechanical Effects of Arterial Compliance Mismatch.* Applied Bionics and Biomechanics, 2015. **2015**: p. 1-6.

212. Surovtsova, I., *Effects of compliance mismatch on blood flow in an artery with endovascular prosthesis.* Journal of Biomechanics, 2005. **38**: p. 2078-2086.
213. Steinman, D.A., D.A. Vorp, and C.R. Ethier, *Computational modeling of arterial biomechanics: Insights into pathogenesis and treatment of vascular disease.* Journal of Vascular Surgery, 2003. **37**: p. 1118-1128.
214. Szafron, J.M., et al., *Optimization of tissue-engineered vascular graft design using computational modeling.* Tissue Engineering Part C: Methods, 2019. **25**(10): p. 561-570.
215. Stewart, S.F.C. and D.J. Lyman, *Effects of an artery/vascular graft compliance mismatch on protein transport: a numerical study.* Annals of biomedical engineering, 2004. **32**: p. 991-1006.
216. Szafron, J., et al., *Immuno-driven and mechano-mediated neotissue formation in tissue engineered vascular grafts.* Annals of biomedical engineering, 2018. **46**(11): p. 1938-1950.
217. Wise, S.G., et al., *A multilayered synthetic human elastin/polycaprolactone hybrid vascular graft with tailored mechanical properties.* Acta Biomaterialia, 2011. **7**: p. 295-303.
218. Cheung, D.K., et al. *Adaptive clutter filter design for micro-ultrasound color flow imaging of small blood vessels*. in *2010 IEEE International Ultrasonics Symposium*. 2010. IEEE.
219. Gong, X., et al., *Physiological pulsatile flow culture conditions to generate functional endothelium on a sulfated silk fibroin nanofibrous scaffold.* Biomaterials, 2014. **35**: p. 4782-4791.
220. Kim, Y., et al., *Flow dynamics across end-to-end vascular bypass graft anastomoses.* Annals of biomedical engineering, 1993. **21**(4): p. 311-320.
221. Anderson, D.E., et al., *Biomimetic modification of poly (vinyl alcohol): encouraging endothelialization and preventing thrombosis with antiplatelet monotherapy.* Acta biomaterialia, 2019. **86**: p. 291-299.
222. Anderson, D.E., et al., *Improving surgical methods for studying vascular grafts in animal models.* Tissue Engineering Part C: Methods, 2018. **24**(8): p. 457-464.
223. Wijeyaratne, S.M. and L. Kannangara, *Safety and efficacy of electrospun polycarbonate-urethane vascular graft for early hemodialysis access: first clinical results in man.* The Journal of Vascular Access, 2011. **12**(1): p. 28-35.
224. Ferraresso, M., et al., *Early experience with a newly developed electrospun polycarbonate-urethane vascular graft for hemodialysis access.* The journal of vascular access, 2013. **14**(3): p. 252-256.
225. Banerjee, M.K., R. Ganguly, and A. Datta, *Effect of pulsatile flow waveform and Womersley number on the flow in stenosed arterial geometry.* ISRN Biomathematics, 2012. **2012**.
226. Gayathri, K. and K. Shailendhra, *Pulsatile blood flow in large arteries: comparative study of Burton's and McDonald's models.* Applied Mathematics and Mechanics, 2014. **35**(5): p. 575-590.
227. Ramnarine, K.V., et al., *Validation of a new blood-mimicking fluid for use in Doppler flow test objects.* Ultrasound in medicine & biology, 1998. **24**(3): p. 451-459.
228. Samavat, H. and J. Evans, *An ideal blood mimicking fluid for doppler ultrasound phantoms.* Journal of Medical Physics/Association of Medical Physicists of India, 2006. **31**(4): p. 275.
229. Ramnarine, K.V., et al., *Doppler backscatter properties of a blood-mimicking fluid for Doppler performance assessment.* Ultrasound in medicine & biology, 1999. **25**(1): p. 105-110.
230. Brindise, M.C., et al., *Hemodynamics of stent implantation procedures in coronary bifurcations: An in vitro study.* Annals of biomedical engineering, 2017. **45**(3): p. 542-553.

231. Geoghegan, P.H., M.C. Jermy, and D.S. Nobes, *A PIV comparison of the flow field and wall shear stress in rigid and compliant models of healthy carotid arteries.* Journal of Mechanics in Medicine and Biology, 2017. **17**(03): p. 1750041.
232. Rathod, M., et al., *Hybrid polymer microfluidic platform to mimic varying vascular compliance and topology.* Lab on a Chip, 2017. **17**(14): p. 2508-2516.
233. Montini-Ballarin, F., et al., *Mechanical behavior of bilayered small-diameter nanofibrous structures as biomimetic vascular grafts.* Journal of the mechanical behavior of biomedical materials, 2016. **60**: p. 220-233.
234. Polanczyk, A., et al., *Artificial circulatory model for analysis of human and artificial vessels.* Applied Sciences, 2018. **8**(7): p. 1017.
235. Song, G., et al., *Effects of different clipping time of aneurysm clips on common carotid artery wall in rabbits.* Chinese Journal of Cerebrovascular Diseases, 2017. **14**(4): p. 193-196.
236. Byrom, M.J., et al., *Animal models for the assessment of novel vascular conduits.* Journal of vascular surgery, 2010. **52**(1): p. 176-195.
237. Tseng, Y.C., et al., *An in vivo study on endothelialized vascular grafts produced by autologous biotubes and adipose stem cells (ADSCs).* Journal of Materials Science: Materials in Medicine, 2017. **28**(10): p. 166.
238. Sharath, U., et al., *Radial arterial compliance measurement by fiber Bragg grating pulse recorder.* Journal of Human Hypertension, 2014. **28**: p. 736-742.
239. Chirinos, J.A., *Arterial Stiffness: Basic Concepts and Measurement Techniques.* Journal of Cardiovascular Translational Research, 2012. **5**: p. 243-255.
240. Standard, A.N., *American National Standard Ansi / Iso.* 2010. **2008**.
241. Lovett, M., et al., *Tubular silk scaffolds for small diameter vascular grafts.* Organogenesis, 2010. **6**(4): p. 217-224.
242. Colombo, A., et al., *Cyclic strain amplitude dictates the growth response of vascular smooth muscle cells in vitro: role in in-stent restenosis and inhibition with a sirolimus drug-eluting stent.* Biomechanics and modeling in mechanobiology, 2013. **12**(4): p. 671-683.
243. Lehoux, S.p. and A. Tedgui, *Signal transduction of mechanical stresses in the vascular wall.* Hypertension, 1998. **32**(2): p. 338-345.
244. Potter, C.M., et al., *Shape and compliance of endothelial cells after shear stress in vitro or from different aortic regions: scanning ion conductance microscopy study.* PloS one, 2012. **7**(2): p. e31228.
245. Fillinger, M.F., et al., *The effect of endothelial cell coculture on smooth muscle cell proliferation.* Journal of vascular surgery, 1993. **17**(6): p. 1058-1068.
246. Golledge, J., *Vein grafts: haemodynamic forces on the endothelium—a review.* European journal of vascular and endovascular surgery, 1997. **14**(5): p. 333-343.
247. Tsaousi, A., et al., *Wnt4/β-catenin signaling induces VSMC proliferation and is associated with intimal thickening.* Circulation research, 2011. **108**(4): p. 427-436.
248. Administration, F.a.D., *Recognized Consensus Standards.*
249. Pashneh-Tala, S., S. MacNeil, and F. Claeyssens, *The Tissue-Engineered Vascular Graft—Past, Present, and Future.* Tissue Engineering Part B: Reviews, 2016. **22**: p. 68-100.
250. Soletti, L., et al., *A bilayered elastomeric scaffold for tissue engineering of small diameter vascular grafts.* Acta Biomaterialia, 2010. **6**: p. 110-122.
251. Luisada, A.A. and S.J. Sarnoff, *Paroxysmal pulmonary edema consequent to stimulation of cardiovascular receptors: II. Mechanical and neurogenic elements.* American Heart Journal, 1946. **31**(3): p. 282-292.

252. Zarka, M., et al., *Mechanical loading activates the YAP/TAZ pathway and chemokine expression in the MLO-Y4 osteocyte-like cell line.* Laboratory Investigation, 2021. **101**(12): p. 1597-1604.
253. Wang, S., et al., *The crosstalk between hippo-YAP pathway and innate immunity.* Frontiers in Immunology, 2020. **11**: p. 323.
254. Ho, R.X.-Y., et al., *The cell adhesion molecule IGPR-1 is activated by and regulates responses of endothelial cells to shear stress.* Journal of Biological Chemistry, 2019. **294**(37): p. 13671-13680.
255. Papaioannou, T.G. and C. Stefanadis, *Vascular wall shear stress: basic principles and methods.* Hellenic J Cardiol, 2005. **46**(1): p. 9-15.
256. Chiu, C.-Z., B.-W. Wang, and K.-G. Shyu, *Effects of cyclic stretch on the molecular regulation of myocardin in rat aortic vascular smooth muscle cells.* Journal of Biomedical Science, 2013. **20**(1): p. 1-12.
257. Liu, S.Q. and J. Goldman, *Role of blood shear stress in the regulation of vascular smooth muscle cell migration.* IEEE transactions on biomedical engineering, 2001. **48**(4): p. 474-483.
258. Ueba, H., M. Kawakami, and T. Yaginuma, *Shear stress as an inhibitor of vascular smooth muscle cell proliferation: role of transforming growth factor-β1 and tissue-type plasminogen activator.* Arteriosclerosis, thrombosis, and vascular biology, 1997. **17**(8): p. 1512-1516.
259. Sun, L., et al., *Shear stress induces phenotypic modulation of vascular smooth muscle cells via AMPK/mTOR/ULK1-mediated autophagy.* Cellular and molecular neurobiology, 2018. **38**(2): p. 541-548.
260. Yang, W., et al., *Roles of AMP-activated protein kinase (AMPK) in mammalian reproduction.* Frontiers in Cell and Developmental Biology, 2020. **8**: p. 593005.
261. Bono, N., et al., *Unraveling the role of mechanical stimulation on smooth muscle cells: A comparative study between 2D and 3D models.* Biotechnology and bioengineering, 2016. **113**(10): p. 2254-2263.
262. Stegemann, J.P., H. Hong, and R.M. Nerem, *Mechanical, biochemical, and extracellular matrix effects on vascular smooth muscle cell phenotype.* Journal of applied physiology, 2005. **98**(6): p. 2321-2327.
263. Song, L., et al., *Downregulation of miR-223 and miR-153 mediates mechanical stretch-stimulated proliferation of venous smooth muscle cells via activation of the insulin-like growth factor-1 receptor.* Archives of biochemistry and biophysics, 2012. **528**(2): p. 204-211.
264. Hu, Y., et al., *Activation of PDGF receptor α in vascular smooth muscle cells by mechanical stress.* The FASEB Journal, 1998. **12**(12): p. 1135-1142.
265. Williams, B., *Mechanical influences on vascular smooth muscle cell function.* Journal of hypertension, 1998. **16**(12): p. 1921-1929.
266. Berk, B.C., *Vascular smooth muscle growth: autocrine growth mechanisms.* Physiological reviews, 2001. **81**(3): p. 999-1030.
267. Zhou, J., et al., *PDGF-BB promotes vascular smooth muscle cell migration by enhancing Pim-1 expression via inhibiting miR-214.* Annals of Translational Medicine, 2021. **9**(23).
268. Shimizu, N., et al., *Cyclic strain induces mouse embryonic stem cell differentiation into vascular smooth muscle cells by activating PDGF receptor β.* Journal of applied physiology, 2008. **104**(3): p. 766-772.
269. Standley, P.R., et al., *Cyclic stretch induces vascular smooth muscle cell alignment via NO signaling.* American Journal of Physiology-Heart and Circulatory Physiology, 2002. **283**(5): p. H1907-H1914.

270. Smith, J., et al., *Cyclic stretch induces the expression of vascular endothelial growth factor in vascular smooth muscle cells.* Endothelium, 2001. **8**(1): p. 41-48.
271. Wang, Y., et al., *Arterial wall stress induces phenotypic switching of arterial smooth muscle cells in vascular remodeling by activating the YAP/TAZ signaling pathway.* Cellular Physiology and Biochemistry, 2018. **51**(2): p. 842-853.
272. Liu, T., et al., *YAP1 up-regulation inhibits apoptosis of aortic dissection vascular smooth muscle cells.* Eur Rev Med Pharmacol Sci, 2017. **21**(20): p. 4632-4639.
273. Nappi, F., et al., *Compliance mismatch and compressive wall stresses drive anomalous remodelling of pulmonary trunks reinforced with Dacron grafts.* Journal of the mechanical behavior of biomedical materials, 2016. **63**: p. 287-302.
274. Bateman, G.A., *Vascular compliance in normal pressure hydrocephalus.* American Journal of Neuroradiology, 2000. **21**(9): p. 1574-1585.
275. Shirwany, N.A. and M.-h. Zou, *Arterial stiffness: a brief review.* Acta Pharmacologica Sinica, 2010. **31**(10): p. 1267-1276.
276. DeLoach, S.S. and R.R. Townsend, *Vascular stiffness: its measurement and significance for epidemiologic and outcome studies.* Clinical Journal of the American Society of Nephrology, 2008. **3**(1): p. 184-192.
277. Bardini, R., et al., *Anastomosis.* World journal of surgery, 1994. **18**(3): p. 373-378.
278. Yao, Y., et al., *Rabbit Surgery Protocol for End-to-End and End-to-Side Vascular GraftVascular grafts AnastomosisAnastomoses*, in *Vascular Tissue Engineering: Methods and Protocols*, F. Zhao and K.W. Leong, Editors. 2022, Springer US: New York, NY. p. 177-189.
279. Qiu, Y. and J.M. Tarbell, *Computational simulation of flow in the end-to-end anastomosis of a rigid graft and a compliant artery.* ASAIO Journal (American Society for Artificial Internal Organs: 1992), 1996. **42**(5): p. M702-9.
280. Steinman, D., et al., *A numerical simulation of flow in a two-dimensional end-to-side anastomosis model.* 1993.
281. Al-Sukhun, J., et al., *Microvascular stress analysis: Part I: Simulation of microvascular anastomoses using finite element analysis.* British Journal of Oral and Maxillofacial Surgery, 2007. **45**(2): p. 130-137.
282. Longest, P.W. and C. Kleinstreuer, *Numerical simulation of wall shear stress conditions and platelet localization in realistic end-to-side arterial anastomoses.* J. Biomech. Eng., 2003. **125**(5): p. 671-681.
283. Carroll, J., et al., *Reduction in anastomotic flow disturbance within a modified end-to-side arteriovenous fistula configuration: Results of a computational flow dynamic model.* Nephrology, 2019. **24**(2): p. 245-251.
284. Pousset, Y., et al., *Numerical model study of flow dynamics through an end-to-side anastomosis: choice of anastomosis angle and prosthesis diameter.* Annals of vascular surgery, 2006. **20**(6): p. 773-779.
285. Ramezanpour, M., M. Maerefat, and M. Mokhtari-Dizaji, *The effects of compliance mismatch on the End to Side bypass graft.* Modares Mechanical Engineering, 2015. **15**(5): p. 279-286.
286. *ibidi Pump System*. Available from: https://ibidi.com/perfusion-system/112-ibidi-pump-system.html.
287. Birjiniuk, J., et al., *Pulsatile flow leads to intimal flap motion and flow reversal in an in vitro model of type B aortic dissection.* Cardiovascular engineering and technology, 2017. **8**(3): p. 378-389.

288. Cutiongco, M.F.A., et al., *Composite scaffold of poly (vinyl alcohol) and interfacial polyelectrolyte complexation fibers for controlled biomolecule delivery.* Frontiers in bioengineering and biotechnology, 2015. **3**: p. 3.
289. Elshazly, T.H., *Characterization of PVA hydrogels with regards to vascular graft development*. 2004, Georgia Institute of Technology.
290. Pohan, G., et al., *Effect of Ethylene Oxide Sterilization on Polyvinyl Alcohol Hydrogel Compared with Gamma Radiation.* Tissue Engineering Part A, 2020.
291. Menon, E.S., *Chapter 7 - Pipe Strength and Wall Thickness*, in *Pipeline Planning and Construction Field Manual*, E.S. Menon, Editor. 2011, Gulf Professional Publishing. p. 105-121.
292. Kim, H., S. Han, and Y. Seo, *Novel Dual Curing Process for a Stereolithographically Printed Part Triggers A Remarkably Improved Interlayer Adhesion and Excellent Mechanical Properties.* Langmuir, 2020.
293. Leone, G., et al., *PVA/STMP based hydrogels as potential substitutes of human vitreous.* Journal of Materials Science: Materials in Medicine, 2010. **21**(8): p. 2491-2500.
294. Peppas, N.A., et al., *Hydrogels in biology and medicine: from molecular principles to bionanotechnology.* Advanced materials, 2006. **18**(11): p. 1345-1360.
295. Puy, N.M.B.C., O. McCarty, and M. Hinds. *Thrombogenicity of poly (Vinyl) alcohol hydrogels is dependent on the crosslinking agent*. in *42nd Society for Biomaterials Annual Meeting and Exposition 2019: The Pinnacle of Biomaterials Innovation and Excellence*. 2019. Society for Biomaterials.
296. XIONG, D.-s., *Synthesis and properties of physically crosslinked poly (vinyl alcohol) hydrogels.* Journal of China University of Mining and Technology, 2008. **18**(2): p. 271-274.
297. Chen, H., et al., *Thermo-and water-induced shape memory poly (vinyl alcohol) supramolecular networks crosslinked by self-complementary quadruple hydrogen bonding.* Polymer Chemistry, 2016. **7**(43): p. 6637-6644.
298. Court, R., M. Sutcliffe, and S. Tavakoli, *Ageing of adhesively bonded joints—fracture and failure analysis using video imaging techniques.* International journal of adhesion and adhesives, 2001. **21**(6): p. 455-463.
299. Ahmed, A.A., et al., *Infrared spectroscopic characterization of phosphate binding at the goethite–water interface.* Physical Chemistry Chemical Physics, 2019. **21**(8): p. 4421-4434.
300. Peppas, N.A. and E.W. Merrill, *Differential scanning calorimetry of crystallized PVA hydrogels.* Journal of Applied Polymer Science, 1976. **20**(6): p. 1457-1465.
301. Lack, S., et al., *Hydrogels based on pullulan crosslinked with sodium trimetaphosphate (STMP): rheological study.* Polymer Bulletin, 2004. **52**(6): p. 429-436.
302. Wolf, G., H.-G. Schmidt, and K. Bohmhammel, *Differential scanning calorimetry. A reliable method of enthalpy calibration.* Thermochimica acta, 1994. **235**(1): p. 23-29.
303. Markiewicz, M.R., R. Ord, and R.P. Fernandes, *Local and Regional Flap Reconstruction of Maxillofacial Defects*, in *Maxillofacial surgery*. 2017, Elsevier. p. 616-635.
304. Wise, S.G., et al., *A multilayered synthetic human elastin/polycaprolactone hybrid vascular graft with tailored mechanical properties.* Acta biomaterialia, 2011. **7**(1): p. 295-303.
305. Konig, G., et al., *Mechanical properties of completely autologous human tissue engineered blood vessels compared to human saphenous vein and mammary artery.* Biomaterials, 2009. **30**(8): p. 1542-1550.
306. Krejza, J., et al., *Carotid artery diameter in men and women and the relation to body and neck size.* Stroke, 2006. **37**(4): p. 1103-1105.

307. Sarkar, S., et al., *The mechanical properties of infrainguinal vascular bypass grafts: their role in influencing patency.* European journal of vascular and endovascular surgery, 2006. **31**(6): p. 627-636.
308. Hansen, F., et al., *Diameter and compliance in the human common carotid artery—variations with age and sex.* Ultrasound in medicine & biology, 1995. **21**(1): p. 1-9.
309. Fung, Y.-C., *Biomechanics: circulation*. Shock. Vol. 9. 1998. 155.
310. Kambric, H., A. Kantrowitz, and P. Sung, *Vascular Graft Update, ASTM Publication 04-898000-54*. 1984, American Society for Testing and Materials, Philadelphia, PA.
311. Catanese III, J., et al., *Mechanical properties of medical grade expanded polytetrafluoroethylene: the effects of internodal distance, density, and displacement rate.* Journal of Biomedical Materials Research: An Official Journal of The Society for Biomaterials, The Japanese Society for Biomaterials, and The Australian Society for Biomaterials, 1999. **48**(2): p. 187-192.
312. Biglino, G., et al., *Rapid prototyping compliant arterial phantoms for in-vitro studies and device testing.* Journal of Cardiovascular Magnetic Resonance, 2013. **15**(1): p. 2.
313. Gao, J., et al., *Effect of wall structures on mechanical properties of small caliber PHBHHx vascular grafts.* Fibers and Polymers, 2019. **20**(11): p. 2261-2267.
314. Nezarati, R.M., et al., *Electrospun vascular grafts with improved compliance matching to native vessels.* Journal of Biomedical Materials Research Part B: Applied Biomaterials, 2015. **103**(2): p. 313-323.
315. Zhu, X.-K. and B.N. Leis, *Evaluation of burst pressure prediction models for line pipes.* International Journal of Pressure Vessels and Piping, 2012. **89**: p. 85-97.
316. Holloway, J.L., A.M. Lowman, and G.R. Palmese, *The role of crystallization and phase separation in the formation of physically cross-linked PVA hydrogels.* Soft Matter, 2013. **9**(3): p. 826-833.
317. Peppas, N.A., *Turbidimetric studies of aqueous poly (vinyl alcohol) solutions.* Die Makromolekulare Chemie: Macromolecular Chemistry and Physics, 1975. **176**(11): p. 3433-3440.
318. Otsuka, E. and A. Suzuki, *A simple method to obtain a swollen PVA gel crosslinked by hydrogen bonds.* Journal of applied polymer science, 2009. **114**(1): p. 10-16.
319. Peacock, A.J. and A. Calhoun, *Polymer Chemistry: Properties and Application*. 2012: Carl Hanser Verlag GmbH Co KG.
320. Yu, L.Y., A.E. Daugaard, and A.L. Skov. *Adhesion between polydimethylsiloxane layers by crosslinking*. in *Advances in Science and Technology*. 2013. Trans Tech Publ.
321. Abraham, G., P. Frontini, and T. Cuadrado, *Molding of biomedical segmented polyurethane delamination events and stretching behavior.* Journal of applied polymer science, 1998. **69**(11): p. 2159-2167.
322. Peiffer, D.G. and L.E. Nielsen, *Preparation and mechanical properties of thick interlayer composites.* Journal of Applied Polymer Science, 1979. **23**(8): p. 2253-2264.
323. Nautiyal, P., B. Boesl, and A. Agarwal, *Harnessing three dimensional anatomy of graphene foam to induce superior damping in hierarchical polyimide nanostructures.* Small, 2017. **13**(10): p. 1603473.
324. Srinivasan, E., T. Vanchinathan, and G. Siva Kumar, *Fabrication of Microcontroller Based Dip-Casting for Thin Films Depositions.*
325. Awaja, F., et al., *Adhesion of polymers.* Progress in polymer science, 2009. **34**(9): p. 948-968.

326. Wu, T., Taylor, S., Vijayaraghavan, S., Danelon, R, *Improving the Manufacturing Process for Biocompatible Vascular Grafts*, in *2019 Chemical Engineering Capstone Design Projects*. 2019, University of Waterloo: University of Waterloo.
327. Al-Owaisi, S., et al., *An experimental investigation of the effect of defect shape and orientation on the burst pressure of pressurised pipes.* Engineering Failure Analysis, 2018. **93**: p. 200-213.
328. Zlokarnik, M., *Scale-up in chemical engineering*. 2006: John Wiley & Sons.
329. Zhong, Q., et al., *Advances of microfluidics in biomedical engineering.* Advanced materials technologies, 2019. **4**(6): p. 1800663.
330. Wojasiński, M., M. Pilarek, and T. Ciach, *Comparative studies of electrospinning and solution blow spinning processes for the production of nanofibrous poly (L-lactic acid) materials for biomedical engineering.* Polish Journal of Chemical Technology, 2014. **16**(2).
331. Kamali, A.R. and D.J. Fray, *Large-scale preparation of graphene by high temperature insertion of hydrogen into graphite.* Nanoscale, 2015. **7**(26): p. 11310-11320.
332. Padilla-Zakour, O.I., *Good manufacturing practices.* Microbiologically safe foods, 2009: p. 395.
333. Narloch, J.A. and M.E. Brandstater, *Influence of breathing technique on arterial blood pressure during heavy weight lifting.* Archives of physical medicine and rehabilitation, 1995. **76**(5): p. 457-462.
334. Atlan, M., et al., *Design, characterization and in vivo performance of synthetic 2 mm-diameter vessel grafts made of PVA-gelatin blends.* Scientific reports, 2018. **8**(1): p. 1-12.
335. Lu, Q.-B., et al., *Chicoric acid prevents PDGF-BB-induced VSMC dedifferentiation, proliferation and migration by suppressing ROS/NFκB/mTOR/P70S6K signaling cascade.* Redox biology, 2018. **14**: p. 656-668.
336. Xiao, J., et al., *Conditional knockout of TFPI-1 in VSMCs of mice accelerates atherosclerosis by enhancing AMOT/YAP pathway.* International Journal of Cardiology, 2017. **228**: p. 605-614.
337. Zhong, L. and J.Y. Su, *Isoflurane activates PKC and Ca2+-calmodulin-dependent protein kinase II via MAP kinase signaling in cultured vascular smooth muscle cells.* The Journal of the American Society of Anesthesiologists, 2002. **96**(1): p. 148-154.
338. Hu, M., et al., *PVA/carbon dot nanocomposite hydrogels for simple introduction of Ag nanoparticles with enhanced antibacterial activity.* Macromolecular Materials and Engineering, 2016. **301**(11): p. 1352-1362.
339. 2022; Available from: https://www.lifelinecelltech.com/shop/culture-media/smooth-muscle-culture-media/vasculife-smooth-muscle-cell-medium-ll-0014/?gclid=Cj0KCQjwtvqVBhCVARIsAFUxcRsnIqQ-C4P7L2g2slSKJ-jtmOkv-1OmRnlcnu56qh5BkO4b2zvnO3saAtkeEALw_wcB.
340. Abcam. *ab219801 EdU Proliferation Kit (iFluor 488)*. Available from: https://www.abcam.com/ps/products/219/ab219801/documents/EdU-assay-staining-Proliferation-Kit-iFluor-488-protocol-book-v2b-ab219801%20(website).pdf.
341. *General Protocol for Western Blotting*. Bio-Rad.
342. Scientific, T.F. *Pierce BCA Protein Assay Kit*. Available from: https://www.thermofisher.com/document-connect/document-connect.html?url=https://assets.thermofisher.com/TFS-Assets%2FLSG%2Fmanuals%2FMAN0011430_Pierce_BCA_Protein_Asy_UG.pdf.

343. Morton, R.C., D. Mangroo, and G.E. Gerber, *A novel method of complete activation by carbonyldiimidazole: application to ester synthesis.* Canadian journal of chemistry, 1988. **66**(7): p. 1701-1705.
344. Paulin, D. and Z. Li, *Desmin: a major intermediate filament protein essential for the structural integrity and function of muscle.* Experimental cell research, 2004. **301**(1): p. 1-7.
345. Kacem, K., J. Seylaz, and P. Aubineau, *Differential processes of vascular smooth muscle cell differentiation within elastic and muscular arteries of rats and rabbits: an immunofluorescence study of desmin and vimentin distribution.* The Histochemical Journal, 1996. **28**(1): p. 53-61.
346. Schwartz, S.M., G.R. Campbell, and J.H. Campbell, *Replication of smooth muscle cells in vascular disease.* Circulation research, 1986. **58**(4): p. 427-444.
347. Heo, S.-J., et al., *Differentiation alters stem cell nuclear architecture, mechanics, and mechano-sensitivity.* Elife, 2016. **5**: p. e18207.
348. Foster, J.W., et al., *Differential nuclear expression of Yap in basal epithelial cells across the cornea and substrates of differing stiffness.* Experimental eye research, 2014. **127**: p. 37-41.
349. Kim, J.-Y., et al., *Apamin inhibits PDGF-BB-induced vascular smooth muscle cell proliferation and migration through suppressions of activated Akt and Erk signaling pathway.* Vascular pharmacology, 2015. **70**: p. 8-14.
350. Bandaru, P., et al., *Mechanical Cues Regulating Proangiogenic Potential of Human Mesenchymal Stem Cells through YAP-Mediated Mechanosensing.* Small, 2020. **16**(25): p. 2001837.
351. Keogh, M.B., F.J. O'Brien, and J.S. Daly, *Substrate stiffness and contractile behaviour modulate the functional maturation of osteoblasts on a collagen–GAG scaffold.* Acta biomaterialia, 2010. **6**(11): p. 4305-4313.
352. Johnson, J.L., et al., *Injury induces dedifferentiation of smooth muscle cells and increased matrix-degrading metalloproteinase activity in human saphenous vein.* Arteriosclerosis, thrombosis, and vascular biology, 2001. **21**(7): p. 1146-1151.
353. Duboeuf, F., et al., *Investigation of PVA cryogel Young's modulus stability with time, controlled by a simple reliable technique.* Medical physics, 2009. **36**(2): p. 656-661.
354. Duck, F.A., *Physical properties of tissues: a comprehensive reference book*. 2013: Academic press.
355. Hneino, M., et al., *Density-dependent shift of transforming growth factor-beta-1 from inhibition to stimulation of vascular smooth muscle cell growth is based on unconventional regulation of proliferation, apoptosis and contact inhibition.* Journal of vascular research, 2009. **46**(2): p. 85-97.
356. Sun, Y.-y., et al., *MicroRNA expression profile and functional analysis reveal their roles in contact inhibition and its disruption switch of rat vascular smooth muscle cells.* Acta Pharmacologica Sinica, 2018. **39**(5): p. 885-892.
357. Gambillara, V., et al., *Effects of reduced cyclic stretch on vascular smooth muscle cell function of pig carotids perfused ex vivo.* American journal of hypertension, 2008. **21**(4): p. 425-431.
358. Thacher, T., et al., *Reduced cyclic stretch, endothelial dysfunction, and oxidative stress: an ex vivo model.* Cardiovascular Pathology, 2010. **19**(4): p. e91-e98.
359. Absher, M., et al., *Characterization of vascular smooth muscle cell phenotype in long-term culture.* In vitro cellular & developmental biology, 1989. **25**(2): p. 183-192.
360. Ashino, T., et al., *Unexpected role of the copper transporter ATP7A in PDGF-induced vascular smooth muscle cell migration.* Circulation research, 2010. **107**(6): p. 787-799.

361. Tannenberg, P., et al., *Extracellular retention of PDGF-B directs vascular remodeling in mouse hypoxia-induced pulmonary hypertension.* American Journal of Physiology-Lung Cellular and Molecular Physiology, 2018. **314**(4): p. L593-L605.
362. Lyle, A.N. and U. Raaz, *Killing me unsoftly: causes and mechanisms of arterial stiffness.* Arteriosclerosis, thrombosis, and vascular biology, 2017. **37**(2): p. e1-e11.
363. Igata, M., et al., *Adenosine monophosphate-activated protein kinase suppresses vascular smooth muscle cell proliferation through the inhibition of cell cycle progression.* Circulation research, 2005. **97**(8): p. 837-844.
364. Yonemitsu, Y., et al., *Transfer of wild-type p53 gene effectively inhibits vascular smooth muscle cell proliferation in vitro and in vivo.* Circulation research, 1998. **82**(2): p. 147-156.
365. Liu, X., et al., *A necessary role of miR-221 and miR-222 in vascular smooth muscle cell proliferation and neointimal hyperplasia.* Circulation research, 2009. **104**(4): p. 476-487.
366. George, S.J. and A. Dwivedi, *MMPs, cadherins, and cell proliferation.* Trends in cardiovascular medicine, 2004. **14**(3): p. 100-105.
367. Rawson, S., S. Cartmell, and J. Wong, *Suture techniques for tendon repair; a comparative review.* Muscles, ligaments and tendons journal, 2013. **3**(3): p. 220.
368. Riemer, K., et al., *Determining haemodynamic wall shear stress in the rabbit aorta in vivo using contrast-enhanced ultrasound image velocimetry.* Annals of Biomedical Engineering, 2020. **48**(6): p. 1728-1739.
369. Hofer, M., et al., *Numerical study of wall mechanics and fluid dynamics in end-to-side anastomoses and correlation to intimal hyperplasia.* Journal of biomechanics, 1996. **29**(10): p. 1297-1308.
370. Karimi, A., et al., *Experimental verification of the healthy and atherosclerotic coronary arteries incompressibility via digital image correlation.* Artery Research, 2016. **16**: p. 1-7.

Appendix

Preliminary data for Computational Fluid Dynamic Simulation

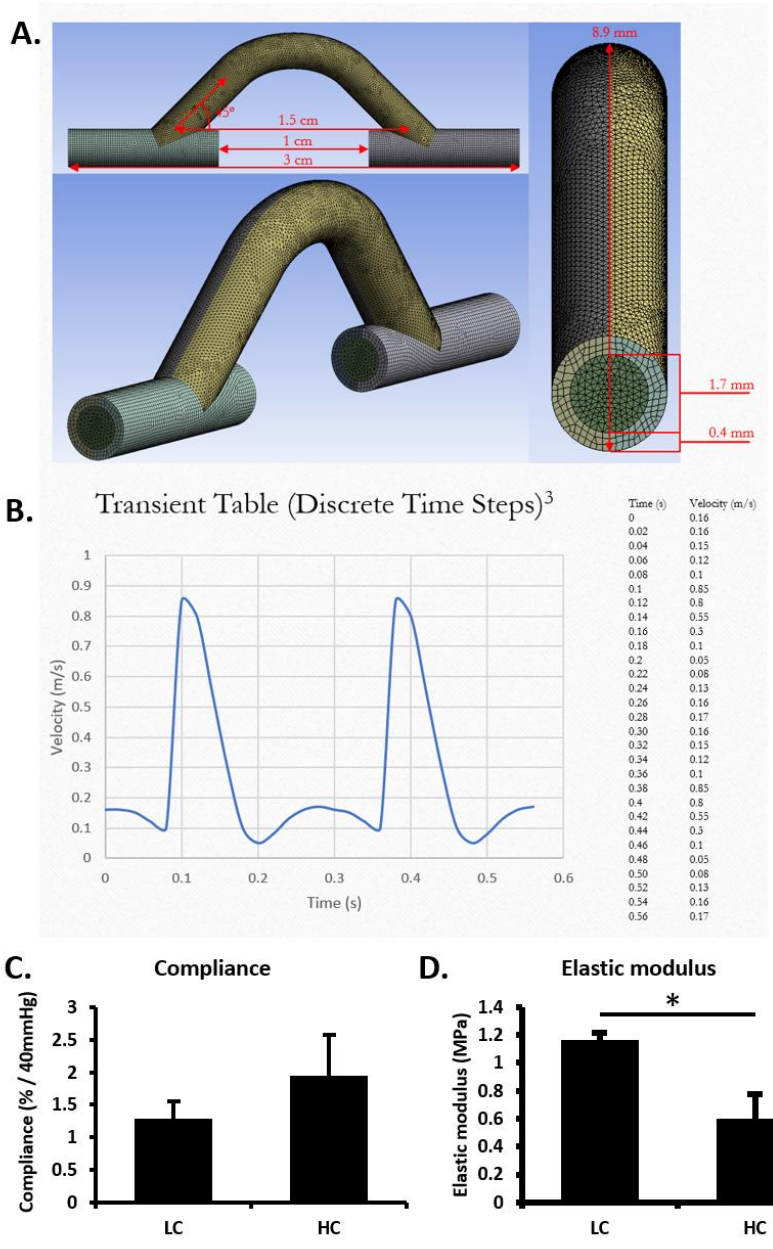

Figure A.1. Simulation parameters. (A) Dimension of the object used for the simulation. (B) input flow rate used [368]. (C) Compliance of the implanted PVA grafts used to compare with the simulation data. LC – low compliance, HC – high compliance. (D) Elastic modulus of the implanted PVA grafts. * indicates statistical difference between indicated groups with $p<0.05$. T-test used for statistical analysis. N=3.

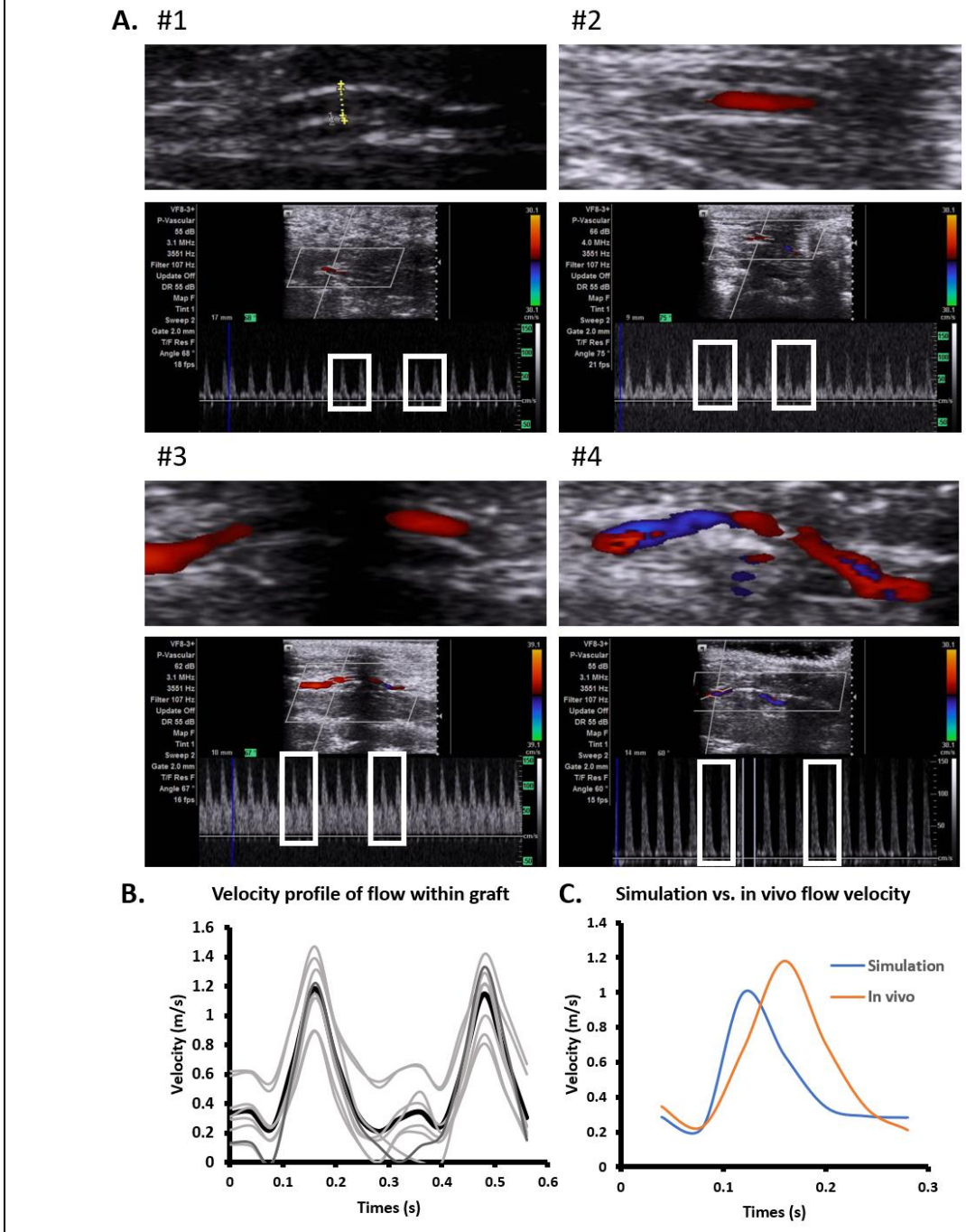

Figure A.2. Comparison between the simulation parameters and in vivo measurement. (A) Ultrasound images and blood flow profile from PVA grafts implanted in rabbit common carotid artery. (B) The velocity of blood flow measured from the ultrasound records. Black line – average flow velocity. (C) plot of the flow velocity from simulation (blue) and in vivo (orange).

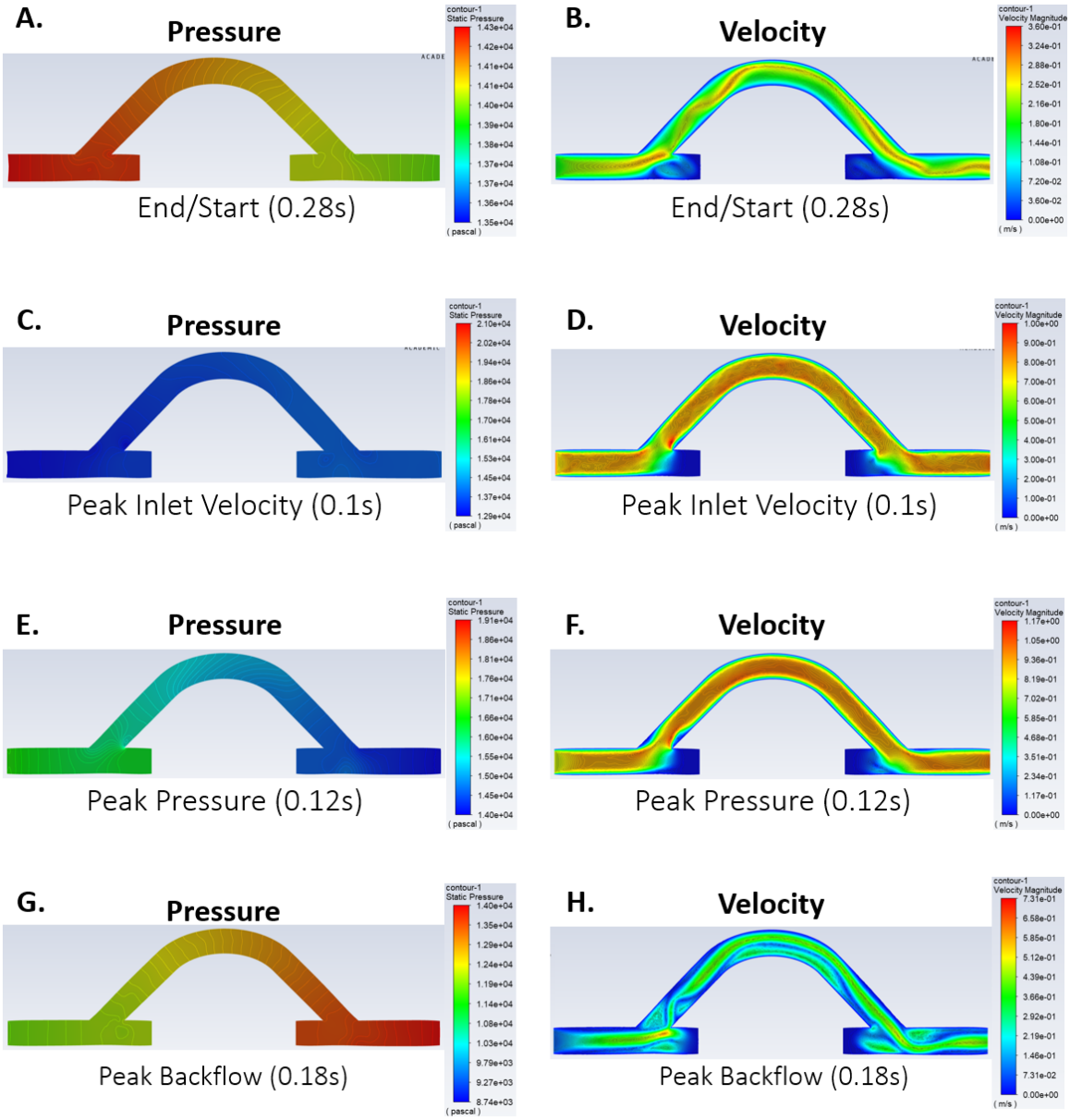

Figure A.3. Pressure and flow velocity of model without compliance mismatch. Elastic modulus of 0.55 MPa was used for all regions of the model [369, 370]. (A) Pressure throughout the model at 0.28 seconds. (B) Velocity throughout the model at 0.28 seconds. (C) Pressure throughout the model at 0.1 seconds. (D) Velocity throughout the model at 0.1 seconds. (E) Pressure throughout the model at 0.12 seconds. (F) Velocity throughout the model at 0.12 seconds. (G) Pressure throughout the model at 0.18 seconds. (H) Velocity throughout the model at 0.18 seconds.

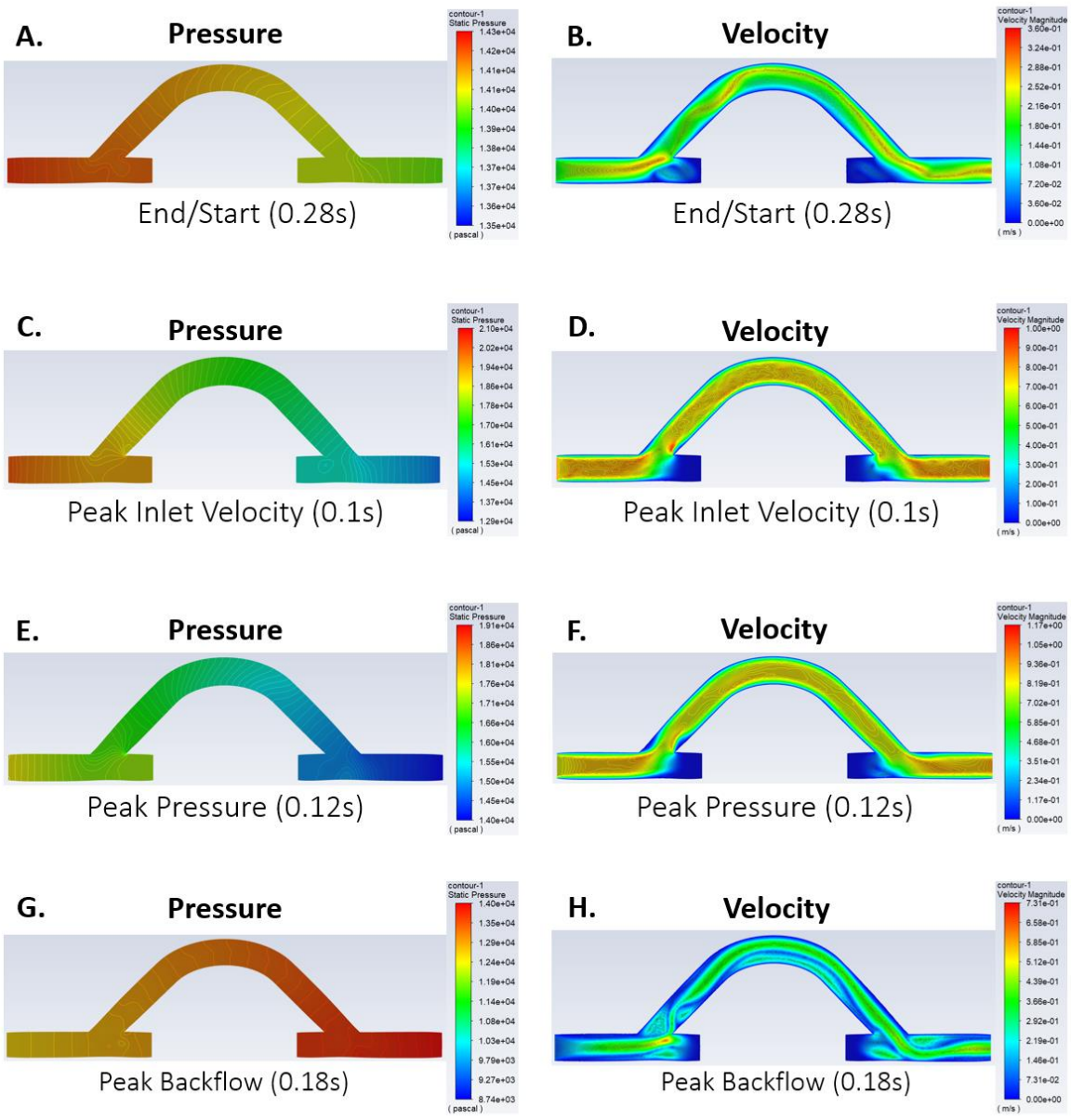

Figure A.4. Pressure and flow velocity of model with compliance mismatch at the graft region. Elastic modulus of 0.55 MPa was used for artery regions of the model [369, 370]. Elastic modulus of 5 MPa was used for graft region of the model. (A) Pressure throughout the model at 0.28 seconds. (B) Velocity throughout the model at 0.28 seconds. (C) Pressure throughout the model at 0.1 seconds. (D) Velocity throughout the model at 0.1 seconds. (E) Pressure throughout the model at 0.12 seconds. (F) Velocity throughout the model at 0.12 seconds. (G) Pressure throughout the model at 0.18 seconds. (H) Velocity throughout the model at 0.18 seconds.

Simulation was developed by Michael Tong under the Supervision of Dr. Keng Hwee Chiam and YeJin Jeong. The shape and dimensions of the model used in simulation is shown in Figure A.1A. The dimension was chosen to reflect the shape and dimension of the poly(vinyl alcohol) (PVA) graft

implanted in rabbit right common carotid artery model. The input velocity that was used in the simulation is shown in Figure A.1B [368]. Compliance and elastic modulus of the PVA grafts used *in vivo* are shown in Figure A.1C and Figure A.1D. The graft section of the model used the elastic modulus of low compliance (Fig. A.1C) to assess the accuracy of the simulation setup. The resulting flow was compared to the ultrasound measurements of the blood flow through the implanted graft. Figure A.2.B is the velocity measured using ultrasound data shown in Figure A.2A. The comparison between the *in vivo* and simulation data is shown in Figure A.2C. The model was then used determine the pressure and velocity of the blood through the conduit without compliance mismatch (Fig. A.3). The result was compared to the compliance mismatch simulation, which used 5 MPa for the graft section of the model (Fig. A.4). The pressure was significantly higher for the compliance mismatch model at 0.1 seconds (Fig. A.3C and Fig. A.4C) and 0.12 seconds (Fig. A.3E and Fig. A.4E). Also, it was observed that the velocity of not compliance mismatched model was higher than the compliance mismatched model at 0.1 seconds (Fig. A.3D and Fig. A.4D) and 0.12 seconds (Fig. A.3F and Fig. A.4F). This is unexpected as higher pressure should occur along with higher velocity. This, along with the fact that the simulation velocity did not accurately reflecting the in vivo measurements as shown in Figure A.2C, could be due to the errors in simulation parameters. The simulation parameters should be further investigated so that the model can be used to investigate the effects of compliance mismatch with direct comparison to the *in vivo* data.